Reliability of Finite Element Method for Time Harmonic Electromagnetic Problems Involving Moving Bodies

Applied Electromagnetics Laboratory

Department of Naval, Electrical, Electronic and Telecommunications Engineering

(DITEN)

University of Genoa, Italy

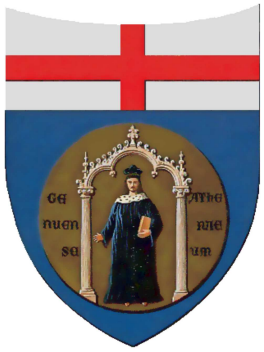

A thesis presented for the degree of
Doctor of Philosophy
by

Praveen Kalarickel Ramakrishnan

Advisor: Prof. Mirco Raffetto

March 1, 2018

Abstract

This work is mainly concerned about the time-harmonic electromagnetic problems involving moving bodies. Such a formulation is possible when the boundaries between different moving objects are stationary and the sources involved are time-harmonic. Even simple media present bianisotropic properties when they are in motion. This kind of problems find applications in diverse fields. Numerical solution is required for most of the practical problems. We examined the reliability of finite element simulator developed for solving such problems. A detailed error analysis was carried out for two dimensional problems involving moving objects by comparing the numerical solution with a semi analytic solution which is available for a simple test case. The results were satisfactory for a wide range of parameters. The solution for the component of the field polarized along that of the incident wave is very robust and has a quadratic convergence rate with respect to the size of the mesh. This is the same behaviour as that of the motionless case. The additional cross polarized component, present because of the bianisotropic effect due to motion is important for the reconstruction of velocity profiles of moving objects using inverse scattering techniques. The cross polarized component turns out to be more difficult to approximate and the convergence rate is only linear in the size of the mesh. Also for very small velocities, this component turns out to be too small and round-off error may become significant. In spite of this, the solution was found to be reliable for a large range of velocities and other parameters. The finite element simulator was used to find solution for three dimensional problems also. A series solution was implemented for such a problem involving rotating sphere and was used to compare the accuracy of finite element simulator for this kind of problems. Good agreement was found in the results. The same simulator was used for some more three dimensional problems involving bianisotropic materials and the convergence behaviour was observed. Thus the work is able to establish the reliability of finite element simulator for solving the interesting problems involving time-harmonic moving objects and other bianisotropic media.

Declaration

I declare that this thesis was composed by me and is the outcome of the original work done in the Applied Electromagnetics (AEM) Laboratory in the Department of Naval, Electrical, Electronic and Telecommunications Engineering (DITEN) of University of Genova, Italy. Due references have been provided on all supporting literatures and resources. The work contained here has not been submitted in support of another degree or professional qualification from this or any other university or institute of learning.

Acknowledgement

Foremost, I would like to express my sincere gratitude to my advisor Prof. Mirco Raffetto for the continuous support of my Ph.D study and research. His guidance helped me in developing the necessary skills for conducting the research. His patience, enthusiasm, warmth and immense knowledge will always remain inspiring to me.

Besides my advisor, I will like to thank all the members of Applied Electromagnetics Laboratory. I thank Prof. Matteo Pastorino, Prof Andrea Randazzo and Prof Gian Luigi Gragnani for their support. I express my sincere gratitude to the other researchers in the laboratory, Alessandro Fedeli, Mario Clemente, Emanuele Tavanti, Massimo Brignone, who were always helpful and friendly.

I thank all the teachers who inspired me to learn. I would like to thank all the friends I have made in Italy for giving me the energy to complete the work. I thank all my friends from whom I have learned immensely and who have given me emotional support.

I thank my family, my mother Lalitha Bai and my brother Arun Kumar for their support and love throughout my life.

Contents

1 Introduction **15**

1.1 General Description of the Topic 16

1.2 Previous Results in Literature 17

1.2.1 One Dimensional Problems 17

1.2.2 Two Dimensional Problems 17

1.2.3 Three Dimensional Problems 18

1.3 New Results obtained 18

1.3.1 Axially Moving Cylinders 18

1.3.2 Rotating Axisymmetric Objects 19

1.4 Thesis Overview 19

2 Background and Methodology **21**

2.1 Introduction 21

2.2 Time Domain Description 21

2.3 Frequency Domain Formulation 24

2.4 Variational Formulation and Well-Posedness of the Problem 27

2.5 Galerkin and Finite Element Approximation 29

2.6 Conclusions 31

3 Error Analysis of Finite Element Solutions for Two Dimensional Problems Involving Axially Moving Cylinders **32**

3.1 Introduction 32

3.2 Mathematical formulation of the problem 34

3.3 Finite element approximation 38

3.4 Definition of a test case and of the relevant errors 40

3.5 Numerical results 47

3.5.1 Numerical results related to E_z 47

3.5.2 Numerical results related to $\mathbf{E}_t$ and H_z 52

3.5.3 Problematic results related to $\mathbf{E}_t$ and H_z 54
3.6 **Issues related to numerical solution procedure** 59
3.7 Conclusions 61

4 Reliability of Finite Element Simulators for Three Dimensional Problems Involving Rotating axisymmetric Objects and Other Bianisotropic Materials 63
4.1 Introduction 63
4.2 Problem Definition 65
4.3 Numerical Results 68
4.3.1 Rotating Sphere 68
4.3.2 Rotating Torus 73
4.3.3 Other Problems Involving Bianisotropic Materials 80
4.4 Conclusions 92

5 Conclusions 93

Appendix A Deduction of the Tensor Fields Involved in the Constitutive Relations for Rotating Objects 95

List of Figures

3.1 The configuration of axially moving homogeneous cylinder considered as test problem. The radius of the cylinder is R and the axial velocity is $v_z = c_0\beta$. The cylinder characterized by the permittivity ε_r and permeability $\mu_r = 1$. The incident field is impinging orthogonally on the cylinder. 41

3.2 An example of discretization of the cylindrical numerical domain Ω obtained by using $n = 6$. 43

3.3 Behaviour of $e_{z,a,h1}$, $e_{z,a,l2}$ and $e_{z,a,semi}$ versus h, when the cylinder is at rest or moves with $\beta = 0.25$. The cylinder is assumed to have $R = 0.2$ m and to be made up of a material having $\varepsilon_r = 2$ at rest. Two plots proportional to h and h^2 are provided, too. 48

3.4 Values of E_{hz} along x axis for $\beta = 0$ and $\beta = 0.25$. Real, Imaginary and absolute values of E_{hz} are shown for both cases. The results were obtained for $\varepsilon_r = 2$, $R = 0.2$ m, $f = 1$ GHz and $n = 320$. 49

3.5 Values of E_{hz} along x axis for $\beta = 0$ and $\beta = 0.25$. Real, Imaginary and absolute values of E_{hz} are shown for both cases. The results were obtained for $\varepsilon_r = 2$, $R = 0.2$ m, $f = 1$ GHz and $n = 320$. 50

3.6 Behaviour of $e_{z,r,h1}$ versus h for different values of β and ε_r. In particular, for any value of ε_r one of the largest possible normalized axial speed values is considered in addition, for both cases, to $\beta = 0$. The scatterer radius is $R = 0.2$ m. 51

3.7 Behaviour of $e_{t,a,u2d}$, $e_{t,a,l2}$, $e_{t,a,\Gamma}$ and $e_{t,a,semi}$ versus h, when the cylinder moves with $\beta = 0.25$. Plots proportional to $e_{t,a,semi}$ is also reported for $\beta = 5\ 10^{-m}$, $m = 6, 9$. $C = 5\ 10^7$. The cylinder is assumed to have $R = 0.2$ m and to be made up of a material having $\varepsilon_r = 2$ at rest. Two plots proportional to h and h^2 are provided, too. 52

3.8 Behaviour of $e_{r,hz}$ versus h for different values of β and ε_r. In particular $\varepsilon_r = 1.1$, $\varepsilon_r = 2$ and $\varepsilon_r = 8$ are considered. In each case a value close to the upper bound of β is taken along with $\beta = 5\ 10^{-9}$. Two plots proportional to h and h^2 are provided, too. 53

3.9 Behaviour of $e_{r,hz}$ versus h, when the cylinder moves with $\beta = 5\ 10^{-m}$, $m = 10, \ldots, 15$. The cylinder is assumed to have $R = 0.2$ m and to be made up of a material having $\varepsilon_r = 2$ at rest.. 54

3.10 Behaviour of $e_{r,hz}$ versus h for different values of β and ε_r. We consider $\varepsilon_r = 1.1$ and $\varepsilon_r = 8.0$ with $\beta = 5\ 10^{-m}$ and $m = 10, 11, 12$. 55

3.11 Behaviour of $e_{r,hz}$ versus β for different values of the scatterer radius R and of the frequency f. The values of β which are particularly critical for $e_{r,hz}$ are considered. The cylinder is assumed to be made up of a material having $\varepsilon_r = 2$ at rest. The numerical solutions are computed by using a mesh with $n = 120$. 56

3.12 Values of $\frac{nn+ne}{ne} \frac{|||[e_z]|||}{|||[e_t]|||}$ versus β for different values of ε_r and n. We consider $n = 120$ with $\varepsilon_r = 1.1$,$\varepsilon_r = 2$ and $\varepsilon_r = 8$. In addition the value corresponding to $n = 200$ with $\varepsilon_r = 2$ is also shown. A plot of β^{-1} provided too. 57

3.13 Values of condition number K_A versus h with $\beta = 5 \times 10^{-9}$ and for different values of ε_r. The results are shown for $\varepsilon_r = 1.1, 2, 8$ and for $n = 20, 40, 80, 120, 160, 200$. 58

3.14 The estimate of maximum relative error due to round-off in the transverse component of the field ($\frac{||\Delta[e_t]||}{|||[e_t]|||}$) calculated according to equation (3.25), considering $\delta = 10^{-15}$. It is plotted against β, for $\varepsilon_r = 1.1, 2, 8$ with $n = 120$. One plot for $n = 200$ is also given corresponding to $\varepsilon_r = 2$. 59

4.1 The configuration of rotating sphere considered as test problem. The radius of the sphere is R_s and the rotation is about z axis with angular velocity ω_s. The electric field is in the x-y plane and comes along the direction θ. 69

4.2 Magnitude of the components of electric field plotted against the angle along a circle in x-z plane. The finite element solution is shown in comparison with the series solution provided by De Zutter. 71

4.3 Phase of the components of electric field plotted against the angle along a circle in x-z plane. The finite element solution is shown in comparison with the series solution provided by De Zutter. 72
4.4 Geometry of the toroidal scatterer considered as the test problem. The toroid rotates about the z axis with angular velocity ω_s. R and r are as shown in the figure and are respectively the "major radius" and the "minor radius" of the torus. 73
4.5 The mesh constructed for a toroidal scatterer. First a two-dimensional mesh is created along x-z plane as shown on the left. The circular boundary of the 2d section of the torus is shown in red. The planar mesh is then rotated around z-axis to get the three dimensional mesh shown on the right. The section cut along x-y plane is shown here. . . 74
4.6 Magnitude of E_z along x axis for the toroidal scatterer. The frequency of incident wave is 20 MHz and torus is made of homogeneous material with $\varepsilon_r = 20$ in its rest frame. For $\omega_s = 0$ the solution from the commercial simulator COMSOL as well as that from our Finite Element code are shown and is compared against our solution for $\omega_s = 0.5c_0$ rad/sec. 75
4.7 Magnitude of E_z along y axis for the toroidal scatterer. The frequency of incident wave is 20 MHz and torus is made of homogeneous material with $\varepsilon_r = 20$ in its rest frame. For $\omega_s = 0$ the solution from the commercial simulator COMSOL as well as that from our Finite Element code are shown and is compared against our solution for $\omega_s = 0.5c_0$ rad/sec. 76
4.8 Magnitude of E_z along z axis for the toroidal scatterer. The frequency of incident wave is 20 MHz and torus is made of homogeneous material with $\varepsilon_r = 20$ in its rest frame. For $\omega_s = 0$ the solution from the commercial simulator COMSOL as well as that from our Finite Element code are shown and is compared against our solution for $\omega_s = 0.5c_0$ rad/sec. 77
4.9 Magnitude of E_z along x axis for the toroidal scatterer. The frequency of incident wave is 100 MHz and torus is made of homogeneous material with $\varepsilon_r = 20$ in its rest frame. For $\omega_s = 0$ the solution from the commercial simulator COMSOL as well as that from our Finite Element code are shown and is compared against our solution for $\omega_s = 0.5c_0$ rad/sec. 78

4.10 Magnitude of E_z along y axis for the toroidal scatterer. The frequency of incident wave is 100 MHz and torus is made of homogeneous material with $\varepsilon_r = 20$ in its rest frame. For $\omega_s = 0$ the solution from the commercial simulator COMSOL as well as that from our Finite Element code are shown and is compared against our solution for $\omega_s = 0.5c_0$ rad/sec. 79

4.11 Magnitude of E_z along z axis for the toroidal scatterer. The frequency of incident wave is 100 MHz and torus is made of homogeneous material with $\varepsilon_r = 20$ in its rest frame. For $\omega_s = 0$ the solution from the commercial simulator COMSOL as well as that from our Finite Element code are shown and is compared against our solution for $\omega_s = 0.5c_0$ rad/sec. 80

4.12 Configuration of a rectangular waveguide partially filled with chiral media considered by Wu and Jaggard in [55] 82

4.13 Magnitude of components of electric field along the x-axis for three different sizes of meshes. The parameters used are $a = 23$mm,$b = 10$ mm, $c = 11$ mm, $d = 5$ mm, $w = 40$ mm, frequency $f = 9$ GHz. The media is characterized by $\varepsilon_r = 2.5$, $\mu_r = 1$. The biisotropic media has $\xi_c = 2.5\,10^{-3}$. The corresponding plots for isotropic media is also shown for the comparison which is characterized by $\xi_c = 0$. 84

4.14 Magnitude of components of electric field along the y-axis for three different sizes of meshes. The parameters used are $a = 23$mm,$b = 10$ mm, $c = 11$ mm, $d = 5$ mm, $w = 40$ mm, frequency $f = 9$ GHz. The media is characterized by $\varepsilon_r = 2.5$, $\mu_r = 1$. The biisotropic media has $\xi_c = 2.5\,10^{-3}$. The corresponding plots for isotropic media is also shown for the comparison which is characterized by $\xi_c = 0$. 85

4.15 Magnitude of components of electric field along the z-axis for three different sizes of meshes. The parameters used are $a = 23$mm,$b = 10$ mm, $c = 11$ mm, $d = 5$ mm, $w = 40$ mm, frequency $f = 9$ GHz. The media is characterized by $\varepsilon_r = 2.5$, $\mu_r = 1$. The biisotropic media has $\xi_c = 2.5\,10^{-3}$. The corresponding plots for isotropic media is also shown for the comparison which is characterized by $\xi_c = 0$. 86

4.16 The configuration of rectangular waveguide half filled with bianisotropic material which was considered in [56]. 87

4.17 Magnitude of components of electric field along x axis for the rectangular waveguide with bianisotropic obstacle which was considered in [56].The waveguide is excited with a TE_{10} by applying a frequency of 10 GHz, the waveguide geometry is defined by $a = 0.01$ m and the material is defined by $\kappa = 1.061\,10^{-3}$. Solution is shown with three different sizes of mesh. The result for the case with no obstacle is also shown. 89
4.18 Magnitude of components of electric field along y axis for the rectangular waveguide with bianisotropic obstacle which was considered in [56].The waveguide is excited with a TE_{10} by applying a frequency of 10 GHz, the waveguide geometry is defined by $a = 0.01$ m and the material is defined by $\kappa = 1.061\,10^{-3}$. Solution is shown with three different sizes of mesh. The result for the case with no obstacle is also shown. 90
4.19 Magnitude of components of electric field along z axis for the rectangular waveguide with bianisotropic obstacle which was considered in [56].The waveguide is excited with a TE_{10} by applying a frequency of 10 GHz, the waveguide geometry is defined by $a = 0.01$ m and the material is defined by $\kappa = 1.061\,10^{-3}$. Solution is shown with three different sizes of mesh. The result for the case with no obstacle is also shown. 91

List of Tables

3.1 Details about meshes obtained for different values of n. 44

Chapter 1

Introduction

The problems in electrodynamics of moving objects are very important in diverse fields. Some of them are communication engineering, power engineering, plasma physics, astrophysics, nuclear physics etc...[1]. In communication engineering, the frequency variation and amplitude modulation resulting from the movement of source is important. A case where this is of concern is in applications like moving target detector radars. Power engineers who are involved in the design of rotating machines, electromagnetic launch pads or magnetically levitated transport system also require to consider the effect of motion on electromagnetic fields. In plasma physics and astrophysics, sources moving with relativistic velocities have to be managed.

In this dissertation I present some work done on the time-harmonic electromagnetic boundary value problems involving moving objects. This is an important subclass of the general electromagnetic problems involving moving objects. In particular we are interested in two dimensional problems involving axially moving cylinders and three dimensional problems involving rotating axisymmetric objects. They find many applications in diverse fields. The two dimensional problems involving axially moving cylinders find applications related to moving plasma columns [2], [3], [4] ionized meteor trails [5], jet exhausts [6] or mass flows in pneumatic pipes [7]. Recent results related to inverse scattering problems for reconstructing velocity profiles of moving objects can be found in [8], [9]. Similarly the three dimensional problems are important in the reconstruction of velocity profiles of rotating axisymmetric objects may be important in the applications related to rotating plasma columns, rotating celestial bodies etc.. [10], [11], [12].

In some simple cases it is possible to derive analytical or semi-analytical solutions to these kind of problems [3], [12], [11]. However in most practical problems involving more complex geometry and electromagnetic characteristics, numerical methods

are necessary to compute the solution. However there were very little work in the open literature related to the reliability of such numerical solutions for this kind of problems. Hence I have carried out some analysis on the accuracy of the numerical solutions.

In the remaining part of this chapter I give a brief description of the problem, the results previously available in the literature and the new results obtained and conclude by discussing the overall structure of the thesis.

1.1 General Description of the Topic

The theory of electrodynamics of moving bodies was developed in the framework of relativity by Albert Einstein in his revolutionary paper published in 1905 [13], building upon the work of Maxwell and other scientists before him. An excellent introduction to the electrodynamics of moving bodies is given in [1]. It is well-known that Maxwell's equations remain unaltered in all inertial frames of reference. The electric field, magnetic field, current density and charge density get transformed according to relativistic relationships. The constitutive relations and material boundary conditions have to be transformed from the rest frame of the body to the laboratory frame. A moving media, even if it is isotropic in its rest frame will be perceived as bianisotropic in laboratory frame [14]. The material boundary conditions are also changed unless the velocity is tangential to the boundary. Further there is doppler shift due to which frequency of electromagnetic fields from moving media get modified [1].

In general we have to treat these problems in time domain. But with time-harmonic sources, when the movement takes place in such a way that the boundaries among different linear media are stationary, it is possible to work in frequency domain [1], [14]. The field quantities can be expressed in time-harmonic form and the complex frequency exponential factor $e^{j\omega t}$ can be suppressed. Several important problems come under this category.

There are many practical problems that can be treated in one, two or three dimensions. It may be possible to obtain analytic solution to these problems in very special cases. But in general, we have to resort to numerical solution . In the flowing section I discuss the main results already available in the literature. I also briefly discuss the need for more results which motivates the importance of the present work.

1.2 Previous Results in Literature

1.2.1 One Dimensional Problems

Some results are already available in the case of one dimensional problems. Electromagnetic problems involving moving slabs can often be formulated in one dimension. This problem can be useful in the analysis of relativistic plasmas with complex media parameter profiles. Many analytic as well as numerical approaches to this class of problem are available in the literature [15], [16], [17].

1.2.2 Two Dimensional Problems

Many problems involving axially moving cylinders can be analyzed in two dimensions. Some series solution are available for multilayer elliptic cylinders [18], [19]. For more general problems, numerical methods are necessary. A set of sufficient conditions for the well-posedness and the convergence of finite element approximation of two-dimensional time-harmonic problems with non-conducting moving media was provided in [20]. This result is quite general and consist of some non restrictive requirement on domain, its boundary, its subdomains and their boundary conditions and constitutive parameters. There are a few additional conditions on the constitutive parameters and media involved and of the velocity field, which are met in a broad class of practical cases of interest involving axially moving media.

In the presence of a time-harmonic illumination, the axial motion of cylinders determines, in any reference frame in which the media are not at rest, a bianisotropic effect, which is responsible for the presence of a scattered field having both polarizations: the same as that of the incident field (co-polarized component) and orthogonal one (cross polarized component).

An important application of problems involving axially moving cylinders is in reconstruction problems. Inverse scattering techniques can be used for the reconstruction of permittivity and velocity profiles of moving targets. An efficient algorithm for the solution of these type of problems was developed in [8]. Two different approaches suitable for different ranges of axial velocities were proposed in this work. At large relativistic velocities, the general approach is taken in which both permittivity and velocity profile are treated as unknowns. However, at low velocities a two step approach is considered. In the first step the permittivity is reconstructed by neglecting motion, for which only the co-polarized component is considered. Then the recovered permittivity profile is used in the reconstruction of velocity profile for which the cross-

polarized component becomes important. The second method is more efficient at low velocities but is not so accurate at higher velocity. Thus both methods complement each other.The proposed method was applied and shown to be applicable for a wide range of speed in [9].

1.2.3 Three Dimensional Problems

A few series solutions for three dimensional problems involving moving objects are available for some simpler geometries. This include some results related to rotating cylinders [10], [12] and rotating sphere [21], [11], [22]. In [23], finite element approach for rotating cylinders is discussed. A result for the well-posedness and finite element convergence of three dimensional time-harmonic problems involving bianisotropic media was proved in [24]. However the application of these results require strong hypotheses on losses and hence cannot be applied to the cases we are interested in. General numerical simulator to manage time-harmonic problems with rotating axisymmetric has not been discussed in the literature and hence the reliability of such a solver is yet to be established.

1.3 New Results obtained

The focus of this thesis is on the two dimensional problems involving axially moving cylinders and three dimensional problems involving rotating axisymmetric objects.

1.3.1 Axially Moving Cylinders

Error analysis for the time-harmonic electromagnetic problems involving axially moving cylinders was not available in literature previously. I was involved in the analysis of performance of finite element simulators used for solving this kind of problems. This was the first error analysis carried out for finite element solutions of boundary value problems involving cylinders moving in axial direction [25]. The semi analytic solution provided in [3] was used to compare the results of the finite element simulation. A detailed analysis was carried out to ensure the reliability and limitations of the simulator. These results could suggest what can be expected in other cases and could be considered as benchmarks for any error estimates deduced in future. The work provides the numerical evidence for the convergence of finite element solution. The convergence rate of the co-polarized and the cross-polarized components of the fields are examined. The co-polarized component converges quadratically with the

size of mesh which is the same rate as that of the solution in motionless case. The cross-polarized component is found to be converging only linearly with respect to the mesh size. The limitation of the simulator in giving accurate results for very small velocities is examined and some practical considerations are provided which can indicate whether the solution is reliable or not. Overall, the results obtained are robust for very wide range of parameters of the problems and hence the numerical approach can be applied to wide range of applications.

1.3.2 Rotating Axisymmetric Objects

We have developed the finite element simulator which can solve three dimensional time-harmonic electromagnetic problems involving rotating axially symmetric objects. I implemented the analytic solution provided by [11], which was used as a reference to measure the error in numerical solutions. This was used to carry out the error analysis of finite element solver developed in our lab [26]. Investigation was carried out to examine the evidence for the convergence and accuracy of the finite element simulator for this kind of problems. I was involved in developing the finite element simulators for axisymmetric rotating objects and in the analysis of the reliability of these simulators.

1.4 Thesis Overview

In chapter 2, the available literature is described in more detail and the motivation for the work is expanded. First the description of the electromagnetic fields is provided in the time domain. The proper relativistic transformations are introduced which becomes necessary when fast moving objects are involved. Further the time-harmonic formulation is introduced along with the general constitutive relations and boundary conditions suitable for these problems. The variational formulation is introduced after that and the well-posedness of the problem is discussed. Following that the Galerkin and finite element method are described. Chapter 3 is related to the error analysis of the numerical solution for two dimensional problems involving non conducting cylinders moving in axial direction. After defining the problem, a test case is considered for which a series solution is available. The detailed error analysis is done by varying different parameters involved in the test case. The convergence of the finite element method is demonstrated. The rate of convergence for the co-polarized and cross-polarized components are examined. The error is analyzed to find

the range in which finite element solver is reliable and some indications are provided so that one can be aware when the simulator starts becoming unreliable. In chapter 4 three dimensional problems involving bianisotropic media are analyzed. The problems related to rotating axisymmetric objects come under this category. The ability of the finite element simulator to give accurate solution is examined by comparing it to analytic solution for the simple problem involving rotating sphere. Further the convergence of the finite element solution is examined for some other three dimensional problems involving bianisotropic media. Finally in chapter 5 the main results obtained are summarized. The possibility of extending the work and the directions for further research in the area are indicated briefly.

Chapter 2

Background and Methodology

2.1 Introduction

This chapter reviews the major concepts and results related to electromagnetic problems involving moving bodies. In Section 2.2 some of the basic ideas pertaining to time domain description of electromagnetic field in the presence of moving bodies is recalled. In Section 2.3 the frequency domain formulation is introduced and the differential formulation of the problem is defined. The discussed form is mostly general for problems involving bianisotropic media. The variational formulation and some ideas related to the well-posedness of these problems are discussed in Section 2.4. Section 2.5 discusses the basic ideas related to Galerkin finite element formulation.

2.2 Time Domain Description

Maxwell's equations were developed in its full form in the nineteenth century. However, to deal with the electromagnetic waves in the presence of moving bodies, we need the theory of special relativity developed in the beginning of twentieth century [13]. A good introduction to the practical problems which deal with electrodynamics of moving bodies is given in [1]. In the first part of [13] the author deals with the kinematics when uniformly moving frames are involved. Accordingly we need to apply Lorentz transformation between two inertial frames of reference to get the correct space-time co-ordinates. In the second part of [13], the author turns to Maxwell's equations, the Doppler effect and the radiation pressure exerted by the fields. According to the theory, two postulates hold for any two inertial frames. Firstly, the laws of electrodynamics and optics have the same form in all inertial frames. Secondly, light

always propagates in empty space with a definite speed c_0, independently of the state of motion of the emitting body.

Consider an open connected domain $\Omega \subset \mathbb{R}^3$. The following is the time domain Maxwell's equation valid throughout Ω

$$\begin{aligned} \nabla \times \mathbf{e} &= -\frac{\partial \mathbf{b}}{\partial t} - \mathbf{j}_m \\ \nabla \times \mathbf{h} &= \frac{\partial \mathbf{e}}{\partial t} + \mathbf{j}_e \\ \nabla \cdot \mathbf{d} &= \rho_e \\ \nabla \cdot \mathbf{b} &= \rho_m \end{aligned} \tag{2.1}$$

where $\mathbf{e}$, $\mathbf{h}$ are electric and magnetic fields, $\mathbf{d}$, $\mathbf{b}$ are electric and magnetic flux densities, $\mathbf{j}_e$, $\mathbf{j}_m$ are electric and magnetic current density sources and ρ_e, ρ_m are the electric and magnetic charge density sources respectively.

From the postulates it follows that the Maxwell's equations for empty space should be of the same form in all inertial frames. This then leads to transformation equations for fields and sources from one inertial frame to another. It is then convenient to solve the field problem in a frame where finding a solution is simple, and then transform the result back to the frame of interest.

The transformation laws for the electromagnetic sources and fields can be derived as given in Van Bladel's book [1] (pp 950 -953). Let S be the laboratory frame of reference and S' be an inertial frame which is moving with a velocity $\mathbf{v}$ whose magnitude is $|\mathbf{v}| = \beta c_0$ where c_0 is the speed of light in vacuum. The transformation laws for the charge and current source densities can be derived starting from the equation of conservation of charge in vacuum. This can be done by first applying the Lorentz equations to transform from rest frame to laboratory frame and then remembering that the conservation equation should hold in all inertial frames. The details of this procedure for electric charge density ρ_e and electric current density $\mathbf{j}_e$ is given in the book by Van Bladel. The final form of the transformation equations looks like:-

$$\begin{aligned} \rho'_e &= \frac{\rho_e}{\sqrt{1-\beta^2}} - \frac{\mathbf{v}\cdot\mathbf{j_e}}{c_0^2\sqrt{1-\beta^2}} \\ \rho'_m &= \frac{\rho_m}{\sqrt{1-\beta^2}} - \frac{\mathbf{v}\cdot\mathbf{j_m}}{c_0^2\sqrt{1-\beta^2}} \\ \mathbf{j}'_{e\perp} &= \mathbf{j}_{e\perp} \\ \mathbf{j}'_{m\perp} &= \mathbf{j}_{m\perp} \\ \mathbf{j}'_{e\parallel} &= \frac{\mathbf{j}_{e\parallel}}{\sqrt{1-\beta^2}} - \frac{\mathbf{v}\rho_e}{\sqrt{1-\beta^2}} \\ \mathbf{j}'_{m\parallel} &= \frac{\mathbf{j}_{m\parallel}}{\sqrt{1-\beta^2}} - \frac{\mathbf{v}\rho_m}{\sqrt{1-\beta^2}} \end{aligned} \tag{2.2}$$

where the subscripts $\parallel$ and $\perp$ indicate the components of the vector parallel to and orthogonal to $\mathbf{v}$ respectively.

The electric field $\mathbf{e}$, magnetic field $\mathbf{h}$, electric flux density $\mathbf{d}$ and magnetic flux density $\mathbf{b}$ can be transformed in a similar way. We get

$$\begin{aligned}
\mathbf{e}' &= \mathbf{e}_\parallel + \tfrac{1}{\sqrt{1-\beta^2}}(\mathbf{e}_\perp + \mathbf{v}\times\mathbf{b}) \\
\mathbf{b}' &= \mathbf{b}_\parallel + \tfrac{1}{\sqrt{1-\beta^2}}(\mathbf{b}_\perp - \tfrac{\mathbf{v}\times\mathbf{e}}{c_0^2}) \\
\mathbf{d}' &= \mathbf{d}_\parallel + \tfrac{1}{\sqrt{1-\beta^2}}(\mathbf{d}_\perp + \tfrac{\mathbf{v}\times\mathbf{h}}{c_0^2}) \\
\mathbf{h}' &= \mathbf{h}_\parallel + \tfrac{1}{\sqrt{1-\beta^2}}(\mathbf{h}_\perp - \mathbf{v}\times\mathbf{d})
\end{aligned} \tag{2.3}$$

The constitutive equations in a moving frame can also be derived [1] (p 958), when the medium is in uniform translation with respect to the laboratory frame S. This is done by first finding an inertial frame S' where all the points of the medium are at rest. In such a frame, the traditional constitutive equations for a material at rest holds. Then using the transformation of fields, it is possible to deduce the constitutive relation that holds for the frame S. Assuming that we have traditional constitutive equations for linear isotropic material

$$\mathbf{d}' = \varepsilon\mathbf{e}',\ \mathbf{b}' = \mu\mathbf{h},\ \mathbf{j}' = \sigma\mathbf{e}' \tag{2.4}$$

We get:-

$$\begin{aligned}
\mathbf{d} + \tfrac{\mathbf{v}\times\mathbf{h}}{c_0^2} &= \varepsilon(\mathbf{e} + \mathbf{v}\times\mathbf{b}) \\
\mathbf{b} - \tfrac{\mathbf{v}\times\mathbf{e}}{c_0^2} &= \mu(\mathbf{h} - \mathbf{v}\times\mathbf{d}) \\
\mathbf{j}_e &= \rho_e\mathbf{v} + \sigma\sqrt{1-\beta^2}\mathbf{e}_\parallel + \tfrac{\sigma}{\sqrt{1-\beta^2}}(\mathbf{e}_\perp + \mathbf{v}\times\mathbf{b}).
\end{aligned} \tag{2.5}$$

From the final form of the constitutive relation, it can be seen that the media in motion exhibits bianisotropic effects even when it is isotropic in its rest frame. This means that the field vectors $\mathbf{d}$ and $\mathbf{h}$ depend on both $\mathbf{e}$ and $\mathbf{b}$ but are parallel to neither.

Transformation of the boundary conditions on material interfaces can be done in a similar manner [1] (p. 959). On the interface the traditional condition for the rest frame S' is

$$\begin{aligned}
\mathbf{n}'\times(\mathbf{h}_2' - \mathbf{h}_1') &= \mathbf{j}_{eS}' \\
\mathbf{n}'\times(\mathbf{e}_2' - \mathbf{e}_1') &= \mathbf{j}_{mS}' \\
\mathbf{n}'\cdot(\mathbf{d}_2' - \mathbf{d}_1') &= \rho_{eS}' \\
\mathbf{n}'\cdot(\mathbf{b}_2' - \mathbf{b}_1') &= \rho_{mS}'
\end{aligned} \tag{2.6}$$

where the subscript S denotes the surface density of the source. Transformed to

the laboratory frame S we get

$$\begin{aligned}
&\mathbf{n} \times (\mathbf{h}_2 - \mathbf{h}_1) + (\mathbf{n} \cdot \mathbf{v})(\mathbf{d}_2 - \mathbf{d}_1) = \mathbf{j}_{eS} \\
&\mathbf{n} \times (\mathbf{e}_2 - \mathbf{e}_1) + (\mathbf{n} \cdot \mathbf{v})(\mathbf{b}_2 - \mathbf{b}_1) = \mathbf{j}_{mS} \\
&\mathbf{n} \cdot (\mathbf{d}_2 - \mathbf{d}_1) = \rho_{eS} \\
&\mathbf{n} \cdot (\mathbf{b}_2 - \mathbf{b}_1) = \rho_{mS}
\end{aligned} \tag{2.7}$$

Here $\mathbf{n}$ and $\mathbf{n}'$ are the unit normal vectors to the interface in the respective frames.

An important property of electromagnetic fields in the presence of motion is the Doppler effect. This is the shift in the frequency of electromagnetic fields due to motion, which can be deduced by using the proper transformation of fields. Thus in general, a moving electromagnetic scatterer illuminated by a time-harmonic source of single frequency could produce scattered field with additional frequencies.

2.3 Frequency Domain Formulation

In general the electromagnetic problems involving moving bodies have to be formulated in time domain. However a frequency domain formulation is possible under some conditions. This was point out by Cheng and Kong in [14]. It says that a moving medium can be treated as a stationary bianisotropic one in any reference frame in which the medium itself is not at rest if we are concerned with solving problems involving moving media with stationary boundaries. Therefore when the sources are time-harmonic and the boundaries of moving media are stationary, all the fields in the media will be time-harmonic and we can formulate the problem in frequency domain.

There are numerous practical problems which can be formulated in frequency domain. One case includes the problems involving moving dielectric slabs. There are some results giving analytic solutions to problems of this type [15], [16], [27], [17]. For example in [17], the authors develop a higher order one dimensional finite element method for the analysis of electromagnetic wave scattering off of a moving dielectric slab.

A class of problems involving axially moving cylinders have important applications in nuclear and plasma physics, astrophysics and engineering. Problems involving axially moving plasma columns [2], [3], [28], ionized meteor trails [5], jet exhausts [6] or mass flow in pneumatic pipes [7]. This class of problems can usually be formulated in two dimensions.

Three dimensional frequency domain problems are also of wide applications. Problems involving rotating axisymmetric objects come under this category. This kind of

problems find applications in different areas like in the reconstruction of velocity profiles in pneumatic pipes [7] and the measurement of rotational speed of celestial bodies [11].

Next we try to give a general description of the problem we are interested in solving. Here we try to state the common hypotheses made for such problems and definite the problem more precisely. In particular some hypotheses related to the domain, media involved and the boundary are stated. The formulation in three dimensions are more explicitly developed in this chapter. The two dimensional formulation is also mentioned but a more detailed description about it is given in Chapter 3.

Let us consider an open, bounded, connected subset of $\mathbb{R}^3$ to be the domain Ω where the electromagnetic problem of interest is formulated. Let $\Gamma = \partial\Omega$ be its Lipchitz continuous boundary [29] (p. 4), [30] (pp. 38-39). We denote by $\mathbf{n}$ the outward unit vector normal to Γ. The above hypotheses are summarized below

HD1. $\Omega \subset \mathbb{R}^3$ is open, bounded and connected

HD2. $\Gamma = \partial\Omega$ is Lipchitz continuous.

Further we assume that Ω can be decomposed into separate subdomains.

HD3. Ω can be decomposed into m subdomains (non empty, open and connected subsets of Ω having Lipchitz continuous boundaries) denoting $\Omega_i, i \in I = \{1, ..., m\}$, satisfying $\overline{\Omega} = \overline{\Omega}_1 \cup ... \cup \overline{\Omega}_m$ ($\overline{\Omega}$ is the closure of Ω) and $\Omega_i \cap \Omega_j = \emptyset$ for $i \neq j$

HM1. any material involved is linear and time-invariant and satisfies the following constitutive relations

To link together the time-harmonic quantities $\mathbf{E}$, $\mathbf{H}$, $\mathbf{D}$, $\mathbf{B}$ we need the following constitutive relations

$$\begin{cases} \mathbf{D} = (1/c_0)\, P\, \mathbf{E} + L\, \mathbf{B} & \text{in } \Omega \\ \mathbf{H} = M\, \mathbf{E} + \mathrm{c}_0\, Q\, \mathbf{B} & \text{in } \Omega \end{cases} \tag{2.8}$$

where c_0 is the velocity of light in vacuum and L,M,P and Q are four 3-by-3 matrix-valued complex functions defined almost everywhere in Ω. This is capable of representing any bianisotropic medium and hence in particular it is useful for problems of our interest involving moving media with only stationary boundaries. Equation (2.8) takes account implicitly of the electric current densities. Other equivalent forms of the above constitutive equations are possible [31](pp. 49), [32].

Next we assume some local regularity for the constitutive parameters. Different

inhomogeneous bianisotropic materials will be modelled with this assumption.

HM2. The matrix-valued complex functions representing the effective constitutive parameters satisfy [29](p.3),[30](p.36):

$$P|_{\Omega_k} \in (C^0(\overline{\Omega}_k))^{3\times 3}, Q|_{\Omega_k} \in (C^0(\overline{\Omega}_k))^{3\times 3}, L|_{\Omega_k} \in (C^0(\overline{\Omega}_k))^{3\times 3}, M|_{\Omega_k} \in (C^0(\overline{\Omega}_k))^{3\times 3}, \forall k \in I$$

Such hypothesis is in no way restrictive for all applications of interest since the material properties are just piecewise but not globally continuous.

Before defining the differential problem to be solved, we need to introduce some more definitions. $(L^2(\Omega))^3$ is the usual Hilbert space of square integrable vector fields on Ω with values in $\mathbb{C}^3$ and with scalar product given by $(\mathbf{u}, \mathbf{v})_{0,\Omega} = \int_\Omega \mathbf{v}^* \mathbf{u} dV$, where $\mathbf{v}^*$ denotes the conjugate transpose of the column vector $\mathbf{v}$. In order to deal with the tangential vector fields involved in the boundary condition we define [30](p.48)

$$L_t^2(\Gamma) = \{\mathbf{v} \in (L^2(\Gamma))^3 | \mathbf{v} \cdot \mathbf{n} = 0 \text{ almost everywhere on } \Gamma\}, \tag{2.9}$$

with scalar product denoted by $(\mathbf{u}, \mathbf{v}_{0,\Gamma}) = \int_\Gamma \mathbf{v}^* u dS$. The space where we will seek $\mathbf{E}$ and $\mathbf{H}$ is [30] (p. 82;see also p. 69)

$$U = H_{L^2,\Gamma}(\text{curl}, \Omega) = \{\mathbf{v} \in H(\text{curl}, \Omega) | \mathbf{v} \times \mathbf{n} \in L_t^2(\Gamma)\}, \tag{2.10}$$

with $H(\text{curl}, \Omega) = \mathbf{v} \in (L^2(\Omega))^3 | \text{curl}\, \mathbf{v} \in (L(\Omega))^3$.

The scalar product in the Hilbert space U is given by [30](p. 84, p. 69)

$$(\mathbf{u}, \mathbf{v})_{U,\Omega} = (\mathbf{u}, \mathbf{v})_{0,\Omega} + (\text{curl}\, \mathbf{u}, \text{curl}\, \mathbf{v})_{0,\Omega} + (\mathbf{u} \times \mathbf{n}, \mathbf{v} \times \mathbf{n})_{0,\Gamma}, \tag{2.11}$$

and the induced norm is $||\mathbf{u}||_{U,\Omega} = (\mathbf{u}, \mathbf{u})_{U,\Omega}^{1/2}$. The symbol ω represents the angular frequency, which, without loss of generality for wave problems, is assumed to be real and positive. Moreover, $\mathbf{J}_e$ and $\mathbf{J}_m$ are the electric and magnetic current densities, respectively, prescribed by the sources, Y is the scalar complex admittance involved in impedance boundary condition and $\mathbf{f}_R$ is the corresponding inhomogeneous term. Finally, the admittance Y with domain Γ and range $\mathbb{C}$ is assumed to satisfy

HB1. Y is piecewise continuous and $|Y|$ is bounded.

Now we can state the electromagnetic boundary value problem involving bianisotropic media

Problem 1. *Under the hypotheses HD1-HD2, HM1-HM2,HB1, given* $\omega > 0, \mathbf{J}_e \in$

$(L^2(\Omega))^3, \mathbf{J}_m \in (L^2(\Omega))^3$ *and* $\mathbf{f}_R \in L_t^2(\Gamma)$*, find* $(\mathbf{E}, \mathbf{B}, \mathbf{H}, \mathbf{D}) \in U \times (L^2(\Omega))^3 \times U \times (L^2(\Omega))^3$ *satisfying Maxwell's equations with impedance boundary conditions*

$$\begin{cases} \nabla \times \mathbf{H} - j\omega \mathbf{D} = \mathbf{J}_e & \text{in } \Omega \\ \nabla \times \mathbf{E} + j\omega \mathbf{B} = \mathbf{J}_m & \text{in } \Omega \\ \mathbf{H} \times \mathbf{n} - Y(\mathbf{n} \times \mathbf{E} \times \mathbf{n}) = \mathbf{f}_R & \text{on } \Gamma. \end{cases} \tag{2.12}$$

Note that $(2.12)_3$ with hypothesis HB1 can be used to enforce lowest order absorbing boundary conditions [33](p. 9), so that the above model can be thought of an approximation of a radiation or scattering problem, or boundary conditions at imperfectly conducting surfaces [34](pp. 384-385), so that the above model can be thought of as a realistic formulation of a cavity problem.

2.4 Variational Formulation and Well-Posedness of the Problem

In order to solve the boundary value problem described in Problem 1, it is convenient to use Galerkin finite element method. As a first step to this we can formulate the problem in a variational form. The appropriate variational form for this problem was derived in [24]. We state some of the important results here

Any solution of Problem 1 is fully determined by its $\mathbf{E}$ component through

$$\mathbf{B} = -\frac{1}{j\omega}\mathbf{J}_m - \frac{1}{j\omega}\nabla \times \mathbf{E}, \tag{2.13}$$

$$\mathbf{H} = M\,\mathbf{E} - \frac{c_0}{j\omega}Q\mathbf{J}_m - \frac{c_0}{j\omega}Q\nabla \times \mathbf{E} \tag{2.14}$$

and

$$\mathbf{D} = \frac{1}{c_0}P\,\mathbf{E} - \frac{1}{j\omega}L\mathbf{J}_m - \frac{1}{j\omega}L\nabla \times \mathbf{E} \tag{2.15}$$

This is easy to see since with $\omega > 0$, from $(2.12)_2$ we can we can deduce (2.13). Then by substituting this for $\mathbf{B}$ in (2.8) gives (2.14) and (2.15).

In [24] the authors go on to derive the variational formulation of Problem 1. This is

Problem 2. *Under the hypotheses H1-H4, given* $\omega > 0$*,* $\mathbf{J}_e \in (L^2(\Omega))^3$*,* $\mathbf{J}_m \in (L^2(\Omega))^3$ *and* $\mathbf{f}_R \in L_t^2(\Gamma)$*, find* $\mathbf{E} \in U$ *such that*

$$a(\mathbf{E}, \mathbf{v}) = l(\mathbf{v}) \ \forall \mathbf{v} \in U \tag{2.16}$$

where the sesquilinear form $a(\mathbf{u}, \mathbf{v})$ is defined by

$$\begin{aligned} a(\mathbf{u}, \mathbf{v}) = c_0\big(Q \operatorname{curl} \mathbf{u}, \operatorname{curl} \mathbf{v}\big)_{0,\Omega} - \frac{\omega^2}{c_0}\big(P\,\mathbf{u}, \mathbf{v}\big)_{0,\Omega} \\ -j\omega\big(M\,\mathbf{u}, \operatorname{curl} \mathbf{v}\big)_{0,\Omega} - j\omega\big(L \operatorname{curl} \mathbf{u}, \mathbf{v}\big)_{0,\Omega} \\ +j\omega\big(Y(\mathbf{n} \times \mathbf{u} \times \mathbf{n}), \mathbf{n} \times \mathbf{v} \times \mathbf{n}\big)_{0,\Gamma}, \end{aligned} \tag{2.17}$$

and the antilinear form $l(\mathbf{v})$ if defined by

$$\begin{aligned} l(\mathbf{v}) = -j\omega\big(\mathbf{J}_e, \mathbf{v}\big)_{0,\Omega} - c_0\big(Q\,\mathbf{J}_m, \operatorname{curl} \mathbf{v}\big)_{0,\Omega} \\ +j\omega\big(L\,\mathbf{J}_m, \mathbf{v}\big)_{0,\Omega} - j\omega\big(\mathbf{f}_R, \mathbf{n} \times \mathbf{v} \times \mathbf{n}\big)_{0,\Gamma}. \end{aligned} \tag{2.18}$$

In [24] the authors were able to prove that Problem 1 and Problem 2 were completely equivalent and hence the well-posedness of one implies that of the other.

The well-posedness of the problem of interest is very important in order to develop reliable numerical solvers. One main technique to arrive at such results is the Lax-Milgram lemma [30] (p. 20). This lemma implies that if the sesquilinear form like in Problem 1 is bounded and coercive and the antilinear form is bounded, then the solution is well-posed. In [24] the authors make use of this lemma to arrive at some sufficient conditions for the well-posedness of the above problem. However the additional hypotheses required to prove the well-posedness with this technique was too restrictive and requires a strong requirement for losses in this system. This is very limiting when we want to solve problems involving moving media.

Another effective technique for proving the well-posedness of variational problems under less restrictive hypotheses is to use the generalized Lax-Milgram lemma [30] (p. 21), [20]. This requires us to show that the sesquilinear form and the antilinear form are both continuous and that the sesquilinear form satisfies the following two conditions

- $\sup_{\mathbf{u} \in U} |a(\mathbf{u}, \mathbf{v})| > 0 \ \forall \mathbf{v} \in U, \mathbf{v} \neq 0$. This condition is easy to prove once we prove that the solution to Problem 2 is unique.

- There is a constant α such that $\inf_{\mathbf{u} \in U, ||\mathbf{u}||_U = 1} \sup_{\mathbf{v} \in U, ||\mathbf{v}|| \leq 1} |a(\mathbf{u}, \mathbf{v})| \geq \alpha > 0$.

This technique was used very effectively in proving the well-posedness of problems with two dimensional geometry in [20]. The additional hypotheses required were much less restrictive. The technique has not been applied to the three dimensional problems till now. Although we are currently working on such an extension, it is not discussed further since all the details are not finalized.

2.5 Galerkin and Finite Element Approximation

Galerkin's method is a powerful approach for approximating the solutions of the variational formulation of second order boundary value problems posed in variational form over a space U [35]. This method consists in defining similar problems, called discrete problems, over finite-dimensional subspaces U_h of the space U. A sequence of approximate solutions can be formed by making the discrete problem closer and closer to the original problem in some sense. In order to do this we can consider a sequence $\{U_h\}$, $h \in I$, of finite dimensional subspaces of U, where the set I is a denumerable and bounded set of strictly positive indexes having zero as the only limit point [35] (p. 112).

For any $h \in I$ and for any set of approximate sources $\mathbf{J}_{eh}, \mathbf{J}_{mh} \in (L^2(\Omega))^3$ and $\mathbf{f}_{Rh} \in L_t^2(\Gamma)$ we define the discrete antilinear form

$$\begin{aligned} l_h(\mathbf{v}) = &-j\omega\big(\mathbf{J}_{eh}, \mathbf{v}\big)_{0,\Omega} - c_0\big(Q\,\mathbf{J}_{mh}, \operatorname{curl}\mathbf{v}\big)_{0,\Omega} \\ &+j\omega\big(L\,\mathbf{J}_{mh}, \mathbf{v}\big)_{0,\Omega} - j\omega\big(\mathbf{f}_{Rh}, \mathbf{n}\times\mathbf{v}\times\mathbf{n}\big)_{0,\Gamma}. \end{aligned} \tag{2.19}$$

With this we can write the discrete version of the variational problem. Under the proper hypotheses on domain, boundary, media and with $\omega > 0$, $\mathbf{J}_{eh}$, $\mathbf{J}_{mh} \in (L^2(\Omega))^3$ and $\mathbf{f}_{Rh} \in L_t^2(\Gamma)$ we have to find $\mathbf{E}_h \in U_h$ such that

$$a(\mathbf{E}_h, \mathbf{v}_h) = l_h(\mathbf{v}_h)\ \forall \mathbf{v}_h \in U_h \tag{2.20}$$

It is necessary that the approximation must at least guarantee convergence. The convergence is defined in terms of sequences of the discrete problems. The solution sequence of solutions $\{\mathbf{E}_h\}$ should strongly converge in U to the true solution $\mathbf{E}$ of the original variational problem defined in (2.16).

Such a result was arrived at in [20] under non restrictive hypotheses. The extension of such a result for three dimensional problems is still to be finalized.

Conforming finite element method is a Galerkin method which uses a particular

way of constructing the finite dimensional space U_h, which are then called finite element spaces [35].

The construction of finite element spaces is characterized by three basic aspects. First a triangulation $\mathcal{T}_h$ is established over the set $\bar{\Omega}$ by subdividing it into a number of subsets T, such that

- For each $T \in \mathcal{T}_h$, the set T is closed and its interior $\mathring{T}$ is nonempty and connected.
- For each $T \in \mathcal{T}_h$, the boundary ∂T is Lipchitz continuous
- $\bar{\Omega} = \bigcup_{T \in \mathcal{T}_h} T$
- For each distinct $T_1, T_2 \in \mathcal{T}_h$, one has $\mathring{T}_1 \cap \mathring{T}_2 = \emptyset$

The second aspect of finite element method is related to a condition on the restriction of the finite element space U_h to the sets $T \in \mathcal{T}_h$. Let us define the finite dimensional spaces $P_T = \{v_h|_T; v_h \in U_h\}$, spanned by the restrictions $v_h|_T$ of the functions $v_h \in U_h$ to the sets $T \in \mathcal{T}_h$. Then it is required that the these spaces $P_T, T \in \mathcal{T}_h$ contain polynomials, or, at least, contain functions that are "close to" polynomials.

The third aspect of the finite element method is related to the choice of basis functions for the finite element space U_h. For an N_h dimensional finite element space U_h, we need to choose the basis functions $(\mathbf{w}_k)_{k=1}^{N_h}$ which have supports that are as small as possible. This is to ensure that the matrix in the resulting linear algebraic system has many zeros, and hence is simpler to solve.

Then by writing the solution $\mathbf{E}_h = \sum_{k=1}^{N_h} \alpha_k \mathbf{w}_k$ the Galerkin formulation of (2.20) gives us the following linear algebraic system to be solved

$$\sum_{k=1}^{N_h} a(\mathbf{w}_k, \mathbf{w}_m)\alpha_k = l_h(\mathbf{w}_m),\ 1 \leq m \leq N_h \tag{2.21}$$

In our case, with bianisotropic media we may end up with a non-Hermitian complex matrix $[A]$ whose $(k,m)^{th}$ entry is given by 2.21. We can use iterative methods for the solution of this system as is often done in finite element codes [33](pp. 382, 383, 396-405), [30]. We use different methods like the conjugate gradient on the normal equation (CGNE), biconjugate gradient method (BiCG) [36] etc.. The convergence of these solvers become slower when the condition number of the matrix become worse. Preconditioners help to improve the condition number and hence increase the rate of convergence. One of the simpler options is to use the Jacobi preconditioner.

2.6 Conclusions

In this chapter we recalled the basic ideas related to electromagnetic boundary value problems in the presence of moving media. In the presence of motion the relativistic transformations are required to be applied to solve electromagnetic problems accurately. The moving media presents bianisotropic behaviour even when the materials are simple in their rest frame. The frequency domain formulation is possible when the boundaries of moving media are stationary and the sources are time-harmonic. The variational formulation was introduced which is more convenient for developing a Galerkin finite element approximation to the solution of the problem. In addition the variational formulation is more suitable for the techniques for analyzing the well-posedness of the problem. We recalled that the well-posedness and the convergence of the finite element method were already proved in the literature for two dimensional problems involving axially moving cylinders. However, a result about the error bound is lacking for two dimensional problems. Hence we try to do a detailed error analysis in the next chapter to analyze the accuracy of the finite element solution. As for the three dimensional problems involving rotating axisymmetric objects, similar result for well-posedness and finite element convergence is not yet finalized. In this context, we do a basic analysis of the accuracy and convergence of finite element solution for such problems in Chapter 4.

Chapter 3

Error Analysis of Finite Element Solutions for Two Dimensional Problems Involving Axially Moving Cylinders

3.1 Introduction

One can consider many important applications involving of electromagnetic waves interacting with axially moving cylinders. In particular, one can refer to axially moving plasma columns [2], [3], [4], ionized meteor trails [5], jet exhausts [6] or mass flows in pneumatic pipes [7].

In most cases of interest, which could involve multiple cylinders having irregular shapes, inhomogeneous constitutive parameters and non-constant velocity profiles, numerical methods are required to try to approximate the solutions of interest [37].

Notwithstanding the difficulty related to the presence of materials in motion [1], [38], [14], determining the appearance of bianisotropic materials in any reference frame in which the media themselves are not at rest, the first results related to the well-posedness and the finite element approximability for these problems have been deduced [20].

When simulators are exploited, the results related to the convergence of numerical approximations are not the only aspects of practical interest, however. Error estimates are important, too (particularly, a-priori error estimations), as clearly pointed out in [39] (p. 114). These estimations were not available so far for two dimensional problems

involving moving objects. In particular results are not available for problems involving axially moving cylinders, like the ones of interest in this chapter.

Then, in order to understand what can be expected in practice, we have to perform numerical experiments. Unfortunately, in the presence of axially moving cylinders no numerical analysis seems to be available. This is the reason why, in this chapter, we present a lot of numerical results. They could suggest what can be expected in other cases and could be considered as benchmarks for any error estimate the research community will be able to deduce.

All numerical results which will be presented refer to a simple problem involving a moving cylinder. For such a problem an independent truncated-series solution can be found [3] (see also [40]). In this way we can evaluate the accuracy of our finite element approximations in terms of absolute and relative errors. The effects of all parameters involved in the definition of the simple problem of reference are studied.

As it has already been pointed out, in the presence of a time-harmonic illumination, the axial motion of cylinders determines, in any reference frame in which the media are not at rest, a bianisotropic effect and this, in turn, is responsible for the presence of a scattered field having both polarizations: the same as that of the incident field and the orthogonal one. For the co-polarized component of the field the outcome is absolutely stable. The errors for this component are, in particular, almost independent of the axial velocity and, then, assume almost the same values we get in the presence of motionless media. For the cross-polarized scattered wave the relative errors are very stable, as well, even though it is a-priori known that the previous results cannot be duplicated in this case, due to the fact that this component of the scattered field is known to go uniformly to zero as the axial speed of the scatterers becomes smaller and smaller [8]. Anyway, the errors on this component of the scattered field are indeed stable for a huge range of axial velocity values. By using double precision arithmetic this range can span nine or even more decades, so allowing the use of finite element simulators for velocities varying from a few centimeters per second to many thousands of kilometers per second. That means that the considered finite element method can be reliably used for a set of applications ranging from astrophysics to medicine.

In the chapter we examine the behavior of the error in the co-polarized and cross-polarized components of the field. The results of numerical experiments indicate that the co-polarized component follows quadratic convergence, same as that in the motionless case. On the other hand the results show that the cross-polarized component has linear convergence. However at low values of axial speed we expect that the

round-off error becomes more and more significant, degrading the accuracy of the cross-polarized component. This is because the co-polarized component remains of the same order while the cross-polarized component goes to zero with decreasing velocity. When the ratio of the norm of cross-polarized component to the co-polarized component becomes too large, the result becomes less reliable. Hence this number can be used as a general indicator for checking if the results of the simulation are reliable or not.

The results show, in addition to the previously mentioned applications, that the indicated simulator can be exploited as a reliable solver of forward scattering problems in imaging procedures aiming at the reconstruction of axial velocity profiles [8],[9] and this, by the way, was the initial motivation for our study.

The chapter is organized as follows. In Section 3.2 the mathematical formulation of the problems of interest is recalled together with some of the results available in the open literature. Some new considerations on the properties of the finite element matrices in the presence of moving media are provided in Section 3.3. In order to carry out the error analysis of interest, the definition of a test case is necessary. This is done in Section 3.4, where, in addition, a complete set of relevant absolute and relative errors is defined. The main section of the manuscript, dealing with the error analysis, is Section 3.5. Finally, the chapter is concluded by summarizing the main outcomes.

3.2 Mathematical formulation of the problem

The electromagnetic problems of interest in this chapter are those in which axially moving cylinders (having parallel axes) are illuminated by a time-harmonic source or field. This class of problems has been studied in [20] and we refer to that paper for the definition of all details. Here we recall just the main points to let the readers understand the developments which will be presented in the next sections.

All our problems will present a cylindrical geometry and we denote by z the axis of such a geometry. The time-harmonic sources and the inhomogeneous admittance boundary conditions involved are assumed to be independent of z, too, so that our problems can be formulated in a two-dimensional domain Ω contained in the (x, y) plane. Γ denotes the boundary of Ω. $\mathbf{n}$ and $\mathbf{l}$ are the unit vectors orthogonal (pointing outward) and tangential to Γ, respectively. We have $\mathbf{n} \times \mathbf{l} = \hat{\mathbf{z}}$.

The media involved in our problems can move in the axial direction with respect to the chosen reference frame. In such a frame a velocity field v_z, assumed to be

time-invariant, is naturally defined, even though we will often refer to it in terms of the usual [41] (p. 525) real-valued normalized field $\beta = \frac{v_z}{c_0}$, being c_0 the speed of light in vacuum. Different linear, time-invariant and inhomogeneous materials can be modelled in our problems. Ω_β will denote the subdomain of Ω containing all media in motion.

Under the indicated conditions all fields in all media will be time-harmonic, as the considered sources, and a factor $e^{j\omega t}$, common to all fields of interest, is assumed and suppressed.

Any material involved is isotropic in its rest frame and is there characterized by its relative permittivity ε_r, its relative permeability μ_r and its electric conductivity σ. In the following, any reference to ε_r, μ_r or σ of a moving medium should be interpreted as a reference to the corresponding quantity when the medium is at rest. All moving media will be considered in any case to have $\sigma = 0$ (in order to avoid the difficulties related to the convective currents which could also become surface electric currents and to avoid difficulty related to the no-slip condition which, ultimately, prevents the possibility of using pure two-dimensional models [20]).

By using the subscript "t" to denote the field quantities transverse to the z direction, the constitutive relations for the media in motion are [20]:

$$\mathbf{D}_t = \frac{1 + \mu_r\varepsilon_r - \zeta_1}{c_0^2\mu_0\mu_r}\mathbf{E}_t + \frac{\zeta_2}{c_0\mu_0\mu_r}\hat{\mathbf{z}} \times \mathbf{B}_t, \tag{3.1}$$

$$D_z = \varepsilon_0\varepsilon_r E_z, \tag{3.2}$$

$$\mathbf{H}_t = \frac{\zeta_1}{\mu_0\mu_r}\mathbf{B}_t + \frac{\zeta_2}{c_0\mu_0\mu_r}\hat{\mathbf{z}} \times \mathbf{E}_t, \tag{3.3}$$

$$H_z = \frac{1}{\mu_0\mu_r}B_z, \tag{3.4}$$

where

$$\zeta_1 = \frac{1 - \mu_r\varepsilon_r\beta^2}{1 - \beta^2}, \tag{3.5}$$

$$\zeta_2 = \frac{\beta(\mu_r\varepsilon_r - 1)}{1 - \beta^2}. \tag{3.6}$$

In order to be able to define the problems of interest and to talk of their finite element approximations, it is necessary to introduce some additional notations. $(L^2(\Omega))^n$ is the usual Hilbert space of square integrable vector fields on Ω with values in $\mathbb{C}^n$, $n = 2, 3$, and with scalar product given by $(\mathbf{u}, \mathbf{v})_{0,\Omega} = \int_\Omega \mathbf{v}^*\mathbf{u}\, dS$, where $\mathbf{v}^*$ denotes the conjugate transpose of the column vector $\mathbf{v}$. For a given three-dimensional

complex-valued vector field $\mathbf{A} = (A_x, A_y, A_z) \in (L^2(\Omega))^3$ we consider the operators curl_{2D} and grad_{2D}, defined according to

$$\mathrm{curl}_{2D}\mathbf{A}_t = \frac{\partial A_y}{\partial x} - \frac{\partial A_x}{\partial y}, \tag{3.7}$$

$$\mathrm{grad}_{2D}A_z = \left(\frac{\partial A_z}{\partial x}, \frac{\partial A_z}{\partial y}\right). \tag{3.8}$$

The transverse parts of the electric and magnetic fields will be in the Hilbert space

$$U_{2D} = \left\{\mathbf{A}_t \in (L^2(\Omega))^2 \mid \mathrm{curl}_{2D}\mathbf{A}_t \in L^2(\Omega) \text{ and } \mathbf{A}_t \cdot \mathbf{l} \in L^2(\Gamma)\right\}, \tag{3.9}$$

whose inner product is given by

$$(\mathbf{u}_t, \mathbf{v}_t)_{U_{2D}} = (\mathbf{u}_t, \mathbf{v}_t)_{0,\Omega} + (\mathrm{curl}_{2D}\mathbf{u}_t, \mathrm{curl}_{2D}\mathbf{v}_t)_{0,\Omega} + (\mathbf{u}_t \cdot \mathbf{l}, \mathbf{v}_t \cdot \mathbf{l})_{0,\Gamma}. \tag{3.10}$$

The axial components of the same fields are in the Hilbert space

$$H^1(\Omega) = \left\{A_z \in L^2(\Omega) \mid \mathrm{grad}_{2D}A_z \in (L^2(\Omega))^2\right\}, \tag{3.11}$$

whose inner product is

$$(u_z, v_z)_{1,\Omega} = (u_z, v_z)_{0,\Omega} + (\mathrm{grad}_{2D}u_z, \mathrm{grad}_{2D}v_z)_{0,\Omega}. \tag{3.12}$$

$\gamma_0 u_z$ will denote the boundary values of $u_z \in H^1(\Omega)$ on Γ.

Overall the electric and magnetic fields are in the Hilbert space

$$U = U_{2D} \times H^1(\Omega) \tag{3.13}$$

with inner product given by

$$(\mathbf{u}, \mathbf{v})_U = (\mathbf{u}_t, \mathbf{v}_t)_{U_{2D}} + (u_z, v_z)_{1,\Omega}. \tag{3.14}$$

$\| \|_U$ will denote the corresponding norm. The norms of the different spaces so far introduced will be of particular interest in establishing the accuracy of the results of the finite element simulator considered.

With the indicated notation, the electromagnetic boundary value problem we consider in this chapter is: given $\omega > 0$, the electric and magnetic current densities $\mathbf{J}_e, \mathbf{J}_m \in (L^2(\Omega))^3$, the boundary data $f_{Rz}, f_{Rl} \in L^2(\Gamma)$, find $(\mathbf{E}, \mathbf{B}, \mathbf{H}, \mathbf{D}) \in U \times$

$(L^2(\Omega))^3 \times U \times (L^2(\Omega))^3$ which satisfies

$$\begin{cases} \mathrm{curl}_{2D}\mathbf{H}_t - j\omega D_z = J_{ez} & \text{in } \Omega \\ \mathrm{grad}_{2D}H_z \times \hat{\mathbf{z}} - j\omega\mathbf{D}_t = \mathbf{J}_{et} & \text{in } \Omega \\ \mathrm{curl}_{2D}\mathbf{E}_t + j\omega B_z = -J_{mz} & \text{in } \Omega \\ \mathrm{grad}_{2D}E_z \times \hat{\mathbf{z}} + j\omega\mathbf{B}_t = -\mathbf{J}_{mt} & \text{in } \Omega \\ \mathbf{H}_t \cdot \mathbf{l} + Y\left(\gamma_0 E_z\right) = -f_{Rz} & \text{on } \Gamma \\ \gamma_0 H_z - Y\left(\mathbf{E}_t \cdot \mathbf{l}\right) = f_{Rl} & \text{on } \Gamma \end{cases} \tag{3.15}$$

and the constitutive relations (3.1), (3.2), (3.3) and (3.4).

After some work [20], one can deduce the equivalent variational formulation: given $\omega > 0$, $\mathbf{J}_e, \mathbf{J}_m \in (L^2(\Omega))^3$, $f_{Rz}, f_{Rl} \in L^2(\Gamma)$, find $\mathbf{E} \in U$ such that

$$a(\mathbf{E}, \mathbf{w}) = l(\mathbf{w}) \qquad \forall \mathbf{w} \in U, \tag{3.16}$$

where a is the following sesquilinear form

$$\begin{aligned} a(\mathbf{u}, \mathbf{w}) = &\left(\frac{\zeta_1}{\mu_r}\,\mathrm{grad}_{2D}u_z, \mathrm{grad}_{2D}w_z\right)_{0,\Omega} + \left(\frac{1}{\mu_r}\mathrm{curl}_{2D}\mathbf{u}_t, \mathrm{curl}_{2D}\mathbf{w}_t\right)_{0,\Omega} + \\ &+ j\frac{\omega}{c_0}\left(\frac{\zeta_2}{\mu_r}\,\mathbf{u}_t, \mathrm{grad}_{2D}w_z\right)_{0,\Omega} - j\frac{\omega}{c_0}\left(\frac{\zeta_2}{\mu_r}\,\mathrm{grad}_{2D}u_z, \mathbf{w}_t\right)_{0,\Omega} + \\ &- \frac{\omega^2}{c_0^2}\left(\varepsilon_r\, u_z, w_z\right)_{0,\Omega} - \frac{\omega^2}{c_0^2}\left(\frac{1 + \varepsilon_r\mu_r - \zeta_1}{\mu_r}\,\mathbf{u}_t, \mathbf{w}_t\right)_{0,\Omega} + \\ &+ j\omega\mu_0\left(Y\left(\gamma_0 u_z\right), \gamma_0 w_z\right)_{0,\Gamma} + j\omega\mu_0\left(Y\left(\mathbf{u}_t \cdot \mathbf{l}\right), \mathbf{w}_t \cdot \mathbf{l}\right)_{0,\Gamma} \end{aligned} \tag{3.17}$$

for all $\mathbf{u}, \mathbf{w} \in U$ and l is the following antilinear form

$$\begin{aligned} l(\mathbf{w}) = &-j\omega\mu_0\left(J_{ez}, w_z\right)_{0,\Omega} - \left(\frac{\zeta_1}{\mu_r}\,\hat{\mathbf{z}} \times \mathbf{J}_{mt}, \mathrm{grad}_{2D}w_z\right)_{0,\Omega} - j\omega\mu_0\left(f_{Rz}, \gamma_0 w_z\right)_{0,\Gamma} + \\ &- \left(\frac{1}{\mu_r}J_{mz}, \mathrm{curl}_{2D}\mathbf{w}_t\right)_{0,\Omega} - j\omega\mu_0\left(\mathbf{J}_{et}, \mathbf{w}_t\right)_{0,\Omega} + j\frac{\omega}{c_0}\left(\frac{\zeta_2}{\mu_r}\,\hat{\mathbf{z}} \times \mathbf{J}_{mt}, \mathbf{w}_t\right)_{0,\Omega} + \\ &- j\omega\mu_0\left(f_{Rl}, \mathbf{w}_t \cdot \mathbf{l}\right)_{0,\Gamma} \end{aligned} \tag{3.18}$$

for all $\mathbf{w} \in U$.

The reader can notice that, whenever $\beta = 0$ everywhere in Ω (which implies $\zeta_2 = 0$ in Ω), the problem splits into two disjoint problems, one for the axial component E_z, the other for the transverse part $\mathbf{E}_t$. These two disjoint problems are the traditional, two-dimensional variational problems, formulated in terms of E_z or $\mathbf{E}_t$, in the presence of motionless isotropic media.

In [20] it was shown that under some non-restrictive hypotheses any electromagnetic problem of the class considered is well-posed. In particular, for any problem of interest we can find a unique solution $(\mathbf{E}, \mathbf{B}, \mathbf{H}, \mathbf{D})$ belonging to $U \times (L^2(\Omega))^3 \times U \times (L^2(\Omega))^3$ and depending continuously on $\mathbf{J}_e, \mathbf{J}_m \in (L^2(\Omega))^3$ and on $f_{Rz}, f_{Rl} \in L^2(\Gamma)$. It is worth mentioning that, due to the bianisotropic behaviour of the media in motion, all unknown fields will have, in general, all three components, even if the scatterers are illuminated by simple fields.

3.3 Finite element approximation

Under some additional assumptions, in [20] we also found that a finite element method, based on the above variational formulation and exploiting a first-order Lagrangian approximation for the axial component and a first-order edge element approximation for the transverse part, determines $(\mathbf{E}_h, \mathbf{B}_h, \mathbf{H}_h, \mathbf{D}_h) \in U_h \times (L^2(\Omega))^3 \times (L^2(\Omega))^3 \times (L^2(\Omega))^3$ which converges, as h goes to zero, to $(\mathbf{E}, \mathbf{B}, \mathbf{H}, \mathbf{D})$ in $U \times (L^2(\Omega))^3 \times (L^2(\Omega))^3 \times (L^2(\Omega))^3$. In the previous statement U_h is the finite dimensional subspace of U generated by the indicated elements (first-order Lagrangian and first-order edge elements) for a specific triangulation of Ω and h denotes, as usual, the maximum diameter of all elements of the triangulation [39] (p. 131).

In [20] no specific considerations related to the implementation of finite element codes were provided. These considerations could be useful for our next developments and, for this reason, we present here the main points. Suppose that for any mesh adopted, fixing a given U_h, we order the degrees of freedom by placing those related to E_{hz}, $[e_z] \in \mathbb{C}^{nn}$, in the first part of the vector $[e] \in \mathbb{C}^{nn+ne}$ of the unknowns while those related to $\mathbf{E}_{ht}$, $[e_t] \in \mathbb{C}^{ne}$, are in its second and last part. In the previous formulas, nn (respectively, ne) refers to the number of nodes (respectively, edges) of the mesh considered. With this convention, by firstly considering the nn test functions like $\mathbf{w}_h = (0, 0, w_{hz})$ and, then, the ne test functions like $\mathbf{w}_h = \mathbf{w}_{ht}$, one can easily deduce that the general form of the final matrix equation obtained from (3.16), (3.17) and (3.18), with $\mathbf{E}$, $\mathbf{u}$, $\mathbf{w}$ and U replaced, respectively, by $\mathbf{E}_h$, $\mathbf{u}_h$ $\mathbf{w}_h$ and U_h, is

$$[A][e] = [l], \tag{3.19}$$

where the entries of $[l] \in \mathbb{C}^{nn+ne}$ are given by $l(\mathbf{w}_h)$, for all test functions considered. The order for its entries is given by the order considered for the test functions and, in analogy to the decomposition of $[e]$ in terms of $[e_z]$ and $[e_t]$, we get $[l_z] \in \mathbb{C}^{nn}$, in

the first part of $[l]$ and $[l_t] \in \mathbb{C}^{ne}$ in the second and last one. $[A]$ is given by

$$[A] = \begin{bmatrix} [A_{zz}] & [A_{zt}] \\ [A_{tz}] & [A_{tt}] \end{bmatrix}. \tag{3.20}$$

In this formula, $[A_{zz}]$, $[A_{zt}]$, $[A_{tz}]$ and $[A_{tt}]$ are complex matrices whose entries are deduced directly from (3.17)

$$\begin{aligned}[A_{zz}]_{ij} = &\left(\frac{\zeta_1}{\mu_r}\operatorname{grad}_{2D} w_{hzj}, \operatorname{grad}_{2D} w_{hzi}\right)_{0,\Omega} - \frac{\omega^2}{c_0^2}\left(\varepsilon_r\, w_{hzj}, w_{hzi}\right)_{0,\Omega} + \\ &+ j\omega\mu_0 \left(Y\left(\gamma_0 w_{hzj}\right), \gamma_0 w_{hzi}\right)_{0,\Gamma}, \quad i,j \in 1,\ldots,nn, \end{aligned} \tag{3.21}$$

$$\begin{aligned}[A_{zt}]_{ij} = &\, j\frac{\omega}{c_0}\left(\frac{\zeta_2}{\mu_r}\,\mathbf{w}_{htj}, \operatorname{grad}_{2D} w_{hzi}\right)_{0,\Omega}, \\ &i \in 1,\ldots,nn, \quad j \in 1,\ldots,ne, \end{aligned} \tag{3.22}$$

$$\begin{aligned}[A_{tz}]_{ij} = &-j\frac{\omega}{c_0}\left(\frac{\zeta_2}{\mu_r}\operatorname{grad}_{2D} w_{hzj}, \mathbf{w}_{hti}\right)_{0,\Omega}, \\ &i \in 1,\ldots,ne, \quad j \in 1,\ldots,nn, \end{aligned} \tag{3.23}$$

$$\begin{aligned}[A_{tt}]_{ij} = &\left(\frac{1}{\mu_r}\operatorname{curl}_{2D}\mathbf{u}_{htj}, \operatorname{curl}_{2D}\mathbf{w}_{hti}\right)_{0,\Omega} - \frac{\omega^2}{c_0^2}\left(\frac{1+\varepsilon_r\mu_r-\zeta_1}{\mu_r}\,\mathbf{w}_{htj}, \mathbf{w}_{hti}\right)_{0,\Omega} + \\ &+ j\omega\mu_0\left(Y\left(\mathbf{w}_{htj}\cdot\mathbf{l}\right), \mathbf{w}_{hti}\cdot\mathbf{l}\right)_{0,\Gamma}, \quad i,j \in 1,\ldots,ne. \end{aligned} \tag{3.24}$$

In this case, too, whenever $\beta = 0$ everywhere in Ω, the two matrices $[A_{zt}]$ and $[A_{tz}]$ become trivial and the discrete problem splits into two disjoint parts: one for $[e_z]$, the other for $[e_t]$. These are the classical two-dimensional problems for TM and TE polarized fields, respectively, in the presence of motionless media.

It is important to note that the second and third addends in the right-hand side of (3.21) are independent of β. The same is true for the first and third addends in the right-hand side of (3.24). Taking account of (3.6) one easily deduces that, for small values of the maximum of β, $\zeta_2 \simeq \beta(\mu_r\varepsilon_r - 1)$ and all entries of $[A_{zt}]$ and $[A_{tz}]$ have magnitudes which are smaller or equal to numbers proportional to the maximum of β, under the same conditions. Finally, the addends of the right-hand sides of (3.21) and (3.24) which depend on β, again for small values of the maximum of $\beta|$, involve $\zeta_1 \simeq 1 + (1 - \mu_r\varepsilon_r)\beta^2$ and $1 + \varepsilon_r\mu_r - \zeta_1 \simeq \varepsilon_r\mu_r - (1 - \mu_r\varepsilon_r)\beta^2$. Thus, the considered

quantities are only slightly affected by the motion, if the maximum of β is small.

In order to solve the algebraic linear system (3.19) several algorithms can be adopted. Among these, we consider iterative solvers, which are very popular for the solution of linear systems arising in finite element simulations [33] (pp. 382, 383, 396-405), [30] (p. 334). The stopping criteria we adopt in all cases, which defines when the iterative solution has reached convergence, is "criterion 2" of [36] (p. 60). For the reader convenience we recall that this criterion requires at the beginning the calculation of the Euclidean norm $\|[l]\|$ of $[l]$. At iteration i the approximate solution $[e]_i$ determines an error $\|[A][e]_i - [l]\|$. The iterative process is stopped when the condition $\|[A][e]_i - [l]\| < \delta\|[l]\|$ is satisfied, where δ is the so-called residual. Usually, δ is a small value in the range $[10^{-12}, 10^{-9}]$ when double precision arithmetic is used [36] (pp. 58-60).

If we assume TM polarized plane wave as the incident wave, then as the maximum value of β goes to zero, the Euclidean norm of components of $[e_t]$ goes to zero where as that of components of $[e_z]$ goes to the non zero value in the motionless problem. Hence the loss of number of significant digits due to round-off errors become large for the transverse components. Since for low values of β, $|||[e_t]|||$ becomes proportional to β and $|||[e_z]|||$ remains almost constant, the ratio $\frac{|||[e_t]|||}{|||[e_z]|||}$ becomes proportional to β as well. We know that $\frac{||\Delta[e]||}{||[e]||} \leq K_A \Delta_{roundoff}$. Here $\Delta[e]$ is the error in the solution due to round-off, K_A the condition number of matrix $[A]$. $\Delta_{roundoff} = \left(\frac{||\Delta[A]||}{[A]||} + \frac{||\Delta[l]||}{||[l]||} + \delta\right)$, where $\Delta[A]$ and $\Delta[l]$ denote change in $[A]$ and $[l]$ due to round-off. Now assuming that the round-off errors are uniformly distributed across the elements of $[e]$, it is easy to deduce that $\frac{||\Delta[e_t]||}{|||[e_t]|||} \leq \frac{nn+ne}{ne} \frac{|||[e]|||}{|||[e_t]|||} K_A \Delta_{roundoff}$. At low values of β we can consider $|||[e]||| \approx |||[e_z]|||$ and that $\Delta_{roundoff} \approx \delta$. Thus we can write

$$\frac{||\Delta[e_t]||}{|||[e_t]|||} \leq \frac{nn+ne}{ne} \frac{|||[e_z]|||}{|||[e_t]|||} K_A \delta. \tag{3.25}$$

Thus it can be seen that the residual error on the transverse component can be magnified by a factor of $\frac{nn+ne}{ne} \frac{|||[e_z]|||}{|||[e_t]|||} K_A$ for small β values. If the maximum allowable error is δ_{max}, then it needs to be ensured that $\frac{nn+ne}{ne} \frac{|||[e_z]|||}{|||[e_t]|||} \leq \frac{\delta_{max}}{K_A \delta}$.

3.4 Definition of a test case and of the relevant errors

In order to deduce some results on the accuracy of finite element solutions in the presence of axially moving cylinders we need to consider simple problems which allow

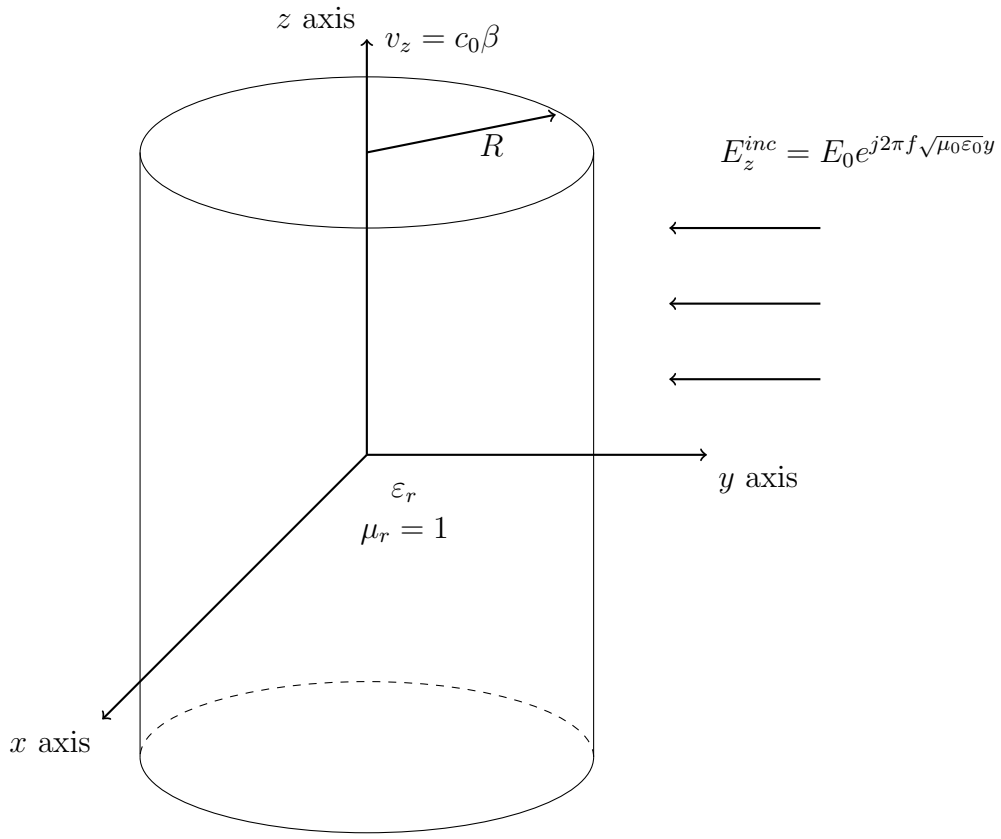

Figure 3.1: The configuration of axially moving homogeneous cylinder considered as test problem. The radius of the cylinder is R and the axial velocity is $v_z = c_0\beta$. The cylinder characterized by the permittivity ε_r and permeability $\mu_r = 1$. The incident field is impinging orthogonally on the cylinder.

the calculation of the fields of interest with other reliable tools. For this reason we consider single canonical cylinders moving in the axial direction. Analogous studies have been performed under the same type of simplifying assumptions related to the inhomogeneity of the media involved, the particular shapes of the scatterers or the illuminating field (see, for example, [30] (p. 188) or [42]). For this reason, we consider the case of a circular cylinder hosted in vacuum and illuminated by a uniform plane wave as indicated in Figure 3.1. In particular, the cylinder axis is assumed to be the z axis and the cylinder cross-section will have a radius $R \leq 0.2$ m. The medium inside the cylinder is assumed to be homogeneous and, in its rest frame, isotropic and not dispersive. It will be characterized by $\mu_r = 1$. We assume that such a medium is in uniform motion along the z axis. Finally, we will consider a TM-polarized incident plane wave impinging orthogonally on the cylinder and defined by $E_z^{inc} = E_0 e^{j2\pi f\sqrt{\mu_0\varepsilon_0}y}$, being the frequency always equal to 1 GHz except for one case when $f = 500$ MHz will be considered. The choice of the simple canonical problem just described was motivated not only by the possibility of finding semi-analytic solutions by using other tools, but also by the possible application of this study to the reconstruction of β profiles, as it will be explained later on. In the following we will consider several different values for the normalized axial speed β of the cylinder, for its relative permittivity ε_r (in its rest frame) and for its radius R.

For problems of this class an efficient semi-analytically procedure, able to compute very good approximations of their solutions was proposed by Yeh [3] (see also Remark 5 of [40]).

The scattering problems just defined are numerically studied by using a finite element simulator based on the considerations reported in the previous section. The domain of numerical investigation we have adopted is in any case a polygon approximating a circle in the (x, y) plane, whose center is at the origin and whose radius is equal to 0.4 m. Such a numerical domain is discretized by using several meshes. In particular, all these meshes are obtained by using n concentric circles and, starting from the center, the innermost circle is divided into 6 segments, the next one in 12 and so on. The domain is thus divided almost uniformly into $6n^2$ triangles, with $1 + 3n + 3n^2$ nodes, $3n + 9n^2$ edges and $6n$ boundary edges. An example of one mesh of this type is shown in Figure 3.2. In the following n will be equal to 20, 40, 80, 120, 160 or 200. Correspondingly, we will get a mesh characterized, respectively, by h equal to 0.0285874, 0.0143858, 0.00721629, 0.00481608, 0.00361402 or 0.00289216 m, with, respectively, 1261, 4921, 19441, 43561, 77281, 120601 nodes, 2400, 9600, 38400, 86400, 153600, 240000 elements, 3660, 14520, 57840, 129960, 230880, 360600 edges,

and 120, 240, 480, 720, 960, 1200 boundary edges. These details are summarized in Table 3.1. All the indicated values of n can be used to discretize scatterers whose radius R is a multiple of 2 cm (respectively, 1 cm if we avoid using $n = 20$).

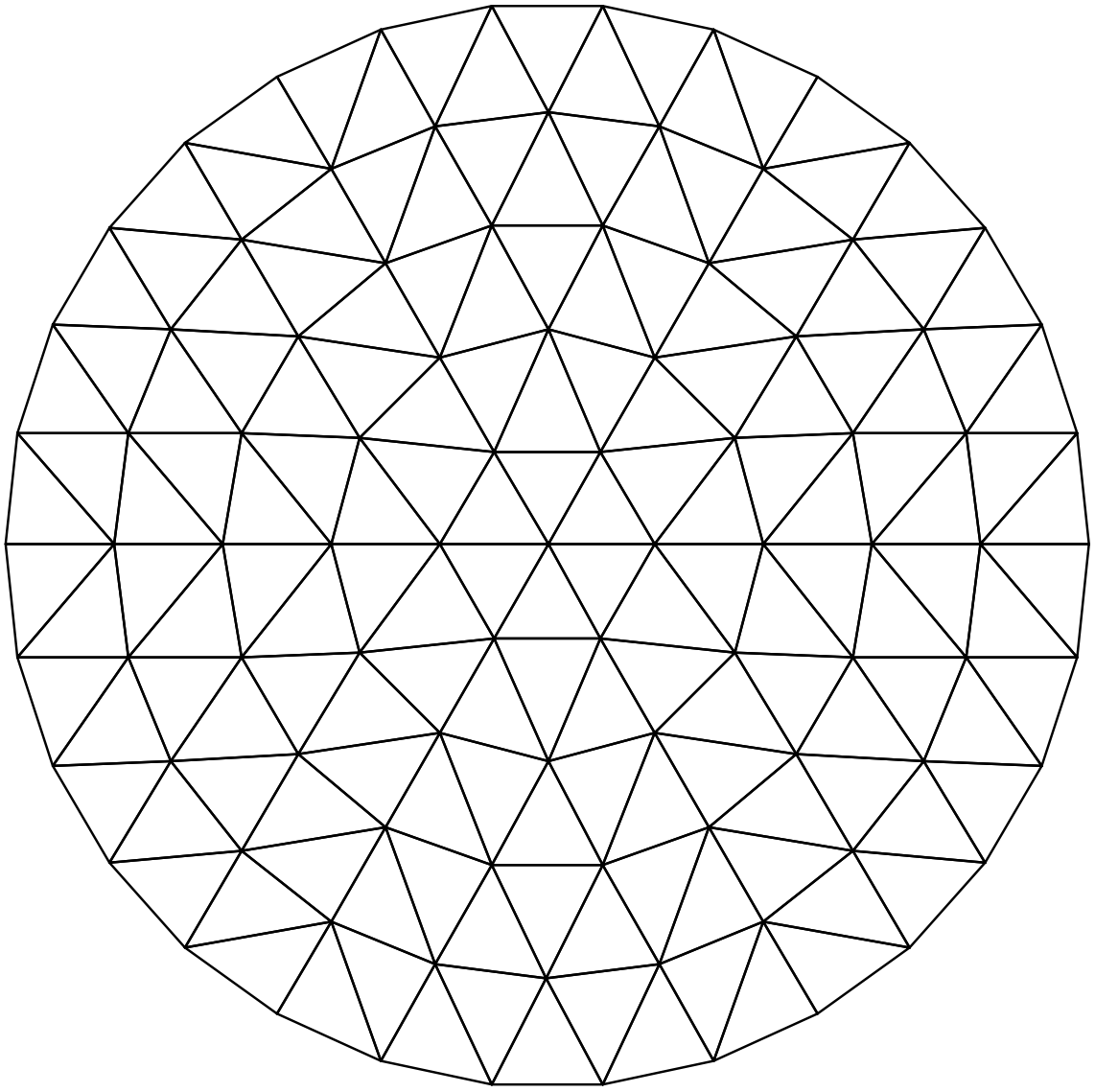

Figure 3.2: An example of discretization of the cylindrical numerical domain Ω obtained by using $n = 6$.

It is very important to point out that, in order to keep the analysis as simple as possible, we avoided considering meshes made up of curved triangles. This means, in particular, that, since the scatterer cross-section is not a polygon, in all our simulation we suffer from a kind of non-conformity [39] (p. 209). As a matter of fact, the scatterer has not the shape of the numerical scatterer and, moreover, the domain of numerical investigation and the numerical scatterer itself change their shapes for

n	h (m)	number of nodes	number of elements	number of edges	number of boundary edges
20	0.0285874	1261	2400	3660	120
40	0.0143858	4921	9600	14520	240
80	0.00721629	19441	38400	57840	480
120	0.00481608	43561	86400	129960	720
160	0.00361402	77281	153600	230880	960
200	0.00289216	120601	240000	360600	1200

Table 3.1: Details about meshes obtained for different values of n.

different values of n. By the same token, we adopted the semi-analytic procedure defined by Yeh [3] (the series are truncated after the first 60 terms for these calculations) to compute the piecewise constant data f_{Rzh} and f_{Rlh} enforcing the inhomogeneous terms in the admittance boundary conditions considered on Γ for the discretized problem (the admittance Y is set to $Y_0 = \sqrt{\frac{\varepsilon_0}{\mu_0}}$ in any case). In this way, we get another violation of conformity, according to [39] (p. 183). The reader should note that these violations of conformity were not considered in [20] and formally the convergence results we deduced there could not be applied. In the following, however, according to a well established approach, we neglect this technical problem and assume that our convergence results do apply to the cases considered. The numerical results we will show provide a heuristic proof of this statement.

An evaluation of the numerical errors of the finite element solutions could now be performed. However, we introduce an additional simplification which allows us to find good estimates of the errors by exploiting finite element calculations. In particular, we will call $E_{z,h,analytic}$ and $H_{z,h,analytic}$ the first-order Lagrangian element expansions which are deduced by evaluating their degrees of freedom with the semi-analytic procedure proposed by Yeh [3]. Analogously, $\mathbf{E}_{t,h,analytic}$ will refer to the first-order edge element expansion which is deduced by evaluating its degrees of freedom with Yeh's procedure. In the above three calculations the series involved in Yeh's procedure are truncated after the first 40 terms. The reader should observe that $H_{z,h,analytic}$ is not related to $\mathbf{E}_{t,h,analytic}$ by the usual Maxwell's curl equation (while H_{hz} is, by definition, equal to $-\frac{1}{j\omega\mu_0\mu_r}\mathrm{curl}_{2D}\mathbf{E}_{ht}$; see equation (3.3) and the considerations below Theorem 5.3 at the end of Section 5 of [20]). As a matter of fact, it is very well-known that the curl of a first-order edge element field is piecewise constant while $H_{z,h,analytic}$ is, as it has already been pointed out, a first-order Lagrangian element field. The decision to consider $H_{z,h,analytic}$ and $\mathbf{E}_{t,h,analytic}$ not related by the usual Maxwell's curl equation was made for the possible application of our results to inverse problem techniques

aiming at the reconstruction of β profile, as it will be further clarified later on.

The previous definitions allow us to introduce a set of (estimates of) absolute errors on E_z, $\mathbf{E}_t$ and H_z by using different relevant norms or seminorms. Thus we have

$$e_{z,a,l2} = \|E_{z,h,analytic} - E_{hz}\|_{0,\Omega}, \tag{3.26}$$

$$e_{z,a,h1} = \|E_{z,h,analytic} - E_{hz}\|_{1,\Omega}, \tag{3.27}$$

$$e_{z,a,semi} = \|\mathrm{grad}_{2D} E_{z,h,analytic} - \mathrm{grad}_{2D} E_{hz}\|_{0,\Omega}, \tag{3.28}$$

$$e_{t,a,l2} = \|\mathbf{E}_{t,h,analytic} - \mathbf{E}_{ht}\|_{0,\Omega}, \tag{3.29}$$

$$e_{t,a,\Gamma} = \|(\mathbf{E}_{t,h,analytic} - \mathbf{E}_{ht}) \cdot \mathbf{l}\|_{0,\Gamma}, \tag{3.30}$$

$$e_{a,hz} = \|H_{z,h,analytic} - H_{hz}\|_{0,\Omega}. \tag{3.31}$$

In the presence of a constant relative permeability $e_{a,hz}$ can be considered as an estimate of $\frac{1}{\omega\mu_0\mu_r} e_{t,a,semi}$, where

$$e_{t,a,semi} = \|\mathrm{curl}_{2D} \mathbf{E}_{t,h,analytic} - \mathrm{curl}_{2D} \mathbf{E}_{ht}\|_{0,\Omega}, \tag{3.32}$$

so that we can also consider

$$e_{t,a,u2d} = \sqrt{e_{t,a,l2}^2 + e_{t,a,\Gamma}^2 + e_{t,a,semi}^2} \tag{3.33}$$

as an estimate of the U_{2D} norm error.

Relative errors are important, too, especially for the problems of interest, due to the huge variation of some of the quantities involved. For this reason, we consider the following relative errors, $e_{z,r,l2}$, $e_{z,r,h1}$, $e_{z,r,semi}$, $e_{t,r,l2}$, $e_{t,r,\Gamma}$ and $e_{r,hz}$, which are defined by dividing the corresponding absolute error by the norm of the "analytic" part involved in the definition of the absolute error itself. Once more, under the indicated condition, $e_{r,hz}$ can be considered as an estimate of $e_{t,r,semi}$.

For the TM-polarized incident field considered, it is important to emphasize that, for a motionless cylinder, the solution presents $\mathbf{E}_t = 0$. Moreover, for small values of $|\beta|$ it is known that $\|\mathbf{E}_t\|_{U_{2D}}$ is small [8]. Thus, all relative errors related to the transverse part of the electric field (that is, $e_{t,r,l2}$, $e_{t,r,\Gamma}$, $e_{r,hz}$, $e_{t,r,semi}$) are expected to become larger and larger as $|\beta|$ goes to zero. At the same time, it could be important to analyze the behaviours of these errors, especially under the indicated conditions, because, on the one hand, good electromagnetic imagining techniques, able to recover the profile of the axial speed, exploits only, for the indicated incident

polarization, data related to $H_z = \frac{j}{\omega\mu_0}\text{curl}_{2D}\mathbf{E}_t$ [8]. On the other hand, the finite element method we are studying can be exploited to provide approximate values of H_z at the measurement points for any trial solution for the β profile considered by the inverse procedure itself [8].

For this reason, in the next section, a part of our numerical analysis will be devoted to considerations related to the reliability of finite element solutions in terms of H_z and, in particular, of $e_{a,hz}$ and $e_{r,hz}$. This part of the analysis was, actually, the initial motivation for this study.

Remark 1. *In many applications the reconstruction of the profiles of ε_r and β are of interest [7]. For the indicated polarization of the incident field, the axial component of the electric field is the most important quantity for the reconstruction of ε_r while the axial component of the magnetic field is crucial for the reconstruction of β [8]. In particular, under some non-restrictive hypotheses, the reconstruction of ε_r can be carried out neglecting any movement and by using data related to E_z only. The estimated ε_r is then adopted as an input data for the reconstruction of the axial speed profile. For the indicated reasons, a finite element code based on a formulation expressed in terms of $\mathbf{E}$ was considered. In our previous considerations we focused in particular on the generation of reliable data for the second step of the reconstruction process, devoted to the estimate of the β profile, simply because the reconstruction algorithms adopted for determining ε_r have been studied for decades [43] while those adopted to recover β are not so standard in the framework of microwave imaging techniques.*

Remark 2. *$e_{r,hz}$ could also be referred to a proper subdomain Ω_m of Ω. We could use e_{r,hz,Ω_m} as an alternative symbol in this case. The subdomain can also be of zero measure (e. g., made up of curves or points) because the involved quantities ($H_{z,h,analytic}$ and H_{hz}) are continuous in Ω. However, in this case we have to change the norm in the definition of the error (the $L^2(\Omega)$ norm is not meaningful anymore).*

The results provided in [20] can be applied to the problems here considered if some conditions involving ε_r and β are satisfied (see, in particular, Section 7 of [20]). In particular, in order to show some examples we can say that in the presence of a cylinder having $\varepsilon_r = 2$ the problem is well-posed and the convergence of finite element approximations is guaranteed (neglecting the conformity violations already pointed out) whenever $|\beta| \leq 0.264308$. For other cylinder media, for example when $\varepsilon_r = 1.1$ or $\varepsilon_r = 8$, the upper bounds for $|\beta|$ are 0.777053 or 0.0826784, respectively. The reader should notice that the corresponding upper bounds for the axial speed values are really impressive (equal to $\simeq$ 232954629 m/s when $\varepsilon_r = 1.1$, $\simeq$ 79237545

m/s when $\varepsilon_r = 2.0$ and $\simeq$ 24786361 m/s when $\varepsilon_r = 8.0$) and that they are not much smaller than the values of the speed of light in the media considered (given by $\frac{1}{\sqrt{1.1}} \simeq 0.953463$, $\frac{1}{\sqrt{2}} \simeq 0.707107$ and $\frac{1}{\sqrt{8}} = \frac{1}{2\sqrt{2}} \simeq 0.353355$, respectively).

3.5 Numerical results

As was already pointed out, for the defined test case we consider several values of ε_r, β, R and n. The effects of these parameters on the errors related to E_z, $\mathbf{E}_t$ and H_z are studied. In particular, the results related to E_z are shown in the first subsection while in the second one we provide considerations on the errors on $\mathbf{E}_t$ and H_z. From these two sub-sections we establish accuracy of the numerical simulations and the convergence behaviour of the components. In the third subsection, we provide the problematic cases where accuracy of the results related to $\mathbf{E}_t$ and H_z start dropping. This is due to the finite precision of the calculations which start to accumulate round-off errors when the bi-anisotropic effect is too weak to give significant cross-polarized component.

3.5.1 Numerical results related to E_z

The first results on E_z we show are all related to cases involving cylinders characterized by $\varepsilon_r = 2$ and $R = 0.2$ m. In particular, in Figure 3.3 we report the absolute errors related to the axial component of the electric field, $e_{z,a,h1}$, $e_{z,a,l2}$ and $e_{z,a,semi}$, versus h for two values of β: $\beta = 0$ and $\beta = 0.25$. As the reader can easily check, it is not possible to distinguish the results of the $\beta = 0$ case from those obtained when $\beta = 0.25$. Many other simulations have been performed, for $\beta = 5\ 10^{-m}$, $m = 1, \ldots, 15$. These additional results are not reported in Figure 3.3 because the plots would be the same as those already shown. In the figure two plots proportional to h and h^2 are provided, too, in order to be able to determine the rate of convergence of the results as functions of h.

As it was pointed out in Section 3.3 the results for the $\beta = 0$ case can be obtained by using a traditional two-dimensional finite element algorithm based on first-order Lagrangian elements (dealing with isotropic media at rest). There is nothing new in the results shown for this case, as it is very well-known [33]; we can simply observe that the absolute errors related to E_z behave like h^2 and that $e_{z,a,semi}$ is much larger than $e_{z,a,l2}$ so determining almost completely $e_{z,a,h1}$.

The results corresponding to $\beta = 0.25$ (determining a huge axial speed of 74948114.5

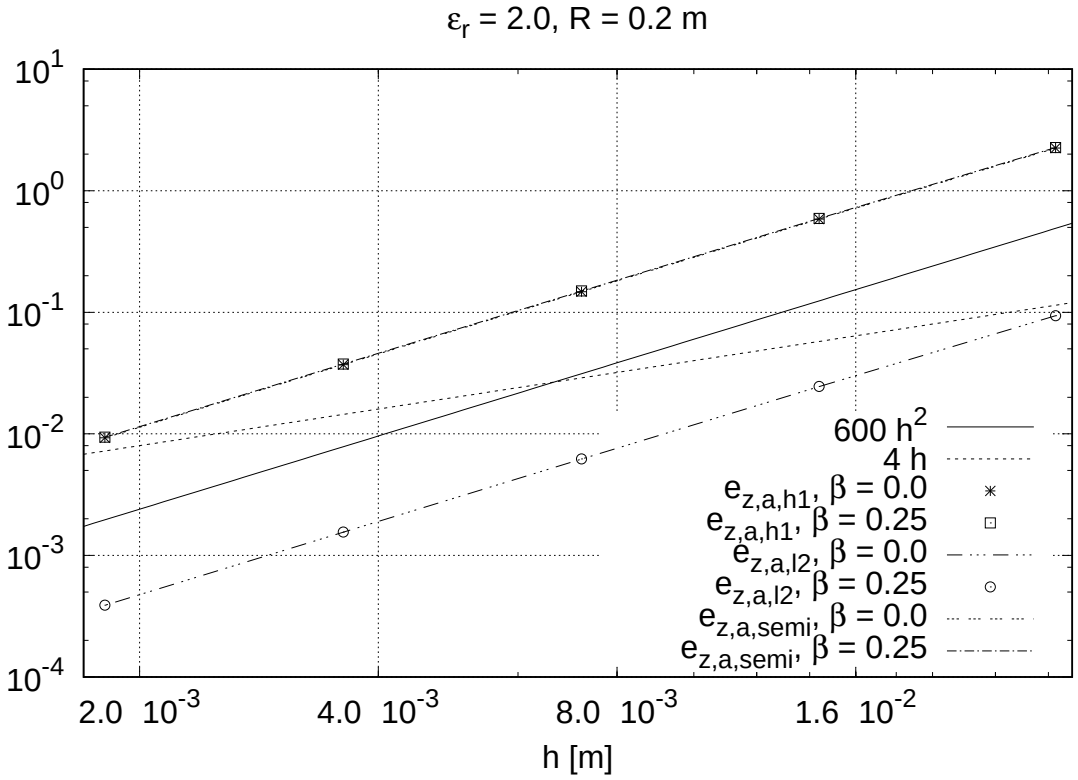

Figure 3.3: Behaviour of $e_{z,a,h1}$, $e_{z,a,l2}$ and $e_{z,a,semi}$ versus h, when the cylinder is at rest or moves with $\beta = 0.25$. The cylinder is assumed to have $R = 0.2$ m and to be made up of a material having $\varepsilon_r = 2$ at rest. Two plots proportional to h and h^2 are provided, too.

m/s) show that the finite element capability of approximating the axial component of the true solution is the same as in the case all media are at rest. In particular, the convergence rate remains quadratic and, taking account of all simulations performed, we can say that this property is completely independent of β. For the same reason, no figure related to the relative errors on E_z is provided.

It could be interesting to observe that $\beta = 0.25$ is close to the upper bound for β reported in Section 3.4 and has a significant effect on E_z. This can be seen in Figure 3.4 and 3.5. We observe that, for example, $Re(E_{hz}) = -0.0549$ V/m at the origin in the $\beta = 0$ case while $Re(E_{hz}) = -0.132$ V/m at the same point when $\beta = 0.25$. Both values are obtained by using a mesh with $n = 320$.

The previous considerations on the independence of the accuracy of the E_z results from the value of β seem to be correct even when the other parameters are changed. For example, if we consider $\varepsilon_r = 1.1$ or $\varepsilon_r = 8$ we get the relative errors shown in Figure 3.6. The reader can easily observe that the error behaviour in both cases does

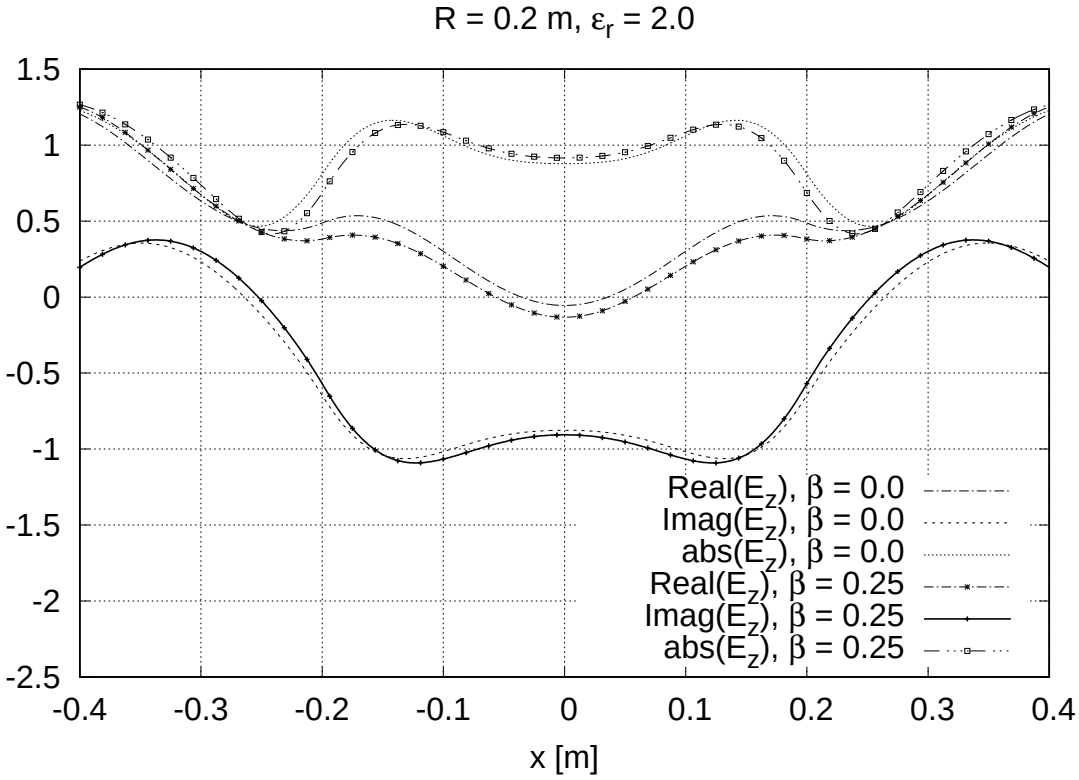

Figure 3.4: Values of E_{hz} along x axis for $\beta = 0$ and $\beta = 0.25$. Real, Imaginary and absolute values of E_{hz} are shown for both cases. The results were obtained for $\varepsilon_r = 2$, $R = 0.2$ m, $f = 1$ GHz and $n = 320$.

not depend on β and that the convergence rate remains $O(h^2)$. However, for any given mesh, the relative errors on E_z are larger for $\varepsilon_r = 8$ than for $\varepsilon_r = 1.1$, due to the reduction of the wavelength in the scatterer by a factor approximately equal to $2\sqrt{2}$. This effect is very well-known and does not require any additional comment [33], [30] (p. 344).

Changes on R are considered, too, but the conclusion for the errors on E_z remains unaltered. When $\varepsilon_r = 2$ and $R = 0.02$ m we get, by using a mesh with $n = 320$, $e_{z,r,h1} = 0.269\,10^{-3}$ if $\beta = 0$ and $e_{z,r,h1} = 0.270\,10^{-3}$ if $\beta = 0.25$. The corresponding quantities obtained when $\varepsilon_r = 2$ and $R = 0.2$ m (with the same mesh) are $e_{z,r,h1} = 0.557\,10^{-3}$ if $\beta = 0$ and $e_{z,r,h1} = 0.563\,10^{-3}$ if $\beta = 0.25$.

Overall we can say that the finite element approximation of E_z, in the presence of axially moving cylinders illuminated by TM-polarized incident plane waves, is as satisfactory as in the presence of motionless scatterers, independently of all values of the parameters considered.

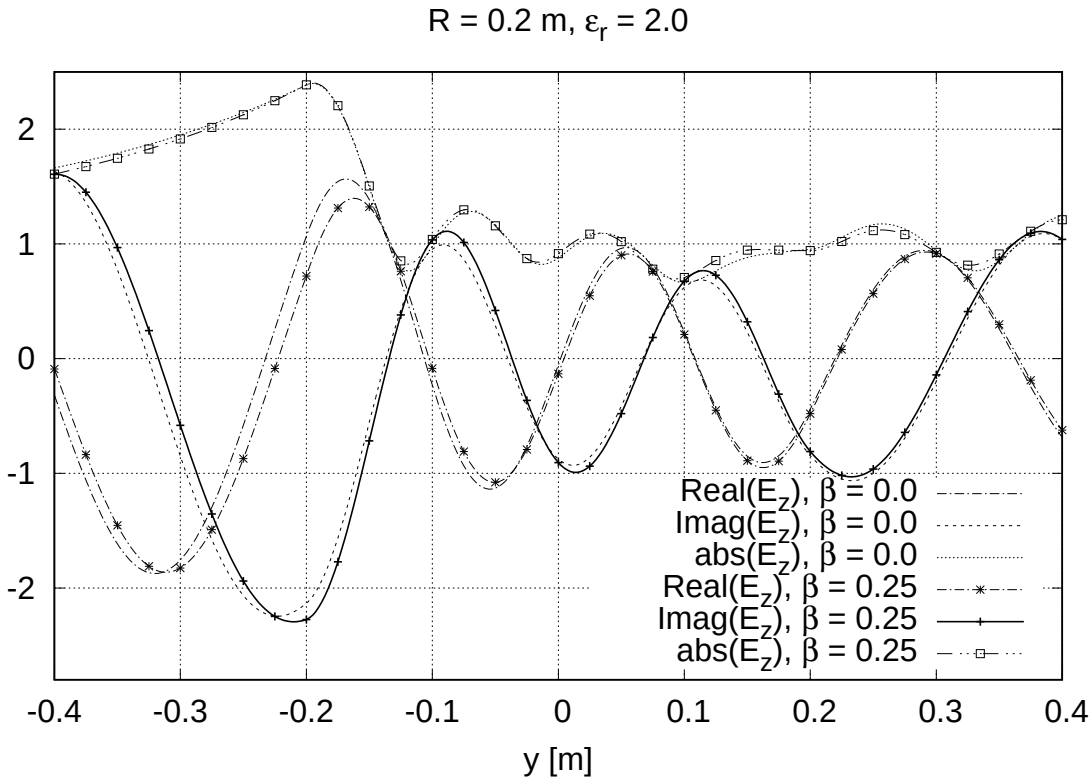

Figure 3.5: Values of E_{hz} along x axis for $\beta = 0$ and $\beta = 0.25$. Real, Imaginary and absolute values of E_{hz} are shown for both cases. The results were obtained for $\varepsilon_r = 2$, $R = 0.2$ m, $f = 1$ GHz and $n = 320$.

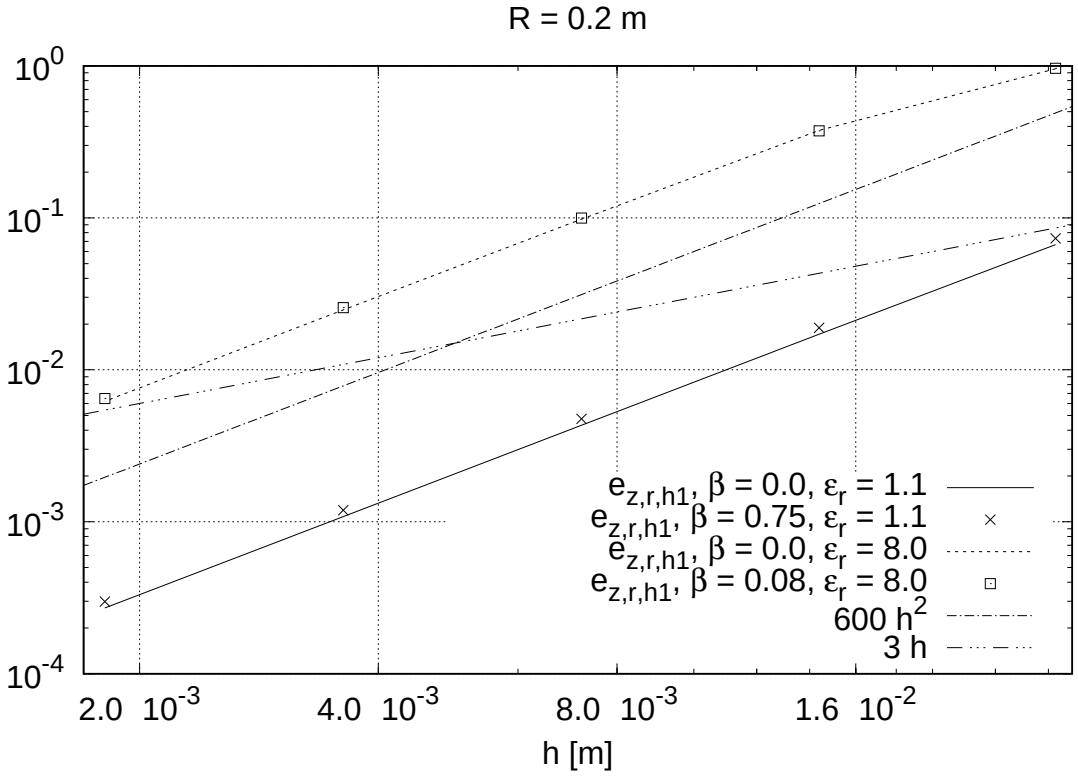

Figure 3.6: Behaviour of $e_{z,r,h1}$ versus h for different values of β and ε_r. In particular, for any value of ε_r one of the largest possible normalized axial speed values is considered in addition, for both cases, to $\beta = 0$. The scatterer radius is $R = 0.2$ m.

3.5.2 Numerical results related to $\mathbf{E}_t$ and H_z

In this sub-section we examine the errors related to the cross-polarized component $\mathbf{E}_t$ and the related magnetic field component H_z. These quantities are zero in the motionless case, and arises because of the bi-anisotropic effect due to motion. The convergence of these components are examined and the accuracy of the simulation is established for a large range of parameters like β, ε_r and R of the scatterer.

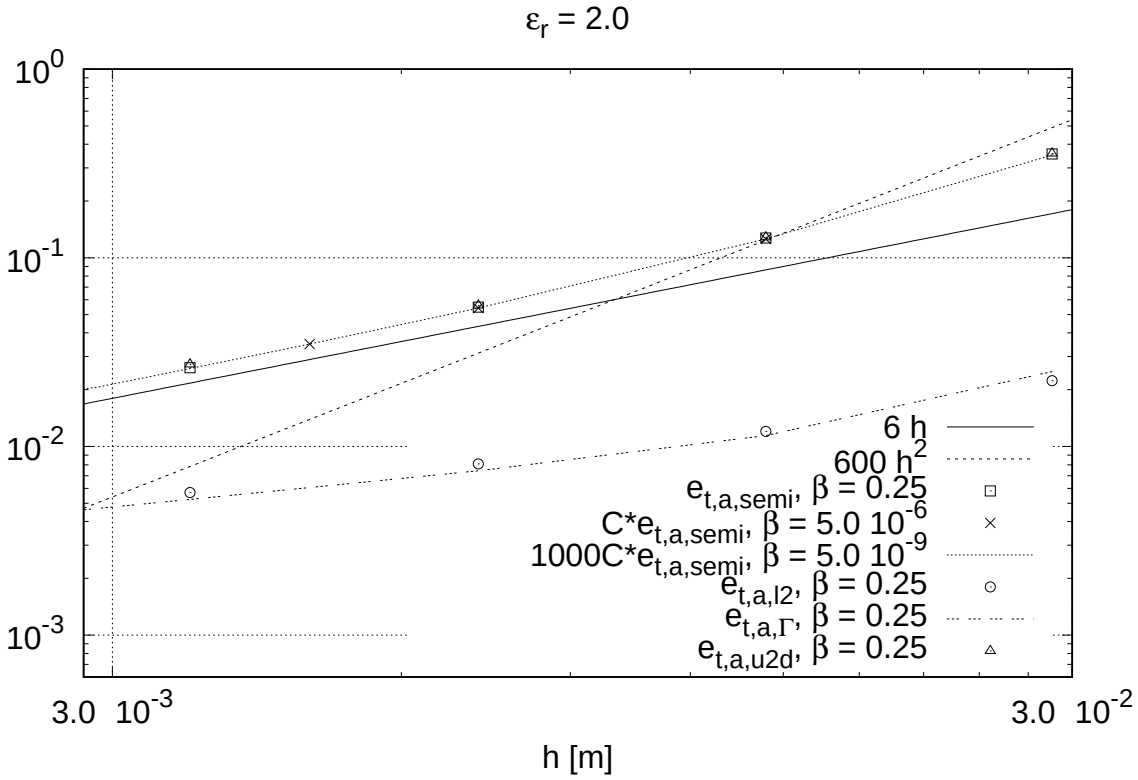

Figure 3.7: Behaviour of $e_{t,a,u2d}$, $e_{t,a,l2}$, $e_{t,a,\Gamma}$ and $e_{t,a,semi}$ versus h, when the cylinder moves with $\beta = 0.25$. Plots proportional to $e_{t,a,semi}$ is also reported for $\beta = 5\ 10^{-m}$, $m = 6, 9$. $C = 5\ 10^7$. The cylinder is assumed to have $R = 0.2$ m and to be made up of a material having $\varepsilon_r = 2$ at rest. Two plots proportional to h and h^2 are provided, too.

In Figure 3.7 some results related to the absolute errors on $\mathbf{E}_t$ are shown. The case $\beta = 0$ is not meaningful for the present analysis because, for the test case considered, the solution has $\mathbf{E}_t = 0$ in Ω and the finite element method is able to compute $\mathbf{E}_{ht} = 0$ in Ω for any mesh considered. For this reason the results refer to cases in which $\beta \neq 0$. A complete set of results is shown for $\beta = 0.25$. One can observe that $e_{t,a,semi}$ is much larger than $e_{t,a,l2}$ and $e_{t,a,\Gamma}$ so that $e_{t,a,u2d} \simeq e_{t,a,semi}$. Moreover, it can be observed that the convergence rate is $O(h)$ for all errors considered. The values of $e_{t,a,semi}$

for $m = 6$ and $m = 9$ are also shown in the figure. Over this large range of β, the convergence behaviour is not affected.

Now we verify what happens when the cylinder is made up of other materials. As in the previous subsection, we will consider $\varepsilon_r = 1.1$ and $\varepsilon_r = 8$ along with $\varepsilon_r = 2$. Figure 3.8 shows the relative error in H_z for these cases. The results are analogous to Figure 3.6 except for the slower rate of convergence. Again, an increase in ε_r results in increase in discretization error, due to the reduction in wavelength. The errors remain largely independent of β over a wide range, with β which could be as low as 5×10^{-9}.

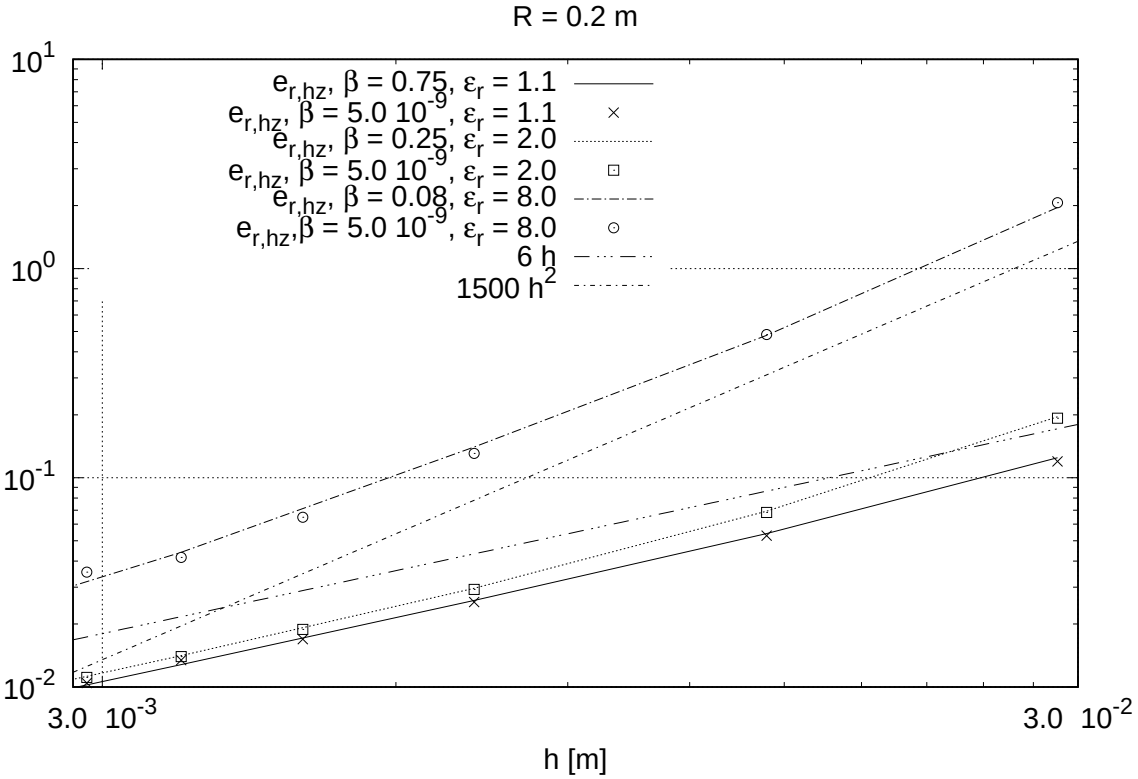

Figure 3.8: Behaviour of $e_{r,hz}$ versus h for different values of β and ε_r. In particular $\varepsilon_r = 1.1$, $\varepsilon_r = 2$ and $\varepsilon_r = 8$ are considered. In each case a value close to the upper bound of β is taken along with $\beta = 5\ 10^{-9}$. Two plots proportional to h and h^2 are provided, too.

Finally we study the effect of changing the radius of scatterer. Along with the $R = 0.2$ m considered for the previous instances, $R = 0.1$ m and $R = 0.05$ m were examined. It is not appropriate to consider too small values of R. This is because of the non-conformity due to polygonal approximation of the circular boundary of the scatterer, as was explained in section 3.4. Instead the frequency is reduced so

that the ratio of R to the wavelength reduces, which is expected to give an equivalent effect on discretization error. Hence we study $f = 500$ MHz in addition to $f = 1$ GHz considered in the preceding cases. The discretization error is not affected much by the reduction in radius of the scatter. With $n = 120$ and $f = 1$ MHz, for $\beta \leq 5\ 10^{-10}$ the relative errors remain 4% for all variations of R considered.As for the effect of reducing f, the discretization error drops below 2% which is expected from the increase in wavelength.

The results in this subsection and the last one show as expected [20], that the finite element approximation is converging to the true solution (notwithstanding the two violations of conformity pointed out in Section 3.4). However, the results related to $\mathbf{E}_t$ and H_z do start becoming worse due to round-off errors when the magnitude of these quantities become small. We consider such cases in the next section.

3.5.3 Problematic results related to $\mathbf{E}_t$ and H_z

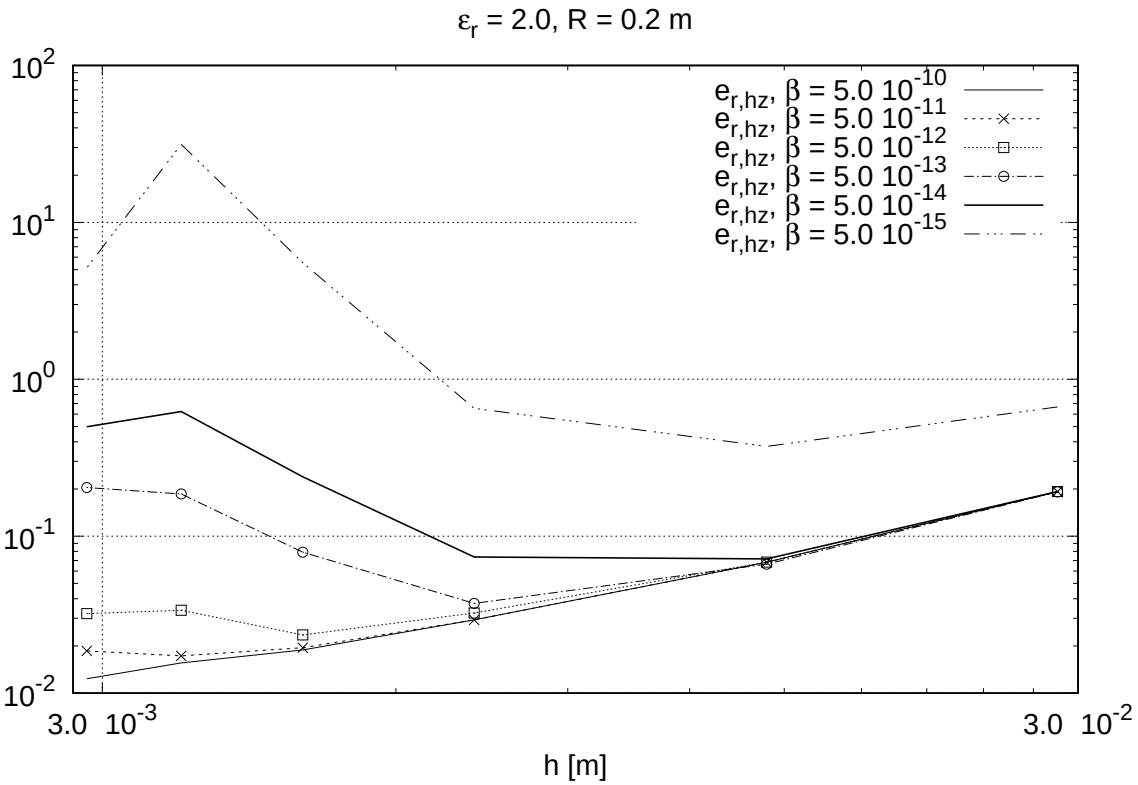

Figure 3.9: Behaviour of $e_{r,hz}$ versus h, when the cylinder moves with $\beta = 5\ 10^{-m}$, $m = 10, \ldots, 15$. The cylinder is assumed to have $R = 0.2$ m and to be made up of a material having $\varepsilon_r = 2$ at rest..

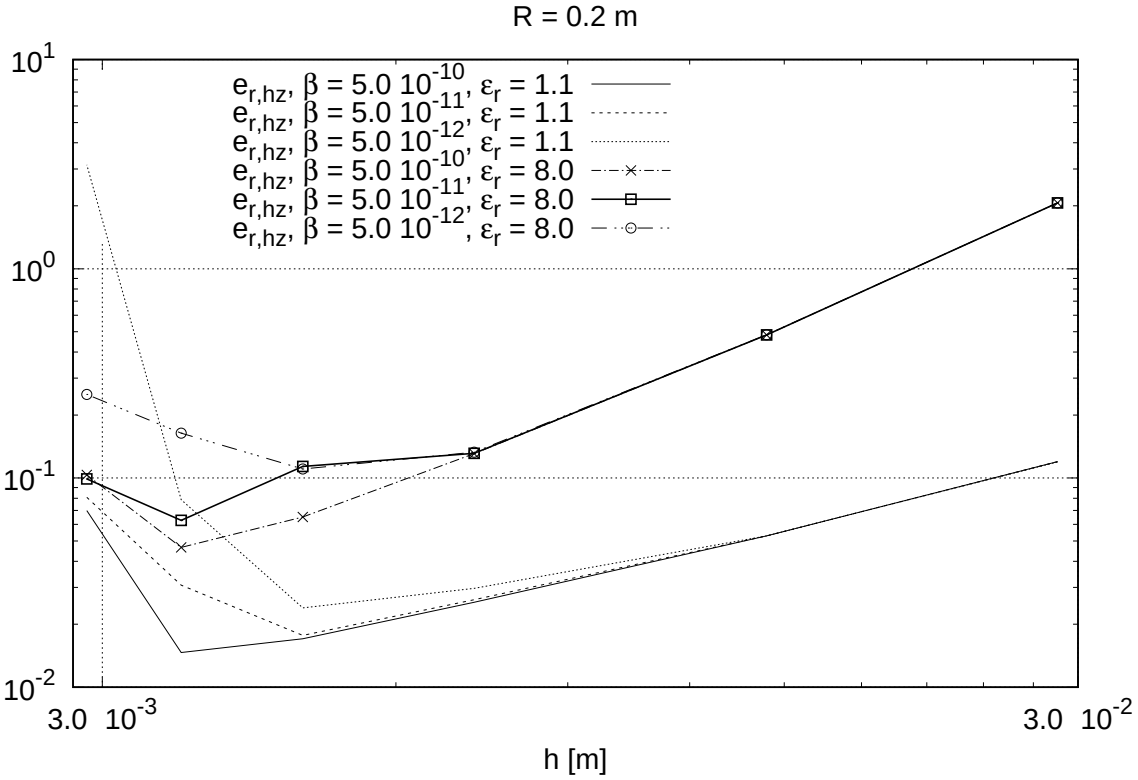

Figure 3.10: Behaviour of $e_{r,hz}$ versus h for different values of β and ε_r. We consider $\varepsilon_r = 1.1$ and $\varepsilon_r = 8.0$ with $\beta = 5\ 10^{-m}$ and $m = 10, 11, 12$.

In this subsection, we consider the cases when the round-off error becomes significant. As indicated by equation (3.25), when the cross-polarized component becomes too low, the round-off error becomes more and more significant. Although we get good accuracy for the co-polarized component, the cross-polarized component could be unreliable. This could be the case with very low values of β, ε_r or R. Hence, in these critical cases, one needs to be careful with the simulations.

In Figure 3.9 the relative errors pertaining to H_z are shown with respect to h for small β values with $m = 10 \ldots 15$. For sufficiently small values of h, although the errors remain less than 10% up to $m = 12$, they start increasing for finer discretization. The results become completely unreliable for smaller values of β. A finer discretization need not produce a decrease in the error in these critical cases, since the increase of round-off error is dominating over the reduction in discretization error. These results suggest that one should be careful in dealing with these delicate cases. One may have to make use of higher precision calculations to accurately solve these problems.

In Figure 3.10 we examine the effect of different permittivity values along with small β. Again $\varepsilon_r = 1.1$ and $\varepsilon_r = 8.0$ are taken and we consider $m = 10, 11, 12$. The

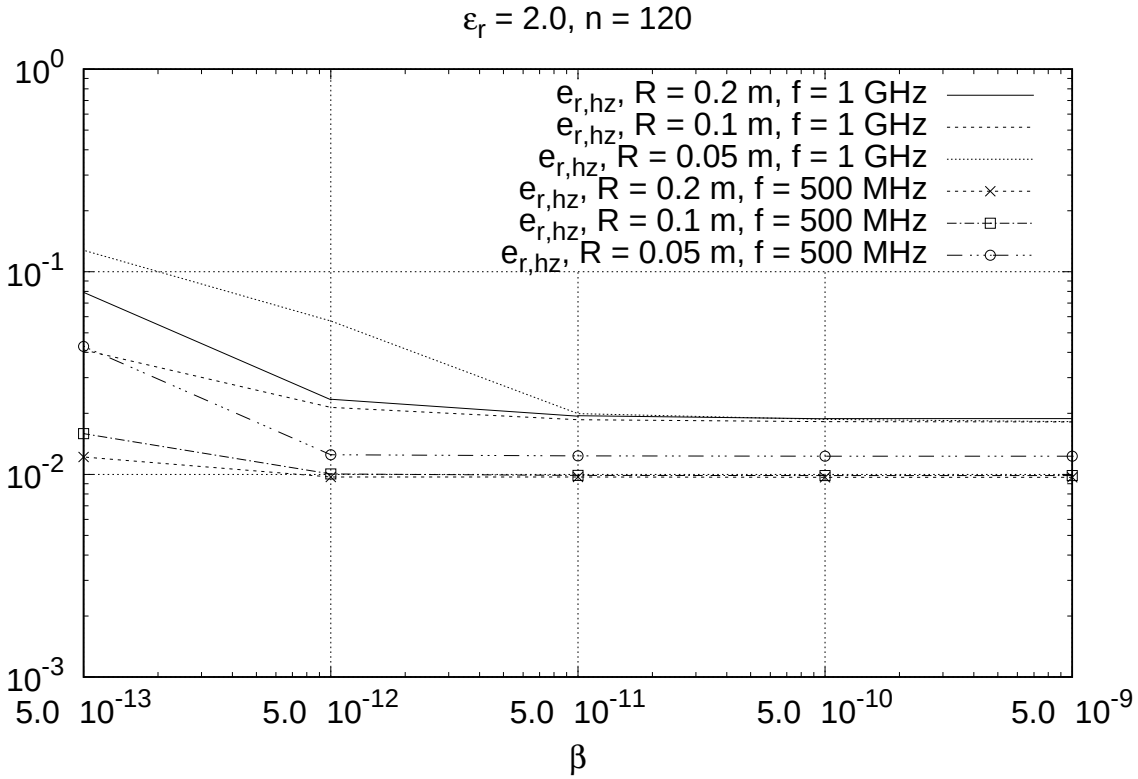

Figure 3.11: Behaviour of $e_{r,hz}$ versus β for different values of the scatterer radius R and of the frequency f. The values of β which are particularly critical for $e_{r,hz}$ are considered. The cylinder is assumed to be made up of a material having $\varepsilon_r = 2$ at rest. The numerical solutions are computed by using a mesh with $n = 120$.

trend remains similar to that for $\varepsilon_r = 2.0$ in Figure 3.9. For $\varepsilon_r = 8.0$, the errors start off large, due to higher discretization error, and goes on becoming worse due to round-off. For $\varepsilon_r = 1.1$, the discretization error is smaller than that for $\varepsilon_r = 2.0$. But once the round-off error becomes significant it can increase very quickly.

In Figure 3.11 the relative error on H_z is plotted against β values. Three different values are considered for the radius of scatterer, $R = 0.2$, $R = 0.1$ and $R = 0.05$ meters. The calculations are done for two frequency values $f = 1$ GHz and $f = 500$ MHz. The bi-anisotropic effect reduces as the scatterer becomes smaller, which might result in a higher round-off error. This could explain why the error starts increasing at $m = 11$ in the case of $f = 1$ GHz where as for all other case the error is stable till $m = 12$.

We can infer that these results are within the bounds of expected round-off errors and is in accordance with the equation (3.25). In order to do this we can calculate the expected maximum error bounds and confirm that the obtained results are within

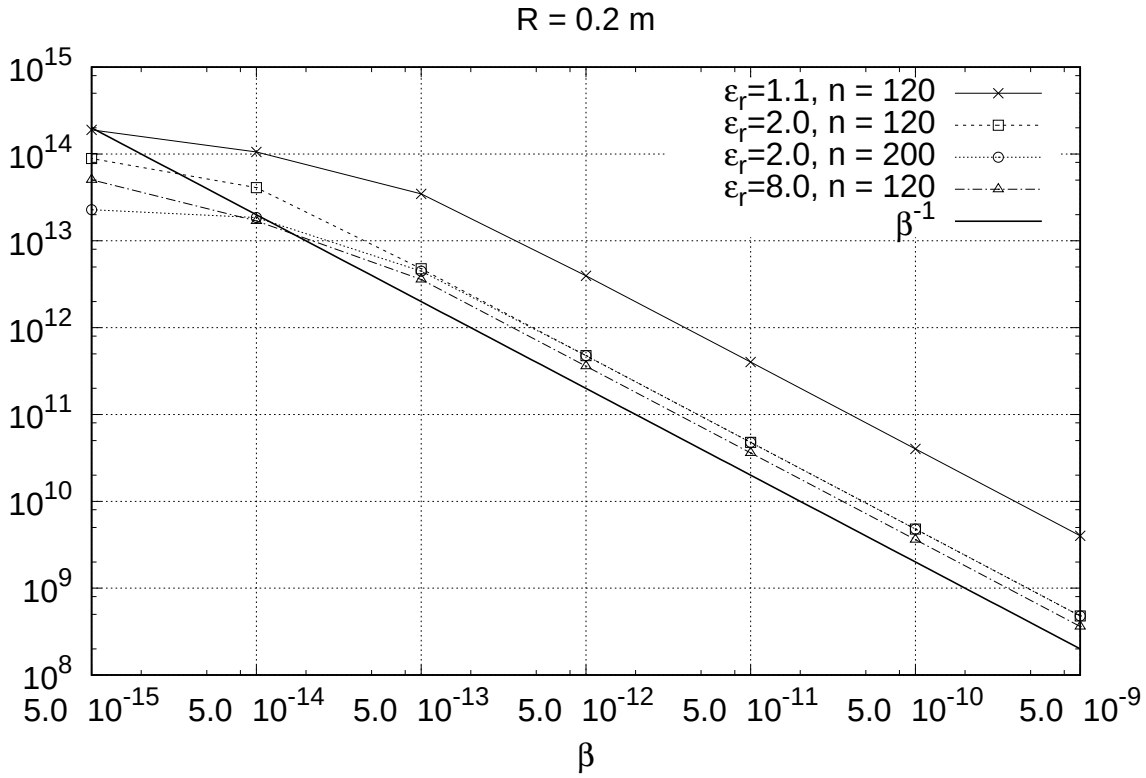

Figure 3.12: Values of $\frac{nn+ne}{ne}\frac{|||[e_z]|||}{|||[e_t]|||}$ versus β for different values of ε_r and n. We consider $n = 120$ with $\varepsilon_r = 1.1$,$\varepsilon_r = 2$ and $\varepsilon_r = 8$. In addition the value corresponding to $n = 200$ with $\varepsilon_r = 2$ is also shown. A plot of β^{-1} provided too.

the predicted limits. This estimate was carried out for the small values of β, below which we start getting less accurate solutions.

It is quite easy to calculate the factor $\frac{nn+ne}{ne}\frac{|||[e_z]|||}{|||[e_t]|||}$ from the algebraic solution obtained from the finite element simulator. In Figure 3.12 we plot the values of $\frac{nn+ne}{ne}\frac{|||[e_z]|||}{|||[e_t]|||}$ versus β for different discretization and permittivity values. As long as the computation of $[e_t]$ is reasonably accurate, the value of $\frac{nn+ne}{ne}\frac{|||[e_z]|||}{|||[e_t]|||}$ is as expected proportional to β^{-1}. For the problem considered here the constant of proportionality is close to 2 in case of $\varepsilon_r = 8$ and $\varepsilon_r = 2$ and close to 20 for $\varepsilon_r = 1.1$. Thus the margin for error steadily decreases in accordance with equation (3.25) as β decreases below $5\ 10^{-9}$ which corroborates the observed results.

The condition number can be more difficult to calculate for a general problem as it might be difficult to get a good estimate in general. It may be required to calculate the eigen values of the algebraic system in order to obtain . For the present problem, we had to solve for the largest and smallest eigen values and take the ratio to get the value of K_A. In figure 3.13 we show the condition number K_A for different

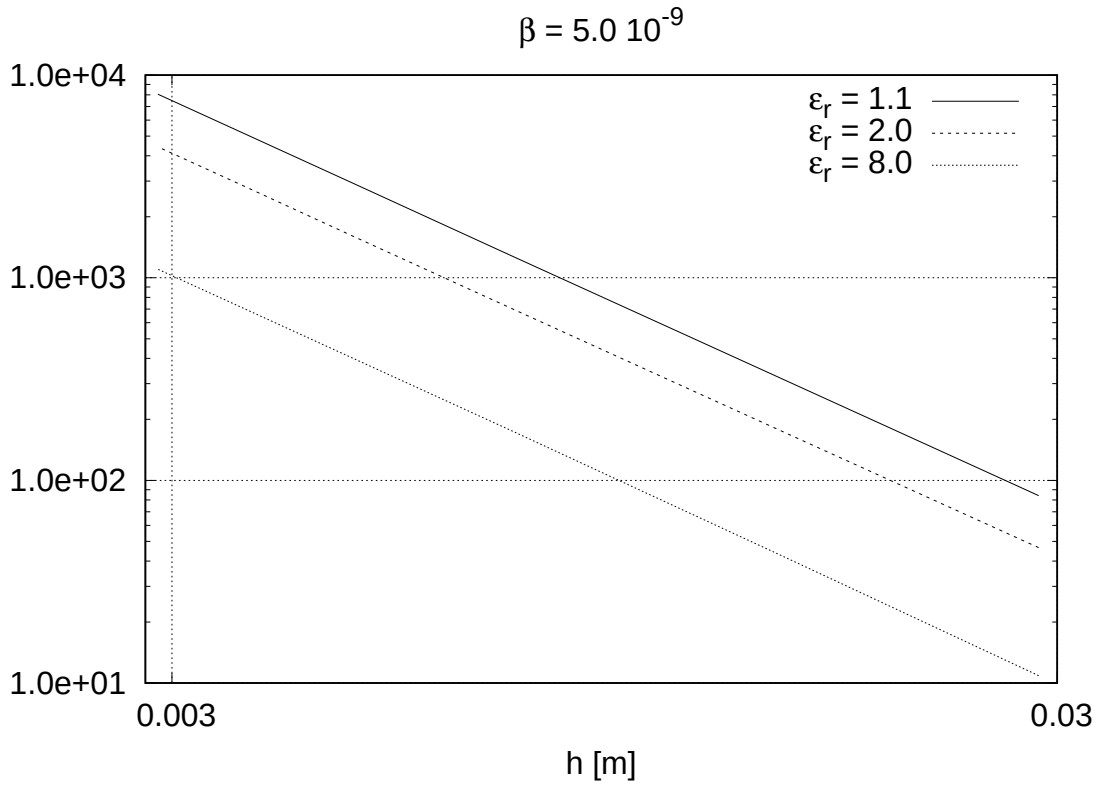

Figure 3.13: Values of condition number K_A versus h with $\beta = 5 \times 10^{-9}$ and for different values of ε_r. The results are shown for $\varepsilon_r = 1.1, 2, 8$ and for $n = 20, 40, 80, 120, 160, 200$.

discretizations for $\beta = 5 \times 10^{-9}$. The condition number is independent of β for small angular velocities. For ε_r we considered the values 1.1, 2 and 8. The condition number is seen to be increasing as the discretization gets finer. Also the value is higher for lower ε_r. The order of magnitude in this case is varying from 10^{-2} to 10^4, resulting in possible loss of two to four significant digits in the solution.

This shows that the round-off error tends to increase for smaller velocities, for finer discretizations and for weaker scatterers. Next we can try to put two results above to get an estimate of the maximum round-off error expected. We took the value of δ in equation (3.25) to be 10^{-15}.

Figure 3.14 confirms what was discussed above. The estimate of maximum relative error of cross-polarized component is plotted against β values less than 10^{-9}. Again the results are shown for $\varepsilon_r = 1.1, 2.0, 8.0$ for $n = 120$. In addition a plot is also given for $n = 200$, $\varepsilon_r = 2.0$. In particular we can see that for all the previous results obtained the relative errors are within the bounds that is obtained here. The error must be less than 10% for values of β less than 10^{-9} which agrees with what we

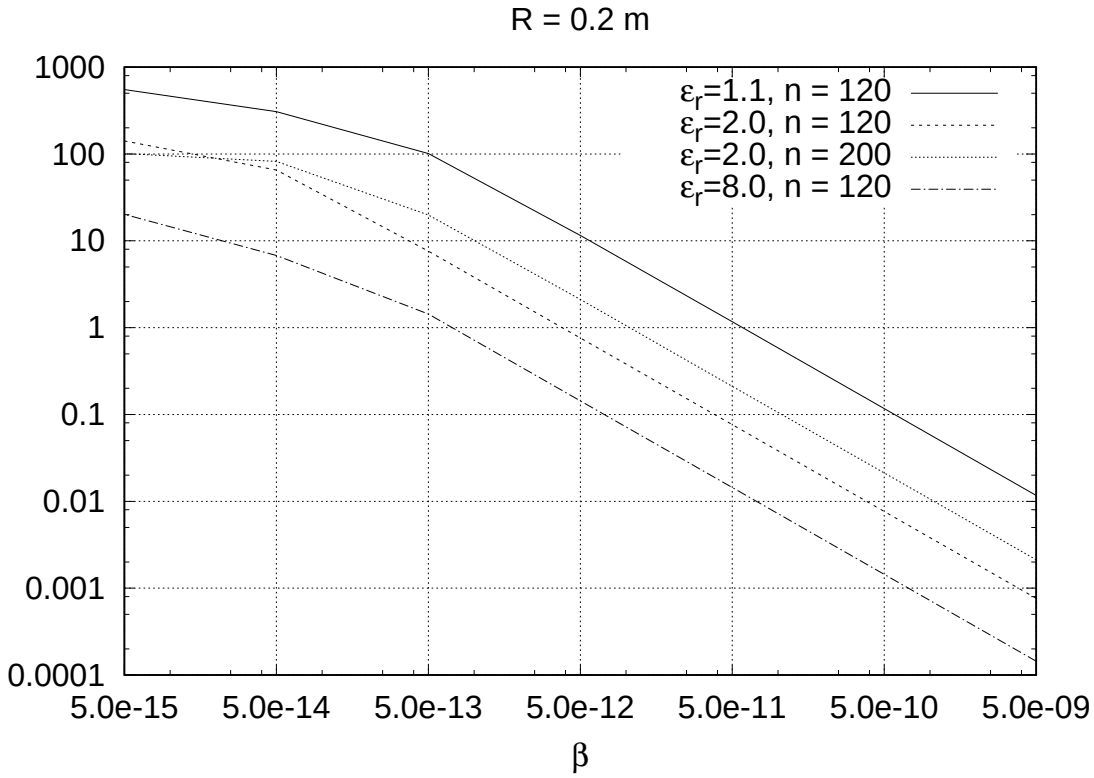

Figure 3.14: The estimate of maximum relative error due to round-off in the transverse component of the field ($\frac{||\Delta[e_t]||}{|||[e_t]|||}$) calculated according to equation (3.25), considering $\delta = 10^{-15}$. It is plotted against β, for $\varepsilon_r = 1.1, 2, 8$ with $n = 120$. One plot for $n = 200$ is also given corresponding to $\varepsilon_r = 2$.

obtained earlier.

The results in this subsection suggests that one must be careful with simulations involving weak bianisotropic effects. One needs to keep in mind the possible corruption of the results due to round-off errors. It may be required to use higher precision calculations to get reliable results in such instances. If one has a good estimate of the condition number then it is possible to gauge the reliability of the result in terms of round-off error as indicated by equation (3.25). However, the results that are obtained for the test case considered here reassures that one can obtain reliable solutions for a very wide span of parameters.

3.6 Issues related to numerical solution procedure

As it was already pointed out, iterative methods are very often exploited to compute the solution of the algebraic linear systems determined by electromagnetic finite

element codes [33] (pp. 382, 383, 396-405). In particular, the BiCG (biconjugate gradient method) [33] (pp. 396-405) is known to be particularly efficient for time-harmonic electromagnetic problems [44] (p. 308) involving only traditional media. However we observed that in our case, this method fails to converge for values of β which are not very small. This is because the structure of the matrix $[A]$ is altered, since its submatrices $[A_{zt}]$ and $[A_{tz}]$ become more significant for higher β values. We may use some alternative iterative methods in such case [36], [**?**]. In particular, CGNE (Conjugate gradient on normal equation) is a simple alternative. However, the condition number is squared in this case resulting in slower convergence and worse round-off errors. Use of preconditioner can help improve the condition number of the system both when BiCG and CGNE are used. Simple Jacobi preconditioner was used for this purpose in the present work and the corresponding methods are denoted as BiCGJP and CGNEJP.

All the results shown in Section 3.5 were calculated by using BiCG, BiCGJP, CGNE or CGNEJP. We give a brief discussion of their performance here. If the algebraic linear system to be solved is $[A][e] = [l]$, as reported in Section 3.3, we initially calculate the euclidean norm $\|[l]\|$ of $[l]$ and do not stop the iterative solver until the approximate solution $[e]_i$ at iteration i satisfies $\|[A][e]_i - [l]\| < \delta\|[l]\|$, with δ always equal to 10^{-p}, $p \in \{10, \ldots, 16\}$. One should avoid using larger values of p when double-precision arithmetic is used [36] (p. 58). In order to avoid presenting unreliable results we computed them at least twice, for two consecutive values of p. When the outcomes were different we considered the next larger value of p and did not stop this process until, for two consecutive values of p, we got the same result (with a tolerance equal to 0.1 %).

Independently of the reliability of the outcome, we find that the BiCGJP is able to compute the solutions for all values of β and p considered and all $n \leq 80$. For finer meshes the convergence of biconjugate iterative solvers is not guaranteed anymore. Consider, for example, some data for the test cases with $\varepsilon_r = 2$, $R = 0.2$ m and $f = 1$ GHz. When $n = 120$, BiCGJP does not converge for $\beta \geq 5\ 10^{-5}$ (for this specific example the smallest residual value seems to be $\simeq 0.26$ which is by far too large to stop the iterations). BiCG fails to converge, with the same n, for $\beta \geq 5\ 10^{-3}$ (the smallest residual value is $\simeq 0.026$). For a mesh obtained by using $n = 160$ BiCG (respectively, BiCGJP) does not converge for $\beta \geq 5\ 10^{-7}$ (respectively, $\beta \geq 5\ 10^{-5}$). When $\beta = 5\ 10^{-7}$ the smallest residual value is $\simeq 3.2\ 10^{-7}$ (respectively, $\simeq 0.28$ for $\beta = 5\ 10^{-5}$). For the same mesh, by using $p = 13$, BiCGJP converges in 20214 steps (with the indicated mesh we have 308161 unknowns) for $\beta = 5\ 10^{-7}$ and in 242643

steps for $\beta = 5\ 10^{-6}$. Finally, when $n = 200$ we have 481201 unknowns and BiCGJP and BiCG fail to converge for $\beta \geq 5\ 10^{-7}$, reaching a minimum residual value, for $\beta = 5\ 10^{-7}$, of $0.45\ 10^{-5}$ and, respectively, 0.5. For this mesh, BiCGJP converges in 22956, 20001, 17834 and 13415 steps for $\beta = 5\ 10^{-m}$, with m respectively equal to $8, 9, 10, 11$ for $p = 15$. It is also interesting to point out that it converges in 3556 steps for $\beta = 0$ (and $p = 15$ as before).

From the previous considerations, one can also understand that most of our results were calculated by using CGNE or CGNEJP. The convergence of this type of algebraic solver, however, is by far too slow, independently of the use of the preconditioner. Even though this is not a surprise [44] (p. 308), [36] (p. 18), it is instructive to report some data. For example, CGNE, for $p = 15$ and $n = 200$, requires 536957 steps to converge for $\beta = 5\ 10^{-6}$ and 710410 steps for $\beta = 0.25$ ($\varepsilon_r = 2$, $R = 0.2$ m, $f = 1$ GHz). The results are not much better when the point Jacobi preconditioner is used. For example, with the usual values of ε_r, R and f, for $n = 120$ and $\beta = 0.25$ CGNEJP converges in 220942 steps (173521 unknowns) while CGNE does the same requiring 233866 steps ($p = 13$ in both cases). In terms of CPU time the difference is even lower (equal, more or less, to 4% on the same computer).

Thus for small values of β BiCG and BiCGJP are suitable for giving fast convergence and lower round-off errors compared to CGNE and CGNEJP. The method breaks down for larger values of β and we can use CGNE or CGNEJP which converge but at a much slower rate.

3.7 Conclusions

The accuracy of finite element results in the presence of axially moving cylinders is analyzed for the first time, to the best of authors' knowledge. The study refers to relative and absolute errors related to two components of the electromagnetic field. The part of the results presented concerning one of the two components is new but the outcome is analogous to the one which is obtained when all media involved are motionless. The second part is related to the field component which is specifically excited by the presence of moving objects. This field component is the most difficult to be approximated. For its information content related to the motion of the objects, it could also be the most important component to be evaluated, at least for some applications.

This study has shown that finite element simulators based on double precision arithmetic could guarantee and extraordinary reliability of all their outcomes. These

performances suggest that the indicated simulators can be exploited and could become the reference method for astrophysics, engineering and medical applications involving media in motion.

Chapter 4

Reliability of Finite Element Simulators for Three Dimensional Problems Involving Rotating axisymmetric Objects and Other Bianisotropic Materials

4.1 Introduction

We have already seen that media in motion are involved in several important electromagnetic problems [1]. In most of these applications the solutions have to be found by using the natural space-time framework defined by the theory of relativity [38], [1]. However, in some cases the movement takes place in such a way that it is still possible to work in the frequency domain [1], [14], for example in the presence of moving media with stationary boundaries [1], [14].

Two classes of particularly interesting problems of this type can be found. The first one is related to problems involving axially moving cylinders. These kind of problems were considered in the previous chapter. In the second class we find problems involving rotating axisymmetric objects. The applications of these problems range from the reconstruction of the dielectric and velocity profiles in pneumatic pipes [7] to the measurement of the rotational speed of celestial bodies [11].

For particular problems, involving single moving objects having simple geometries, it is possible to find series solutions [3], [4], [40], [11], [22]. However, in most cases

of practical interest involving multiple and irregular objects in motion, in order to approximate the solution one has to refer to numerical methods [37], [45].

In the last decades several numerical techniques have been developed to solve time-harmonic electromagnetic boundary value problems [46], [33]. In particular, for problems in which all media are at rest one can find several results on the reliability of numerical methods. This is particularly true for the finite element method [30], [47], [24], [48], [49].

Unfortunately, in the presence of moving media, even in the cases which allow a time-harmonic formulation, the electromagnetic problems to be solved become extremely complex [37], [1], [50]. Such a complexity is essentially due to the fact that even the simplest linear, stationary, homogeneous and isotropic material becomes at least bianisotropic once in motion. It could remain linear provided that the acceleration of the motion is not too large [10], [51].

The indicated complexity could be the reason behind the almost complete lack of results related to the reliability of numerical methods in the presence of moving (and then at least bianisotropic) materials. The reliability of a numerical method could be considered from different perspective. However, it is widely accepted that a reliable method should at least guarantee the convergence of the approximation to the true solution of the problem, as the number of degree of freedom becomes larger and larger [52]. The first results of this type for finite element approximations were provided in [24]. However, such results do not apply to several important cases, preventing, for example the presence of a lossless, standard, isotropic medium in motion [24], at any velocity different from zero. A more general approach was used in [20], where a result of convergence, which holds true under rather weak assumptions, is shown for finite element methods in the presence of axially moving cylinders. Such an approach has not been extended so far to cover cases involving objects which rotate around their axes of rotational symmetry.

In this context, the aim of this chapter is to provide some results showing the good behaviour of finite element approximations for time-harmonic electromagnetic problems involving rotating axisymmetric objects. The rotational speed is considered to be time-invariant in order to give a meaning to the time-harmonic formulation. Moreover, we will assume the objects are made up of linear, stationary, isotropic and lossless materials in their rest frames. In particular, we will present some results obtained by a three-dimensional finite element simulator able to deal with linear bianisotropic media. The effects of the motion on the numerical solutions are discussed, comparing these quantities with the corresponding ones obtained when all media in-

volved are at rest and, in the presence of canonical objects, with the results deduced by using semi-analytical techniques [11]. The problem involving rotating sphere is considered to establish the reliability of our solver. Then the simulator is used for solving problem involving other axisymmetric object. Problem involving rotating toroidal scatterer is considered as a test problem here. No other tool is available to solve this kind of problems. The same simulator can be used for other problems involving bianisotropic materials. Hence we also investigate the convergence of the numerical solution for some of the problems involving this kind of media. For this we take some test problems which were considered previously in the literature. Although the well-posedness and convergence of finite element solution are not proved for these problems, we can expect that an extension of the generalized Max-Milgram lemma used in [20] could provide a confirmation of the convergence result obtained here.

The chapter is organized as follows. In Section 4.2 the mathematical formulation of the problems of interest is provided. The Galerkin finite element formulation is described. The details and results of the numerical experiments are provided in 4.3. Finally, the chapter is concluded by summarizing the main outcomes.

4.2 Problem Definition

Problems involving axisymmetric rotating objects illuminated by time-harmonic electromagnetic field can be considered as a special case of a general time-harmonic problem involving bianisotropic materials. Hence a general mathematical and numerical formulation which can deal with bianisotropic media can be immediately applied to the problems involving rotating axisymmetric objects. A general description of this kind of problem was given in Chapter 2. Here we briefly recall it as applicable to rotating axisymmetric objects.

Let us denote by $\Omega \subset \mathbb{R}^3$ the bounded and connected domain where the problems of interest are formulated. Its boundary Γ is assumed to be Lipschitz continuous. We denote by $\mathbf{n}$ the outward unit vector orthogonal to Γ.

In order to consider different materials abutting and different rotating axisymmetric objects we assume that Ω can be decomposed into m open and connected subdomains of Ω having Lipschitz continuous stationary boundaries. These subdomains are denoted by Ω_i, $i \in M = \{1, \ldots, m\}$, satisfying $\overline{\Omega} = \overline{\Omega}_1 \cup \cdots \cup \overline{\Omega}_m$ ($\overline{\Omega}$ is the closure of Ω) and $\Omega_i \cap \Omega_j = \emptyset$ for $i \neq j$.

In each subdomain we have a linear and time-invariant medium. Moreover, we assume that all the materials involved are isotropic in their rest frames and are there

characterized by the complex-valued fields ε, μ. In order to avoid problems with convective currents, which can become surface currents [22], we assume that all moving media have the electric conductivity $\sigma = 0$. n of the indicated m subdomains, $n \leq m$, are axisymmetric and it is assumed that the materials contained in these regions rotate around the symmetry axes. All inhomogeneities in these n subdomains are axisymmetric, too.

In order to define the problem of interest we introduce the following additional notations and hypotheses. $(L^2(\Omega))^3$ is the usual Hilbert space of square integrable vector fields on Ω with values in $\mathbb{C}^3$ and with scalar product given by $(\mathbf{u}, \mathbf{v})_{0,\Omega} = \int_\Omega \mathbf{v}^* \mathbf{u} \, dV$, where $\mathbf{v}^*$ denotes the conjugate transpose of the column vector $\mathbf{v}$. In order to deal with the tangential vector fields involved in the boundary condition we define [30] (p. 48)

$$L^2_t(\Gamma) = \{\mathbf{v} \in (L^2(\Gamma))^3 \mid \mathbf{v} \cdot \mathbf{n} = 0 \ \text{ almost everywhere on } \Gamma\}, \tag{4.1}$$

with scalar product denoted by $(\mathbf{u}, \mathbf{v})_{0,\Gamma} = \int_\Gamma \mathbf{v}^* \mathbf{u} \, dS$. The space where we will seek the electric and magnetic fields is [30]

$$U = H_{L^2,\Gamma}(\mathrm{curl}, \Omega) = \{\mathbf{v} \in H(\mathrm{curl}, \Omega) \mid \mathbf{v} \times \mathbf{n} \in L^2_t(\Gamma)\}, \tag{4.2}$$

with $H(\mathrm{curl}, \Omega) = \{\mathbf{v} \in (L^2(\Omega))^3 \mid \mathrm{curl}\, \mathbf{v} \in (L^2(\Omega))^3\}$. The scalar product in U is given by [30] (p. 84, p. 69)

$$(\mathbf{u}, \mathbf{v})_{U,\Omega} = (\mathbf{u}, \mathbf{v})_{0,\Omega} + (\mathrm{curl}\, \mathbf{u}, \mathrm{curl}\, \mathbf{v})_{0,\Omega} + (\mathbf{u} \times \mathbf{n}, \mathbf{v} \times \mathbf{n})_{0,\Gamma}, \tag{4.3}$$

and the induced norm is $\|\mathbf{u}\|_{U,\Omega} = (\mathbf{u}, \mathbf{u})^{1/2}_{U,\Omega}$.

For all media in motion with angular velocity values bounded as indicated in [51], the instantaneous rest-frame hypothesis [10] will be assumed. In this case the constitutive equations in the laboratory frame are given by [10] and can be written as

$$\begin{cases} \mathbf{D} = (1/c_0)\, P\, \mathbf{E} + L\, \mathbf{B} & \text{in } \Omega \\ \mathbf{H} = M\, \mathbf{E} + \mathrm{c}_0\, Q\, \mathbf{B} & \text{in } \Omega, \end{cases} \tag{4.4}$$

where P, L, M and Q are matrix-valued fields depending on the dielectric properties of the media in their rest frames and on the velocity fields of the moving materials [10] and c_0 is the speed of light in vacuum.

In the presence of moving and, then, bianisotropic media, the variational formulation of the time-harmonic electromagnetic boundary value problems of interest is

[24]

$$\text{Find } \mathbf{E} \in U : a(\mathbf{E}, \mathbf{v}) = l(\mathbf{v}) \quad \forall \mathbf{v} \in U, \tag{4.5}$$

where $a(\mathbf{u}, \mathbf{v})$ is the sesquilinear form given by

$$\begin{aligned} a(\mathbf{u}, \mathbf{v}) = {} & c_0 \big(Q \operatorname{curl} \mathbf{u}, \operatorname{curl} \mathbf{v}\big)_{0,\Omega} - \frac{\omega^2}{c_0} \big(P \, \mathbf{u}, \mathbf{v}\big)_{0,\Omega} \\ & - j\omega \big(M \, \mathbf{u}, \operatorname{curl} \mathbf{v}\big)_{0,\Omega} - j\omega \big(L \operatorname{curl} \mathbf{u}, \mathbf{v}\big)_{0,\Omega} \\ & + j\omega \big(Y(\mathbf{n} \times \mathbf{u} \times \mathbf{n}), \mathbf{n} \times \mathbf{v} \times \mathbf{n}\big)_{0,\Gamma}, \end{aligned} \tag{4.6}$$

and $l(\mathbf{v})$ is the antilinear form given by:-

$$\begin{aligned} l(\mathbf{v}) = {} & -j\omega \big(\mathbf{J}_e, \mathbf{v}\big)_{0,\Omega} - c_0 \big(Q \, \mathbf{J}_m, \operatorname{curl} \mathbf{v}\big)_{0,\Omega} \\ & + j\omega \big(L \, \mathbf{J}_m, \mathbf{v}\big)_{0,\Omega} - j\omega \big(\mathbf{f}_R, \mathbf{n} \times \mathbf{v} \times \mathbf{n}\big)_{0,\Gamma}. \end{aligned} \tag{4.7}$$

Here $\mathbf{J}_e$ and $\mathbf{J}_m$ represent electric and magnetic sources. Y is the boundary admittance and $\mathbf{f}_R$ is the source term of the boundary conditions enforced on Γ:

$$\mathbf{H} \times \mathbf{n} - Y \left(\mathbf{n} \times \mathbf{E} \times \mathbf{n}\right) = \mathbf{f}_R \quad \text{on } \Gamma. \tag{4.8}$$

These conditions can be used to consider absorbing boundary conditions [33] (p. 9), to model radiation or scattering problems, or boundary conditions at imperfectly conducting surfaces [1] (p. 646), to model metal cavity problems.

Solution of problem 4.5 can be approximated by a Galerkin finite element method, which is a discretization of a variational formulation. To this aim, let us introduce a sequence of finite dimensional subspaces of U denoted by $\{U_h\}_{h \in I}$, being I a denumerable and bounded set of strictly positive indexes having zero as the only limit point. Moreover, let us assume that the capability of U_h to approximate U becomes more and more satisfactory as h is reduced.

For any $h \in I$ and for any set of approximate sources $\mathbf{J}_{eh}$, $\mathbf{J}_{mh}$ and $\mathbf{f}_{Rh}$, the discrete version of problem 4.5 is

$$\text{Find } \mathbf{E}_h \in U_h : a(\mathbf{E}_h, \mathbf{v}_h) = l(\mathbf{v}_h) \quad \forall \mathbf{v}_h \in U_h. \tag{4.9}$$

Whenever problem 4.5 is well-posed, we say that problem 4.9 is a convergent approximation of problem 4.5 if the sequence $\{\mathbf{E}_h\}_{h \in I}$ of solutions of problem 4.9

satisfies

$$\|\mathbf{E}_h - \mathbf{E}\|_U \underset{h\to 0}{\longrightarrow} 0 \tag{4.10}$$

where $\mathbf{E}$ is the solution of problem (4.5).

The sequence of finite dimensional subspaces considered in Galerkin method is built by using the finite element method. This is done by considering a sequence of triangulations $\{\mathcal{T}_h\}_{h\in I}$ of $\overline{\Omega}$, and a specific finite element on each triangulation $\mathcal{T}_h$. We assume that: 1) $\overline{\Omega} = \bigcup_{T\in\mathcal{T}_h} T$; 2) the family $\{\mathcal{T}_h\}$ of triangulation is regular; 3) $\mathcal{T}_h$ is made up of tetrahedra; 4) first order edge elements are used to build U_h, with $h \in I$.

4.3 Numerical Results

The well-posedness and the convergence of finite element method for problems for three dimensional problems have not been proved in the literature yet. Also there is no report on the reliability of solution of numerical simulators for this kind of problems. For this reason we try to investigate the reliability of finite element simulator developed in our lab for solving problems involving bianisotropic media. Firstly we consider the case of rotating sphere. For this kind of problems a series solution is available in [11]. As a result we can compare the results obtained from the finite element method with this solution to establish the validity of the simulator. After this we confirm the convergence behaviour by considering some problems involving bianisotropic materials.

4.3.1 Rotating Sphere

In order to assess the good behaviour and the performances of finite element simulators in the presence of rotating axisymmetric objects we consider simple problems allowing the calculation of the solutions with other reliable tools. In particular, we firstly consider a sphere in vacuum. The sphere has radius denoted by R_s and contains a medium which, in its rest frame, is characterized by constant values of permittivity and permeability, which are denoted, respectively, by ε_r and μ_r. The problem of interest is formulated by considering a spherical domain of numerical investigation of radius R_d. The centers of the spherical object and domain are the same. No current densities are considered in Ω. The sphere is assumed to be illuminated by a uniform plane wave having

$$\mathbf{E}_{inc} = \hat{\mathbf{x}} E_x + \hat{\mathbf{z}} E_z, \tag{4.11}$$

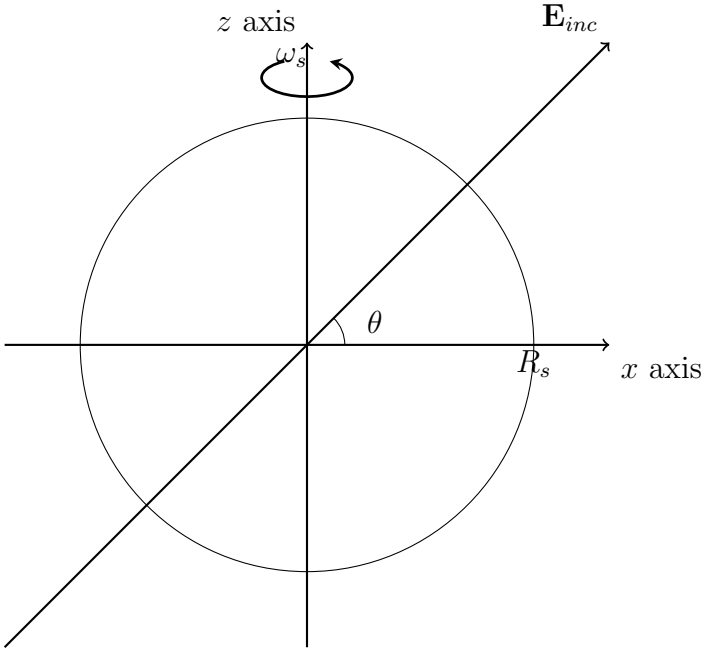

Figure 4.1: The configuration of rotating sphere considered as test problem. The radius of the sphere is R_s and the rotation is about z axis with angular velocity ω_s. The electric field is in the x-y plane and comes along the direction θ.

where

$$E_x = A\cos(\theta)e^{-j\omega\sqrt{\varepsilon_0\mu_0}(x\,\sin(\theta)+z\,\cos(\theta))}, \tag{4.12}$$

$$E_z = -A\sin(\theta)e^{-j\omega\sqrt{\varepsilon_0\mu_0}(x\,\sin(\theta)+z\,\cos(\theta))} \tag{4.13}$$

and θ is the usual elevation angle of the spherical coordinate system. Different values of this angle can be considered in order to deal with different directions of propagation in the (x, z) plane. The z-axis is in any case the axis of rotation of the sphere. We denote by ω_s its angular velocity.

A first order approximation of the solution of any problem of this class was deduced by De Zutter [11]. In addition to the zero-order term due to non-rotating sphere which corresponds to the classical Mie theory, a first order approximation with a term of the order $\frac{\omega_s R_s}{c_0}$ appears. We implemented this series solution against which the solution of finite element simulator was compared.

In order to solve the problems of interest we have to deduce the tensor fields P, L, M, Q involved in the constitutive relations. They are easily deduced for the subdomain outside the spherical object. We have

$$P = c_0\varepsilon_0 I_3, Q = \frac{1}{c_0\mu_0} I_3, L = M = 0, \tag{4.14}$$

being I_3 the identity matrix, and c_0 is the velocity of light in vacuum. Inside the object, starting from the following well-known equations [1] (p. 958) for a generic velocity field $\mathbf{v}$

$$\begin{cases} \mathbf{D} + \frac{1}{c_0^2}\mathbf{v} \times \mathbf{H} = \varepsilon \left(\mathbf{E} + \mathbf{v} \times \mathbf{B}\right) \\ \mathbf{B} - \frac{1}{c_0^2}\mathbf{v} \times \mathbf{E} = \mu \left(\mathbf{H} - \mathbf{v} \times \mathbf{D}\right) \end{cases} \tag{4.15}$$

one easily deduces ($v = |\mathbf{v}|$)

$$\begin{cases} \mathbf{D} - \frac{1}{c_0^2}\left(\mathbf{v} \times \mathbf{D}\right) \times \mathbf{v} = \\ \quad \varepsilon\mathbf{E} - \frac{1}{\mu c_0^4}\left(\mathbf{v} \times \mathbf{E}\right) \times \mathbf{v} + \frac{\mu_r\varepsilon_r - 1}{\mu c_0^2}\left(\mathbf{v} \times \mathbf{B}\right) \\ \mathbf{H} = \frac{\mu_r\varepsilon_r - 1}{\mu}\frac{1}{c_0^2 - v^2}\left(\mathbf{v} \times \mathbf{E}\right) + \\ \quad \frac{1}{\mu}\mathbf{B} - \frac{1}{\mu}\frac{\mu_r\varepsilon_r - 1}{c_0^2 - v^2}\left(\mathbf{v} \times \mathbf{B}\right) \times \mathbf{v}. \end{cases} \tag{4.16}$$

Taking account that, for the problem of interest in this work, the velocity field is along the $\hat{\varphi}$ unit vector (again of the spherical coordinate system) and has a magnitude given by the constant angular velocity ω_s multiplied by the distance of the considered point from the $z-$axis, after some calculations we can deduce the explicit expressions of the matrices representing the tensor fields P, L, M and Q in our Cartesian reference frame. These are the expressions usually managed by finite element simulators and, in particular, by our finite element code. The expressions of the matrices involved in equivalent forms of the constitutive relations [32] can be deduced as well. A little more detail of this derivation is given in Appendix A. Then we get the following expressions for the entries of the P,Q,L, and M matrices

$$\begin{aligned} P_{xz} &= P_{zx} = P_{yz} = P_{zy} = 0, \\ P_{xy} &= P_{yx} = \frac{\omega_s^2 xy(\varepsilon_r\mu_r - 1)}{\mu_0\mu_r c_0\left(c_0^2 - \omega_s^2(x^2+y^2)\right)}, \\ P_{xx} &= \varepsilon_0\varepsilon_r c_0 + \frac{\omega_s^2 x^2(\varepsilon_r\mu_r - 1)}{\mu_0\mu_r c_0\left(c_0^2 - \omega_s^2(x^2+y^2)\right)}, \\ P_{yy} &= \varepsilon_0\varepsilon_r c_0 + \frac{\omega_s^2 y^2(\varepsilon_r\mu_r - 1)}{\mu_0\mu_r c_0\left(c_0^2 - \omega_s^2(x^2+y^2)\right)}, \\ P_{zz} &= \varepsilon_0\varepsilon_r c_0 + \frac{\omega_s^2 (x^2+y^2)(\varepsilon_r\mu_r - 1)}{\mu_0\mu_r c_0\left(c_0^2 - \omega_s^2(x^2+y^2)\right)}, \end{aligned} \tag{4.17}$$

$$\begin{aligned} L_{xx} &= L_{yy} = L_{zz} = L_{xy} = L_{yx} = 0, \\ L_{xz} &= -L_{zx} = \frac{\omega_s x(\varepsilon_r\mu_r - 1)}{\mu_0\mu_r\left(c_0^2 - \omega_s^2(x^2+y^2)\right)}, \\ L_{yz} &= -L_{zy} = \frac{\omega_s y(\varepsilon_r\mu_r - 1)}{\mu_0\mu_r\left(c_0^2 - \omega_s^2(x^2+y^2)\right)}, \end{aligned} \tag{4.18}$$

$$
\begin{aligned}
&M_{xx} = M_{yy} = M_{zz} = M_{xy} = M_{yx} = 0,\\
&M_{xz} = -M_{zx} = \frac{\omega_s x(\varepsilon_r\mu_r - 1)}{\mu_0\mu_r\left(c_0^2 - \omega_s^2(x^2+y^2)\right)},\\
&M_{yz} = -M_{zy} = \frac{\omega_s y(\varepsilon_r\mu_r - 1)}{\mu_0\mu_r\left(c_0^2 - \omega_s^2(x^2+y^2)\right)},
\end{aligned}
\tag{4.19}
$$

$$
\begin{aligned}
&Q_{xz} = Q_{zx} = Q_{yz} = Q_{zy} = 0,\\
&Q_{xy} = Q_{yx} = -\frac{\omega_s^2 xy(\varepsilon_r\mu_r - 1)}{\mu_0\mu_r c_0\left(c_0^2 - \omega_s^2(x^2+y^2)\right)},\\
&Q_{xx} = \frac{1}{\mu_0\mu_r c_0} - \frac{\omega_s^2 x^2(\varepsilon_r\mu_r - 1)}{\mu_0\mu_r c_0\left(c_0^2 - \omega_s^2(x^2+y^2)\right)},\\
&Q_{yy} = \frac{1}{\mu_0\mu_r c_0} - \frac{\omega_s^2 y^2(\varepsilon_r\mu_r - 1)}{\mu_0\mu_r c_0\left(c_0^2 - \omega_s^2(x^2+y^2)\right)},\\
&Q_{zz} = \frac{1}{\mu_0\mu_r c_0} - \frac{\omega_s^2 (x^2+y^2)(\varepsilon_r\mu_r - 1)}{\mu_0\mu_r c_0\left(c_0^2 - \omega_s^2(x^2+y^2)\right)}.
\end{aligned}
\tag{4.20}
$$

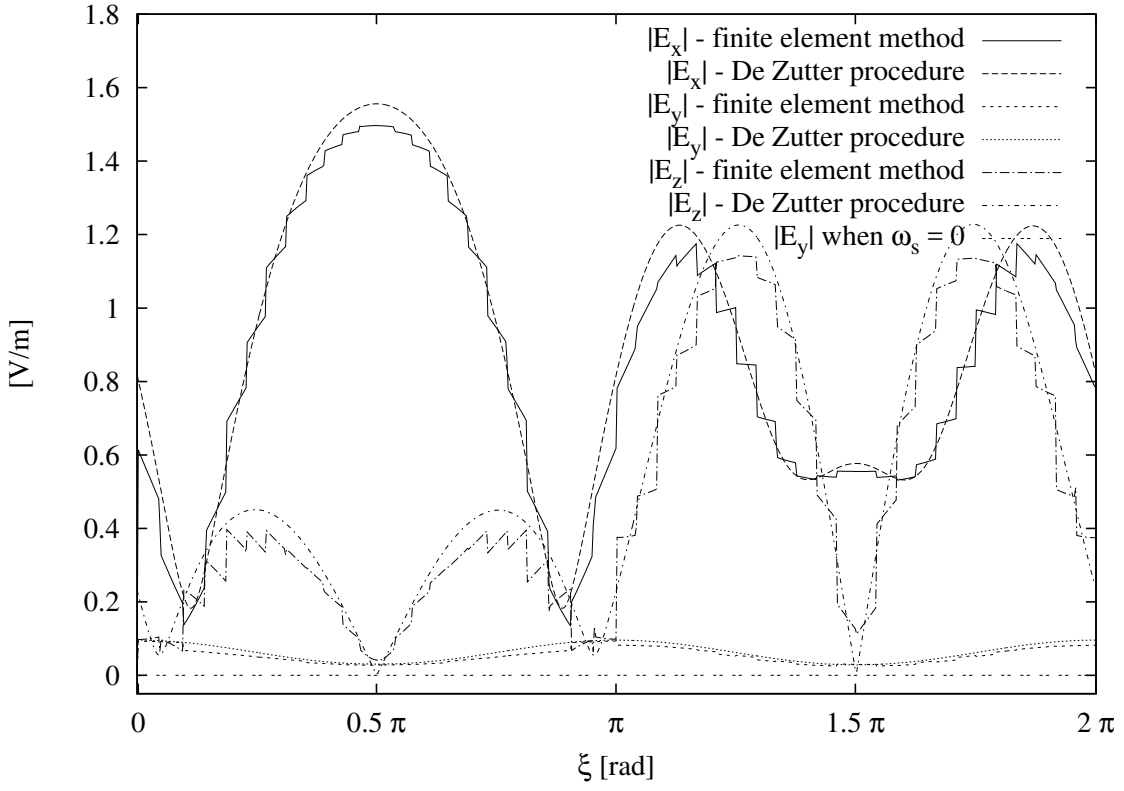

Figure 4.2: Magnitude of the components of electric field plotted against the angle along a circle in x-z plane. The finite element solution is shown in comparison with the series solution provided by De Zutter.

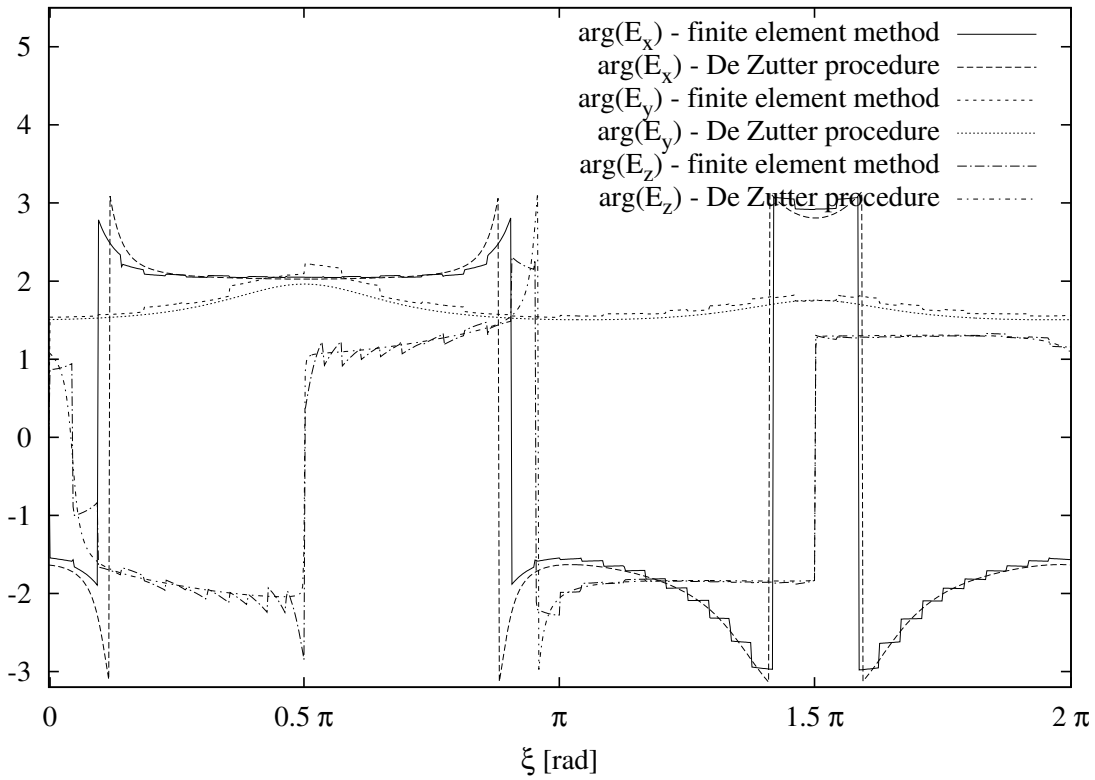

Figure 4.3: Phase of the components of electric field plotted against the angle along a circle in x-z plane. The finite element solution is shown in comparison with the series solution provided by De Zutter.

In figures 4.2 and 4.3 the results obtained when $R_s = 1$ m, $R_d = 4$ m, $\omega = \pi \cdot 10^8$ rad/s ($f = 50$ MHz), $\theta = 0$, $\varepsilon_r = 16$ (for the rotating sphere when the medium is at rest), $\omega_s = 5 \cdot 10^{-3} c_0$. The field components, whose magnitudes (respectively, phases) are shown in Figure 4.2 (respectively, 4.3), are evaluated in a set of points belonging to a circle 1.5 m in radius in the (x, z) plane and centered in the origin.

The mesh adopted for computing the finite element solution is made up of 40 uniform spherical layers. It has not been optimized since the uniformity of the thickness of the layers does not take account of the strong inhomogeneity of the media involved.

The numerical results are in good agreement with the semi analytical ones. The two main components of the electric field (E_x and E_z) are almost completely independent of the motion. The E_y component, on the contrary, is particularly meaningful because it provides much more information on the rotational speed of the scatterer. This is die to the fact that, when $\omega_s = 0$, we get $E_y = 0$. Even if such a component is much smaller in magnitude than E_x and E_z, Figures 4.2 and 4.3 shows that finite element code is able to compute E_y in an accurate way. Such a result on E_y could

be important for inverse scattering procedures dealing with the reconstruction of the rotational speed of the sphere. This could be considered a first step toward the goal of estimating the rotating speed of celestial bodies of more general shapes.

4.3.2 Rotating Torus

From the previous subsection, we are able to verify the reliability of the finite element simulator for rotating axisymmetric objects by comparing the result against the series solution that is available for rotating sphere. Now we can use the same simulator for other rotating axisymmetric objects for which analytic solution is not available. For this we have selected a homogeneous torus rotating about its axis. No other tool is available which can deal with such a problem to the best of our knowledge. Hence the results presented here are novel. This may be a first step in solving more general problems.

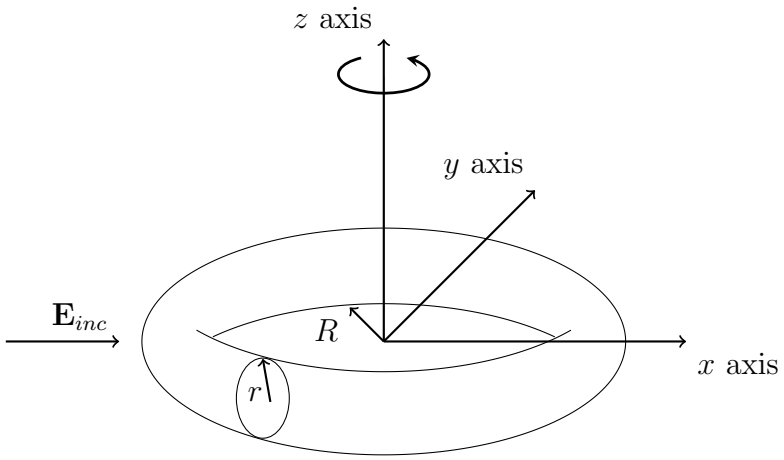

Figure 4.4: Geometry of the toroidal scatterer considered as the test problem. The toroid rotates about the z axis with angular velocity ω_s. R and r are as shown in the figure and are respectively the "major radius" and the "minor radius" of the torus.

The geometry of the test problem considered is described in Figure 4.4. The vales of major radius $R = 0.15$ m and that of minor radius r is also 0.15 m. The torus is made of material with $\varepsilon_r = 20$. The domain of numerical investigation is a sphere of radius 2 m. We consider a plane wave incident along the negative x axis with electric field along the z axis and with magnitude 1 V/m. Two values of frequencies $f = 20$ MHz and $f = 100$ MHz are considered for the incident wave.

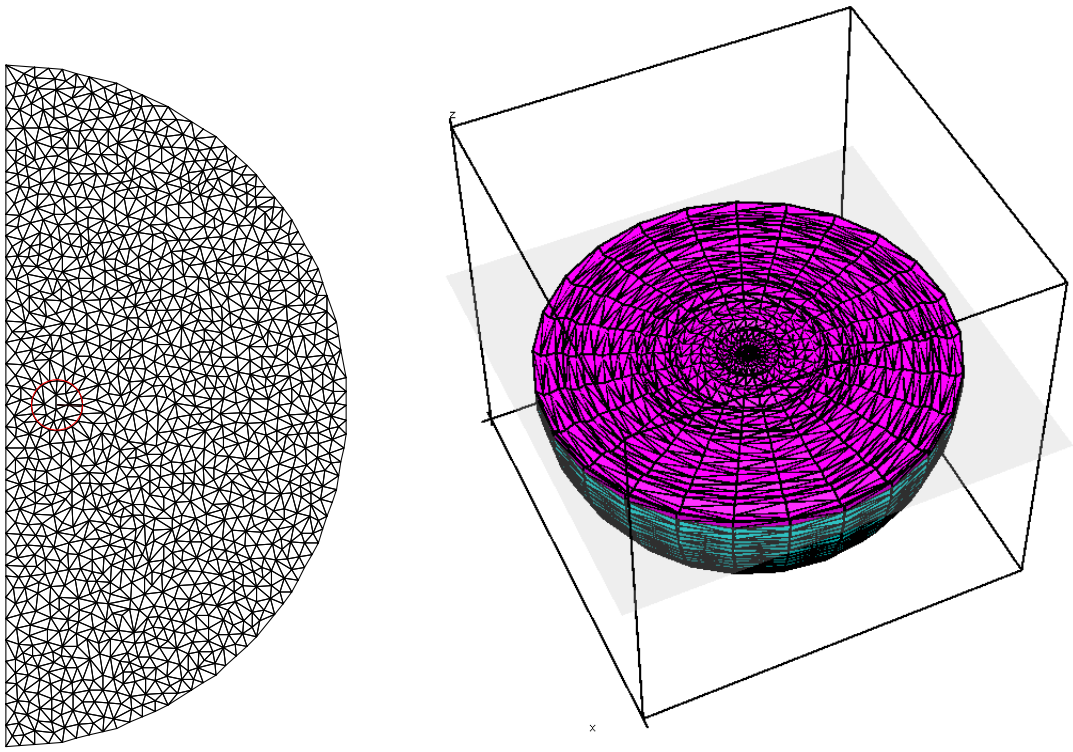

Figure 4.5: The mesh constructed for a toroidal scatterer. First a two-dimensional mesh is created along x-z plane as shown on the left. The circular boundary of the 2d section of the torus is shown in red. The planar mesh is then rotated around z-axis to get the three dimensional mesh shown on the right. The section cut along x-y plane is shown here.

The meshing of the domain was carried out in two steps. First the mesh was created for a two dimensional half plane of the domain. The section along $x-z$ plane is chosen for this step. The freely available software "Triangle" was used for this [53]. The mesh obtained in this step is shown on the left half of Figure 4.5. In the figure the boundary of circular cross section of the planar section of toroid is shown in red. The mesh needs to be such that the triangular elements do not cross this boundary. In the second step, this mesh is rotated about z axis. This gives the three dimensional mesh shown in right half of Figure 4.5. The freely available tool tetview [54] was used for visualizing the 3d mesh. A section cut along x-y plane is shown in the figure. The final three dimensional mesh has 31030 nodes, 180350 elements and 3350 boundary faces.

The results of the simulations for $f = 20$ MHz are shown in Figures 4.6, 4.7 and 4.8. The magnitude of E_z along the three axes is shown. The solution of the problem with toroid at rest is shown both with the commercial software COMSOL as well as by putting $\omega_s = 0$ in our simulator. The solution for $\omega_s = 0.5c_0$ rad/sec is shown.

There is appreciable difference in this case. Especially along y axis, E_z is appreciably changed by the rotation. Similar results are shown for the case $f = 100$ MHz in Figures 4.9, 4.10 and 4.11.

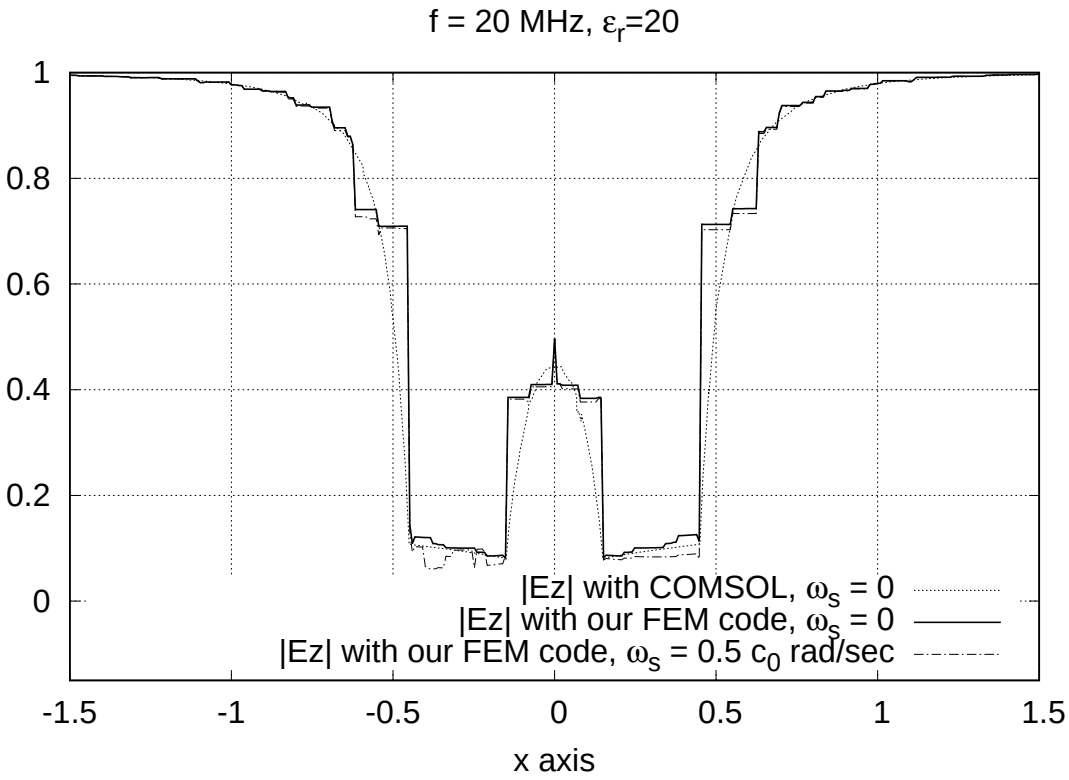

Figure 4.6: Magnitude of E_z along x axis for the toroidal scatterer. The frequency of incident wave is 20 MHz and torus is made of homogeneous material with $\varepsilon_r = 20$ in its rest frame. For $\omega_s = 0$ the solution from the commercial simulator COMSOL as well as that from our Finite Element code are shown and is compared against our solution for $\omega_s = 0.5c_0$ rad/sec.

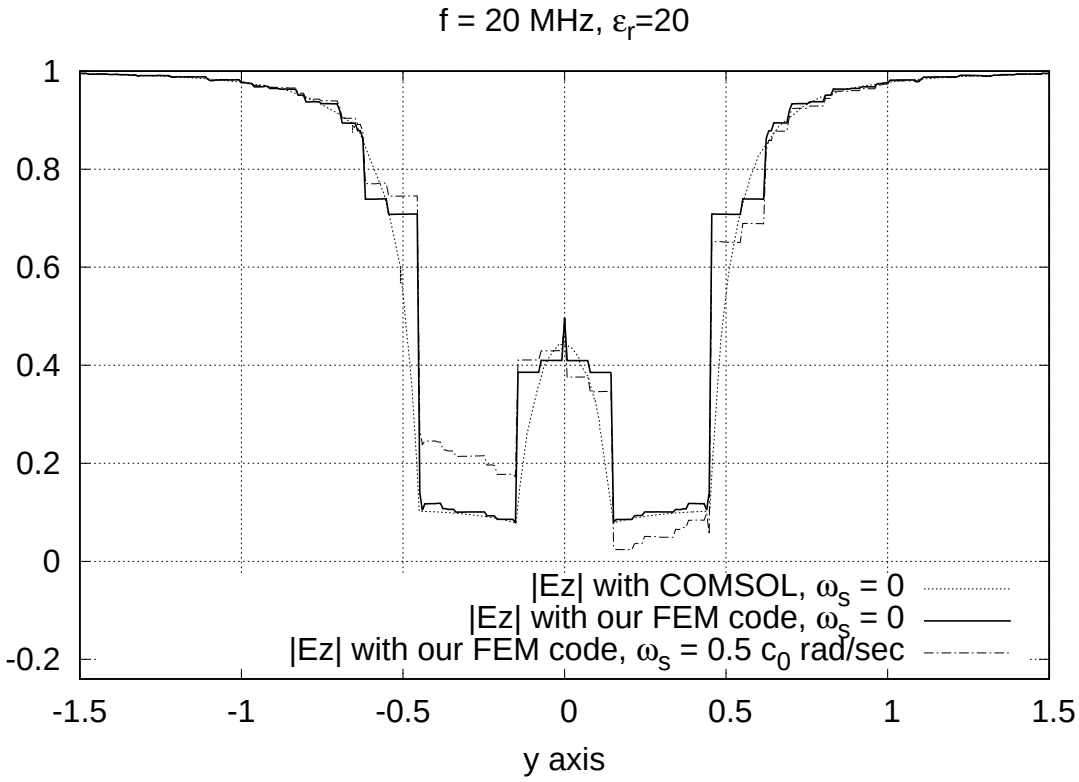

Figure 4.7: Magnitude of E_z along y axis for the toroidal scatterer. The frequency of incident wave is 20 MHz and torus is made of homogeneous material with $\varepsilon_r = 20$ in its rest frame. For $\omega_s = 0$ the solution from the commercial simulator COMSOL as well as that from our Finite Element code are shown and is compared against our solution for $\omega_s = 0.5c_0$ rad/sec.

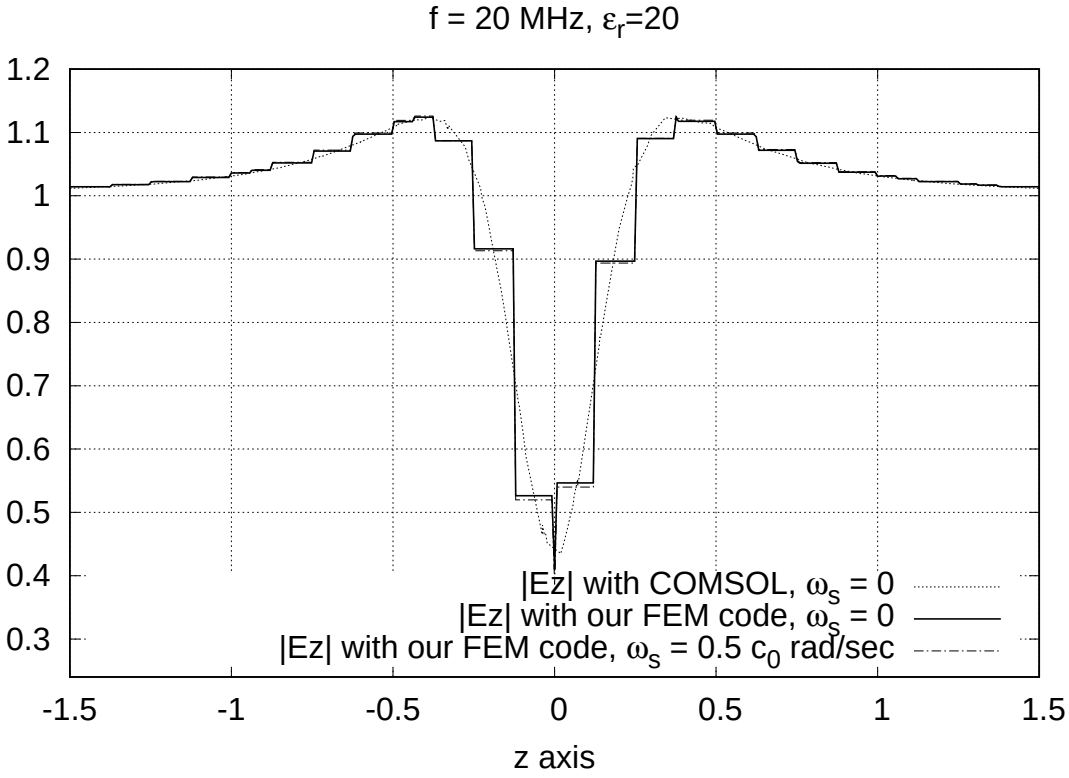

Figure 4.8: Magnitude of E_z along z axis for the toroidal scatterer. The frequency of incident wave is 20 MHz and torus is made of homogeneous material with $\varepsilon_r = 20$ in its rest frame. For $\omega_s = 0$ the solution from the commercial simulator COMSOL as well as that from our Finite Element code are shown and is compared against our solution for $\omega_s = 0.5c_0$ rad/sec.

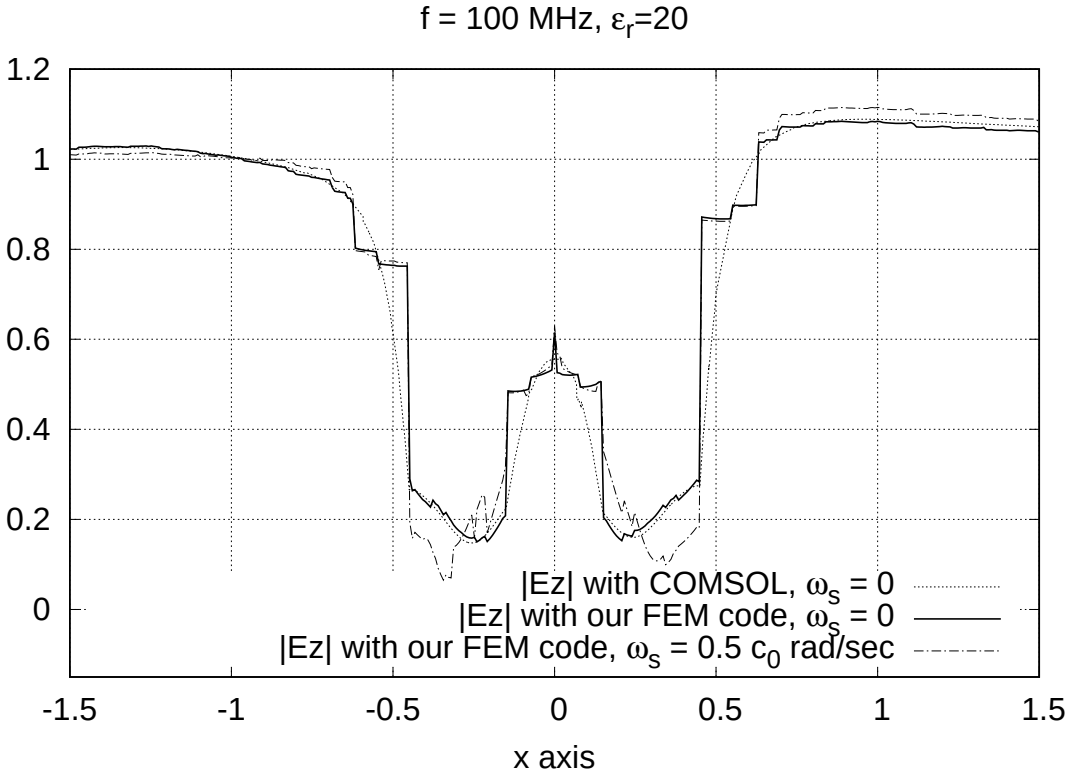

Figure 4.9: Magnitude of E_z along x axis for the toroidal scatterer. The frequency of incident wave is 100 MHz and torus is made of homogeneous material with $\varepsilon_r = 20$ in its rest frame. For $\omega_s = 0$ the solution from the commercial simulator COMSOL as well as that from our Finite Element code are shown and is compared against our solution for $\omega_s = 0.5c_0$ rad/sec.

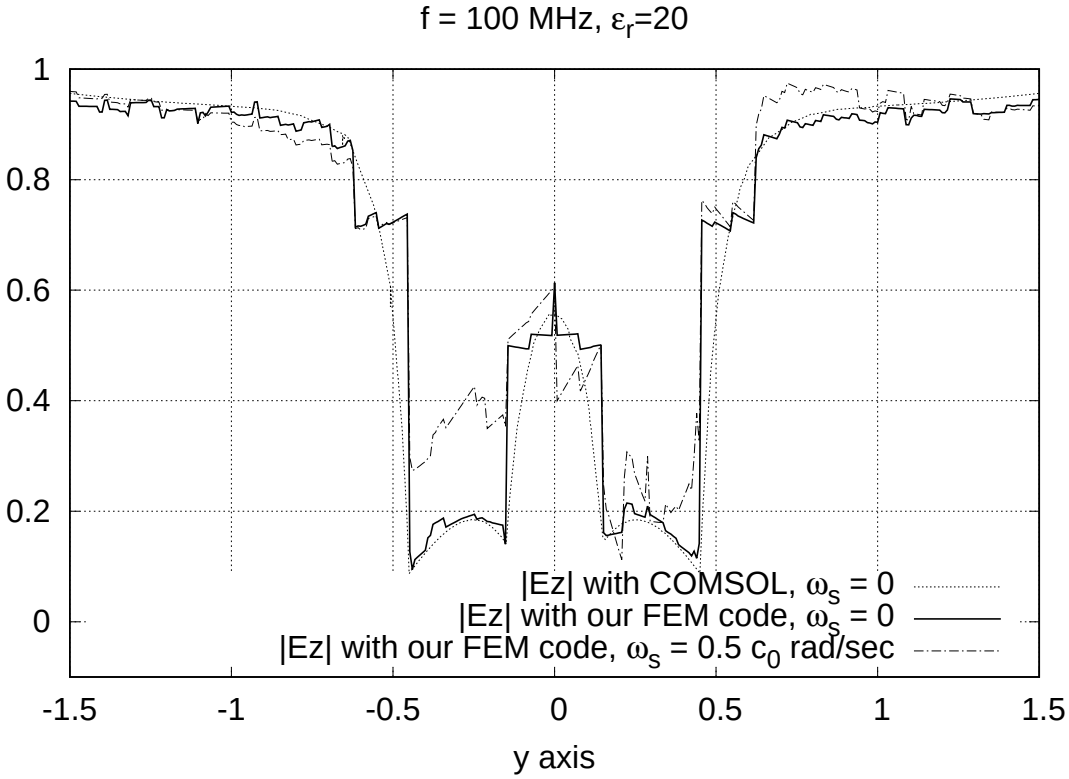

Figure 4.10: Magnitude of E_z along y axis for the toroidal scatterer. The frequency of incident wave is 100 MHz and torus is made of homogeneous material with $\varepsilon_r = 20$ in its rest frame. For $\omega_s = 0$ the solution from the commercial simulator COMSOL as well as that from our Finite Element code are shown and is compared against our solution for $\omega_s = 0.5c_0$ rad/sec.

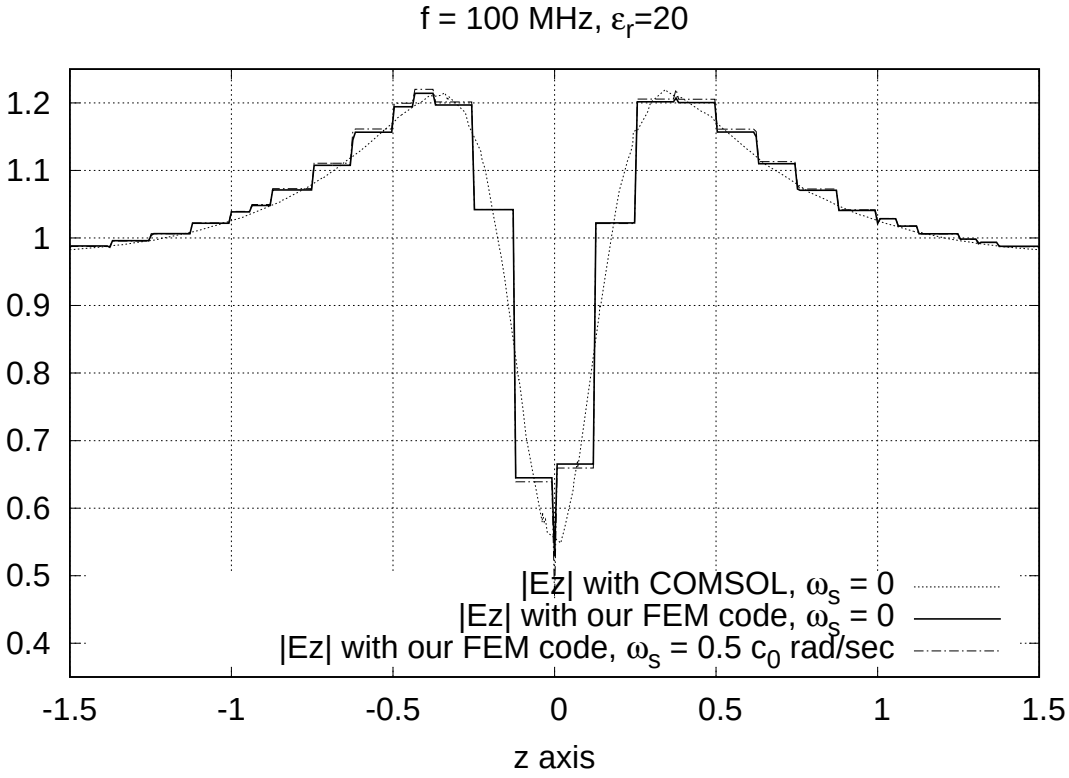

Figure 4.11: Magnitude of E_z along z axis for the toroidal scatterer. The frequency of incident wave is 100 MHz and torus is made of homogeneous material with $\varepsilon_r = 20$ in its rest frame. For $\omega_s = 0$ the solution from the commercial simulator COMSOL as well as that from our Finite Element code are shown and is compared against our solution for $\omega_s = 0.5c_0$ rad/sec.

4.3.3 Other Problems Involving Bianisotropic Materials

Many problems involving bianisotropic materials can be solved using the finite element simulator that was developed in the lab. Now we consider some examples of such problems. The results suggest the convergence behaviour of the solution for such cases. The problems we consider are ones for which the well-posedness and finite element convergence have not been proved so far. However these results can serve as the numerical evidence for convergence of finite element method, once such well-posedness and convergence results are proved for these cases. We consider problems that were discussed by Wu and Jaggard in [55] and by Alotto and Condecasa in [56]. These problems were chosen here because the results deduced in [24] cannot be applied to them. We can expect that a convergence result which may be derived in the future based on generalized Lax-Milgram lemma will be able to extend the applicability of the results to these problems as well. Thus such a general result will

be able to cover a wide range of problems including those involving axisymmetric objects, and in addition the problems involving bianisotropic media considered here. With this general aim in mind, we examine the convergence of finite element solutions for the afore mentioned problems.

Rectangular Waveguide Partially Filled with Chiral Media

First let us consider the biisotropic medium considered by Wu and Jaggard in [55]. They studied about the discontinuities in chirowaveguides. The configuration of the considered waveguide is given in Figure 4.12, which is a metallic waveguide partially filled with biisotropic media, which can be managed by our simulator. The media is characterized by the constitutive relation given in equation (4.21).

$$\begin{cases} \mathbf{D} = \varepsilon_0 \epsilon_r \mathbf{E} - j\xi_c \mathbf{B} \\ \mathbf{H} = \frac{\mathbf{B}}{\mu_0 \mu_r} - j\xi_c \mathbf{E} \end{cases} \tag{4.21}$$

Which gives

$$P = c_0 \varepsilon_0 \varepsilon_r I_3, Q = \frac{1}{c_0 \mu_0 \mu_r} I_3, L = M = -j\xi_c I_3 \tag{4.22}$$

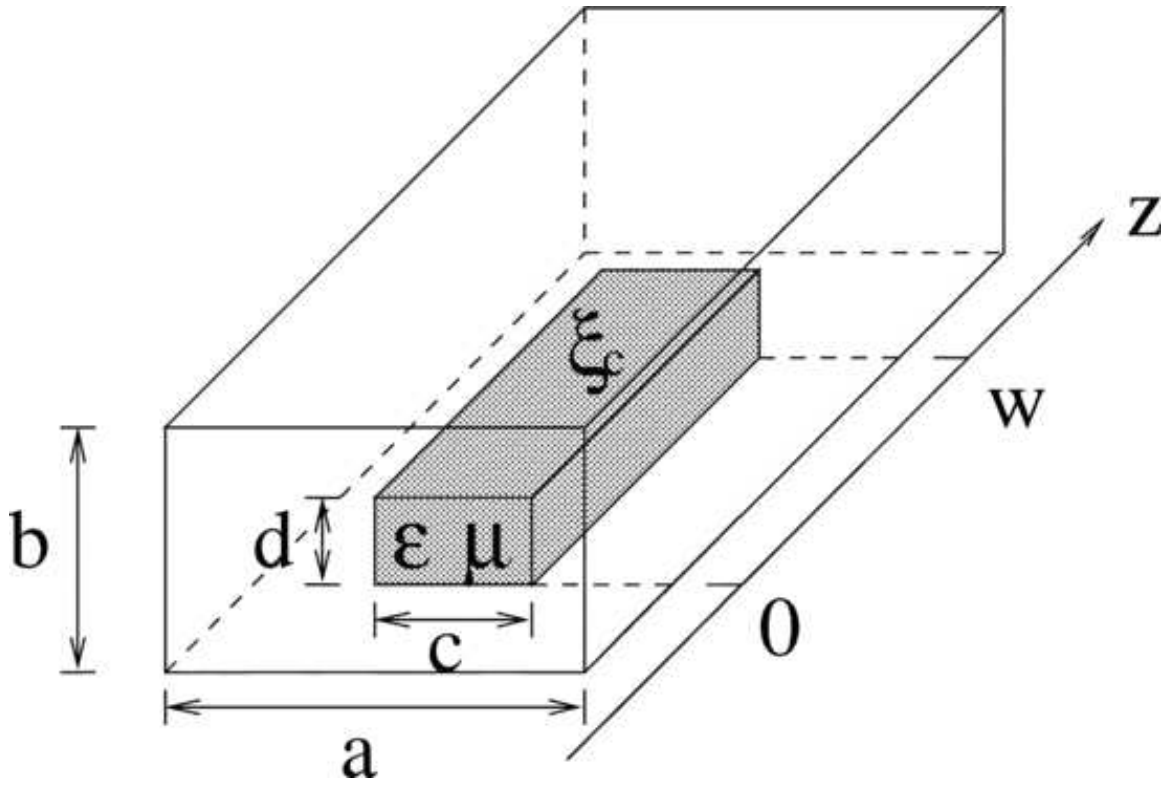

Figure 4.12: Configuration of a rectangular waveguide partially filled with chiral media considered by Wu and Jaggard in [55]

For the evaluation of convergence property of the finite element simulator, we consider the configuration for the waveguide shown in Figure 4.12. The axis of propagation is considered to be z-axis. The rectangular cross section of the waveguide are having the width and height a and b along x and y axes respectively, and the length along the z-axis is w. The waveguide is partially filled with the chiral media as shown in the Figure 4.12. The rectangle formed by the chiral media has a cross section with width c and height d. The geometric parameters considered for the waveguide are $a = 23$ mm, $b = 10$ mm, $c = 11$ mm, $d = 5$ mm, $w = 40$ mm. The frequency considered is $f = 9$ GHz. The biisotropic media is characterized by $\varepsilon_r = 2.5$, $\mu_r = 1$, $\xi_c = 2.5\,10^{-3}$ mho.

The results are calculated for three different sizes of mesh. The meshing is done by splitting the domain into tetrahedra. The coarse mesh has only 24 points along x-axis, 11 points along y axis and 41 points along z-axis. This corresponds to a uniform mesh with 10 segments along y axis and a number of segments to the respective lengths along the other two directions. The finer mesh used has 47 points along x axis, 21 points along y axis and 81 points along z-axis. The finest mesh used is with 70 points along x axis, 31 points along y axis and 121 points along the z-axis.

In the Figure 4.13 magnitudes of the components of electric field along the x-axis computed using the finite element code is shown. The solution for the isotropic case with $\xi_c = 0$ is also shown. The results clearly show that as the mesh becomes finer and finer the difference between the solutions become less and less. This suggests that the finite element simulator is able to converge to the solution. The same conclusion hold also for the solution computed along other directions. This is shown is Figures 4.14 and 4.15 which give the solutions along y axis and z axis respectively.

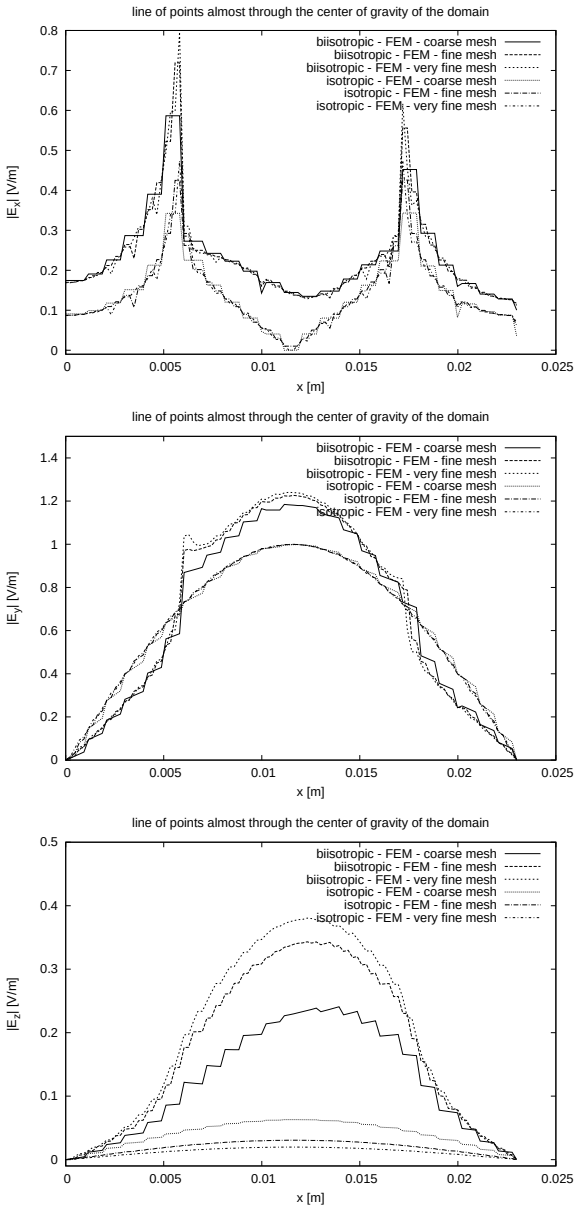

Figure 4.13: Magnitude of components of electric field along the x-axis for three different sizes of meshes. The parameters used are $a = 23$mm,$b = 10$ mm, $c = 11$ mm, $d = 5$ mm, $w = 40$ mm, frequency $f = 9$ GHz. The media is characterized by $\varepsilon_r = 2.5$, $\mu_r = 1$. The biisotropic media has $\xi_c = 2.5\,10^{-3}$. The corresponding plots for isotropic media is also shown for the comparison which is characterized by $\xi_c = 0$.

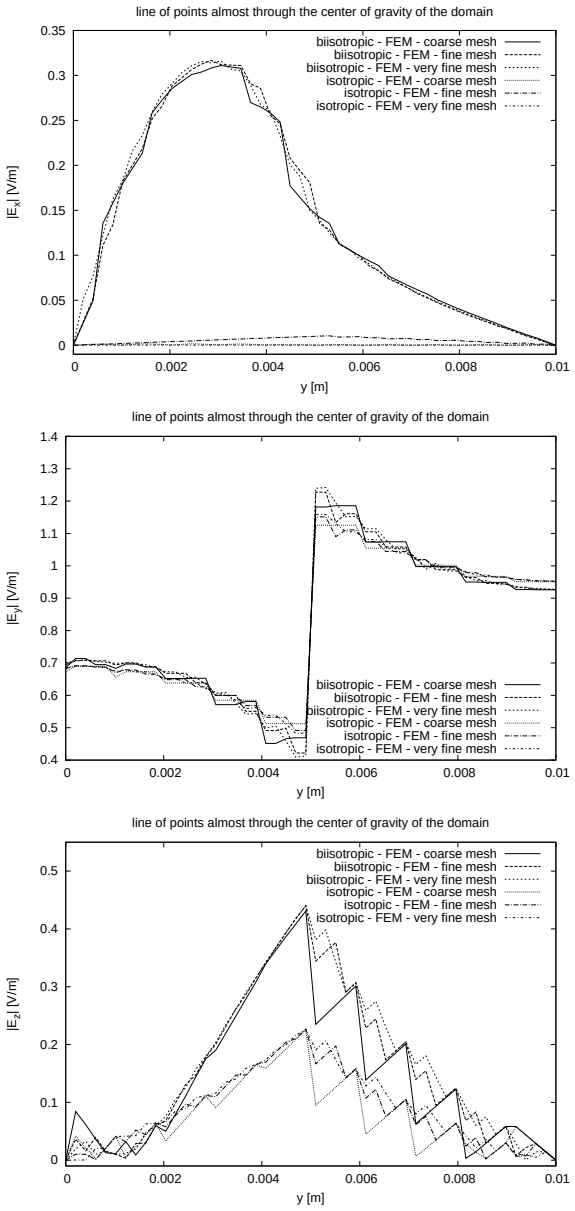

Figure 4.14: Magnitude of components of electric field along the y-axis for three different sizes of meshes. The parameters used are $a = 23$mm,$b = 10$ mm, $c = 11$ mm, $d = 5$ mm, $w = 40$ mm, frequency $f = 9$ GHz. The media is characterized by $\varepsilon_r = 2.5$, $\mu_r = 1$. The biisotropic media has $\xi_c = 2.5\,10^{-3}$. The corresponding plots for isotropic media is also shown for the comparison which is characterized by $\xi_c = 0$.

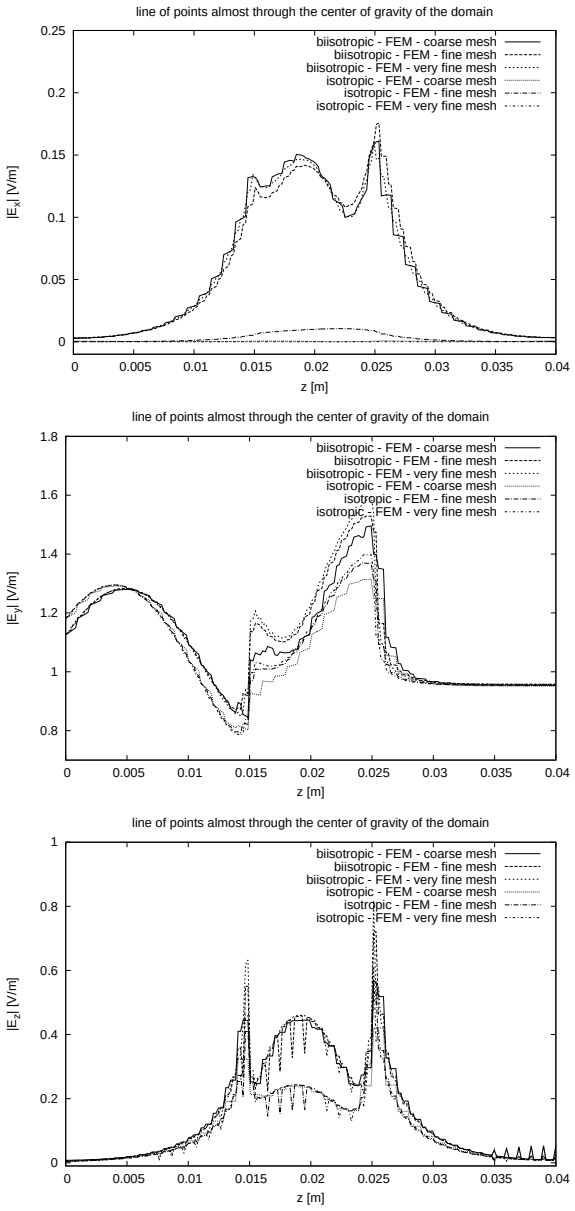

Figure 4.15: Magnitude of components of electric field along the z-axis for three different sizes of meshes. The parameters used are $a = 23$mm,$b = 10$ mm, $c = 11$ mm, $d = 5$ mm, $w = 40$ mm, frequency $f = 9$ GHz. The media is characterized by $\varepsilon_r = 2.5$, $\mu_r = 1$. The biisotropic media has $\xi_c = 2.5\,10^{-3}$. The corresponding plots for isotropic media is also shown for the comparison which is characterized by $\xi_c = 0$.

Rectangular Waveguide Half Filled with Bianisotropic Material

Next we consider the configuration considered by Alotto and Codecasa in [56]. The configuration we consider for our numerical experiment is as shown in Figure 4.16, which is a rectangular waveguide half filled with bianisotropic material. Again the

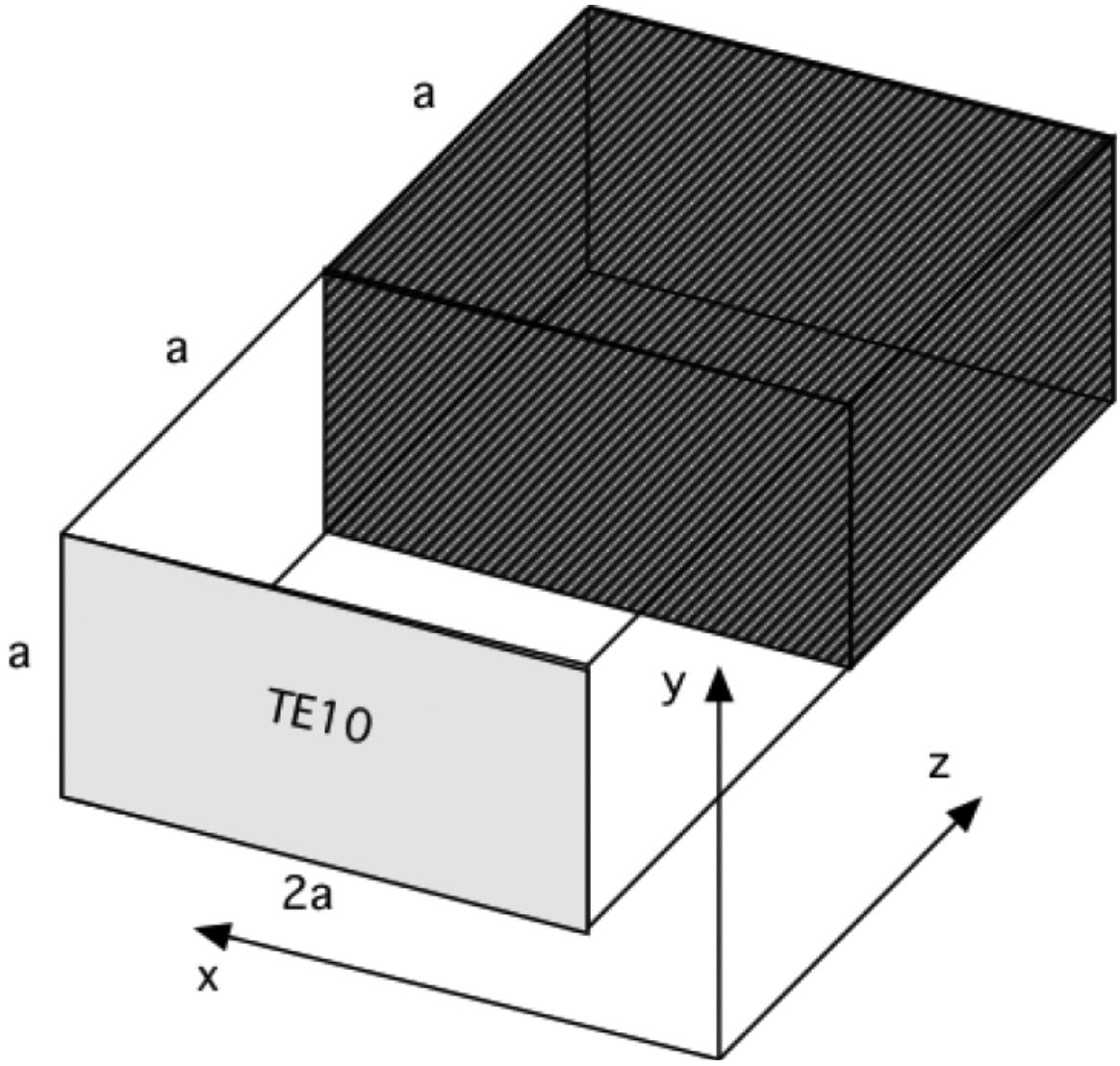

Figure 4.16: The configuration of rectangular waveguide half filled with bianisotropic material which was considered in [56].

axis of propagation is taken as z. The width and height are $2a$ and a and the length is $2a$, half of which is filled with air and the other half is filled with bianisotropic material which acts as obstacle. The material is characterized by the P, Q, M, L tensor fields described by the equation (4.4) which take the form in equation (4.23) in this case

$$\begin{aligned} P &= c_0\epsilon_0 I_3 \\ Q &= \tfrac{1}{c_0\mu_0} I_3 \\ L = M &= j\kappa \begin{bmatrix} 1 & 1 & 0 \\ 1 & 1 & 0 \\ 0 & 0 & 1 \end{bmatrix} \end{aligned} \tag{4.23}$$

where κ is a parameter. For the numerical experiments we consider the value of $\kappa = 1.061\,10^{-3}$. The value of $a = 0.01$ m is considered. A TE_{10} mode is applied at the input port by exciting it with a frequency of 10 GHz and good electric conductor condition is set at the output port. The details of the tetrahedral mesh used is as follows. The coarse mesh has 11 points along the y axis and 21 points along x and z axes. The finer mesh has 21 points along the y axis and 41 points along x and z axes. Finally a very fine mesh is considered with 31 points along the y axis and 61 points along the x and z axes.

The magnitude of the components of electric field is shown in Figures 4.17, 4.18 and 4.19. Again we can observe the convergence behaviour of the finite element solution.

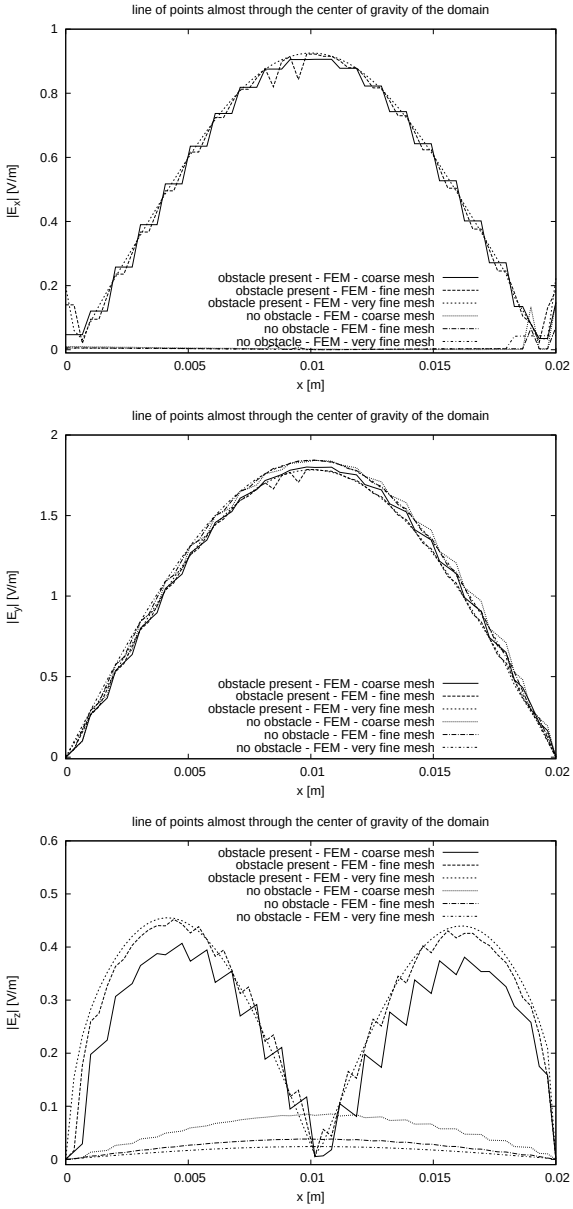

Figure 4.17: Magnitude of components of electric field along x axis for the rectangular waveguide with bianisotropic obstacle which was considered in [56].The waveguide is excited with a TE_{10} by applying a frequency of 10 GHz, the waveguide geometry is defined by $a = 0.01$ m and the material is defined by $\kappa = 1.061\,10^{-3}$. Solution is shown with three different sizes of mesh. The result for the case with no obstacle is also shown.

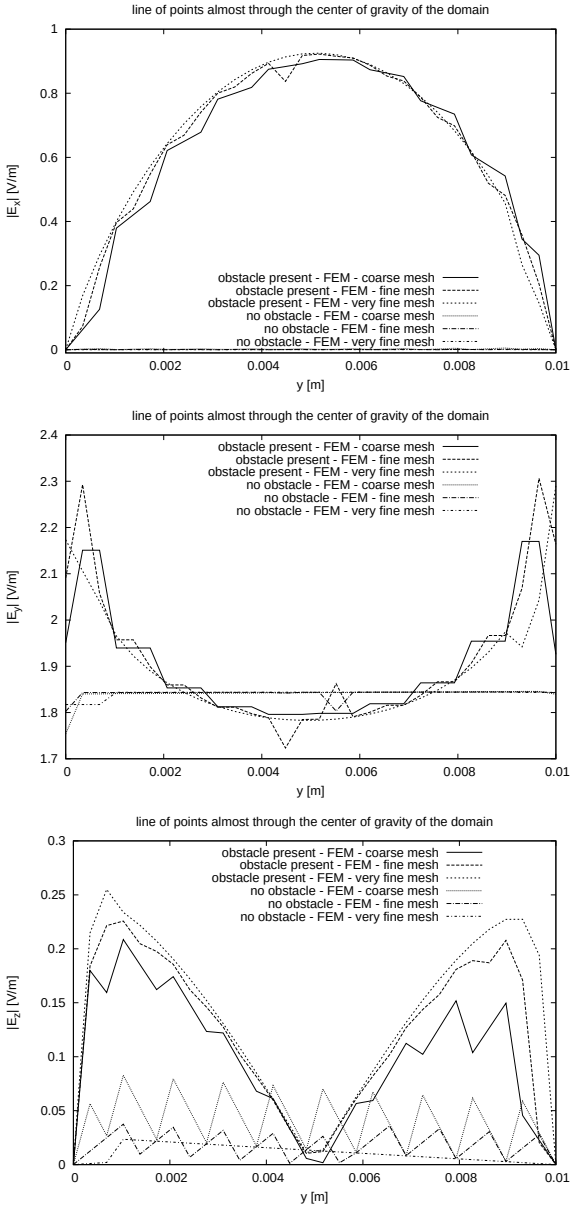

Figure 4.18: Magnitude of components of electric field along y axis for the rectangular waveguide with bianisotropic obstacle which was considered in [56].The waveguide is excited with a TE_{10} by applying a frequency of 10 GHz, the waveguide geometry is defined by $a = 0.01$ m and the material is defined by $\kappa = 1.061\,10^{-3}$. Solution is shown with three different sizes of mesh. The result for the case with no obstacle is also shown.

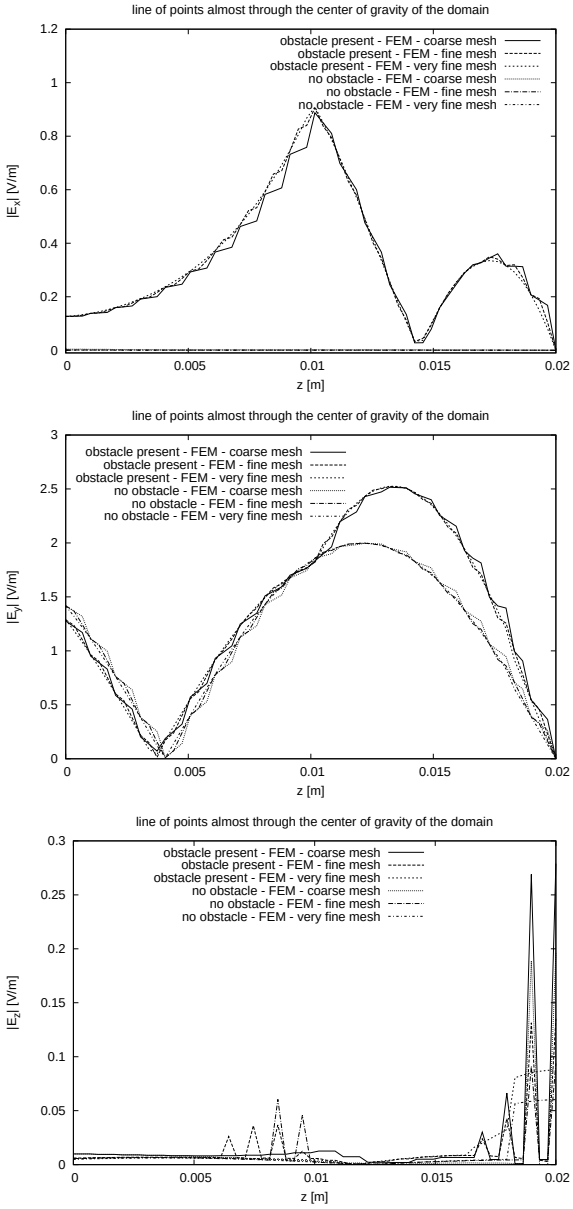

Figure 4.19: Magnitude of components of electric field along z axis for the rectangular waveguide with bianisotropic obstacle which was considered in [56].The waveguide is excited with a TE_{10} by applying a frequency of 10 GHz, the waveguide geometry is defined by $a = 0.01$ m and the material is defined by $\kappa = 1.061\,10^{-3}$. Solution is shown with three different sizes of mesh. The result for the case with no obstacle is also shown.

4.4 Conclusions

The finite element simulator capable of solving problems involving bianisotropic constitutive relations was developed. This could be directly used for solving problems involving rotating axisymmetric objects. The problems we considered are the ones for which the convergence of finite element method is not proved so far. Neither are there any analysis of the accuracy of the numerical solutions for these problems. The finite element simulator was used for the simple problem of rotating sphere and the result was compared against the series solution. This provides evidence for the accuracy of the finite element method for solving such problems involving rotating axisymmetric objects. The simulator was then used for solving problem involving rotating torus. We also studied some other problems involving bianisotropic media. They fall under the category of problems for which the convergence of finite element method is not yet established in literature. The numerical experiments carried out provides further evidence that the finite element method is convergent and can support the theoretical results that may be proved in the future regarding the well-posedness and finite element approximability of such problems. Such a result can be anticipated by the generalization of techniques used in [20] and thus could cover many practical problems with bianisotropic media. The result for rotating axisymmetric object could be a first step in the practical application for the reconstruction of velocity of fast moving axisymmetric objects like the celestial bodies.

Chapter 5

Conclusions

We have seen that the electromagnetic problems involving moving objects have diverse applications. We have mainly considered the problems that could be formulated in frequency domain. Since the solution of many such problems requires numerical solution, we investigated the reliability of finite element method applied to such problems. The main focus were on the two dimensional problems involving axially moving cylinders and three dimensional problems involving rotating axisymmetric objects.

The well-posedness and the convergence of finite element method were proved for the two dimensional problems which mainly include non-conducting cylinders moving in the axial direction. However there were neither any error estimate nor any error analysis for this kind of problems. Hence in this work we provided a detailed error analysis for these kind of problems. These results could be used as a benchmark for any error estimate that the research community will be able to deduce.

We evaluated a simple test case involving non-conducting homogeneous circular cylinder moving in axial direction. A series solution was available to solve such problems. The results obtained could be generalized for more complex cases. The scatterer exhibits a bianisotropic effect due to motion. This gives rise to a cross polarized component of the field in addition to the component polarized along the incident field. The results were very satisfactory in general. The solution was very accurate for the co-polarized field in all the cases and the convergence speed was the same as that of the stationary cylinder. As for the orthogonally polarized component, the convergence was slower. This component is important in the reconstruction of the velocity profiles as it is entirely caused due to the motion. The discretization error was going down in the first power of h as against the h^2 convergence of the co-polarized component. Further, for small velocities, the accuracy in the computation of orthogonally polarized field reduces due to the round-off error. This suggest that

one should be careful in the cases where the scatterer is too weak. The ratio of the algebraic norms of the cross-polarized and co-polarized component can give a simple indication about such limits. Overall, the results are very good and the finite element simulator is able to give accurate solution for very wide range of parameters.

The three dimensional problems involving moving bodies were also considered as part of this work. These problems can again be considered as a subclass of problems involving bianisotropic media. The well-posedness results in the literature are applicable for only very restricted cases. Hence the convergence of finite element solution is not yet proved for the problems of our interest. The rotating axisymmetric objects could be formulated as three dimensional frequency domain problem with bianisotropic media. Hence a finite element simulator developed to solve such general problem can be applied to solve such problem. We implemented a series solution provided in literature for rotating dielectric sphere in vacuum. The finite element solution was found to be in agreement with the series solution. Hence we can be confident about the applicability of the method for this class of problems. Problem involving rotating toroidal scatterer was simulated for the first time. We further evaluated the convergence of the finite element simulator for problems involving other bianisotropic materials. These results are a first step in the application of the method for more complex problems. The simulator can be further extended to more complex geometries and can find application in many practical problems. The reconstruction of velocity profile by inverse scattering techniques could be an important application.

The work can be extended in many directions. As for the two dimensional problems there is a lack of a priori error estimate. The simulator may now be applied to more problems of practical importance.

The lack of an adequate well-posedness result needs to addressed for three dimensional problems. This can lead to a proof of finite element convergence and hence give the theoretical backing for the results provided here. There may be possibility of relaxing many assumptions required earlier and hence get a much more general theory. As stated earlier, the applications to inverse problems for reconstruction of the velocity profile can be of practical importance.

The most general form of the problem will be in the time domain. This may require more effort to tackle but an efficient solution to such problems could be of practical significance.

Appendix A

Deduction of the Tensor Fields Involved in the Constitutive Relations for Rotating Objects

Inside the rotating object we have equations we begin from (A.1) [1]

$$\begin{cases} \mathbf{D} + \frac{1}{c_0^2}\mathbf{v} \times \mathbf{H} = \varepsilon\left(\mathbf{E} + \mathbf{v} \times \mathbf{B}\right) \\ \mathbf{B} - \frac{1}{c_0^2}\mathbf{v} \times \mathbf{E} = \mu\left(\mathbf{H} - \mathbf{v} \times \mathbf{D}\right) \end{cases} \tag{A.1}$$

We can eliminate $\mathbf{H}$ from $(A.1)_1$ by using $\mathbf{H}$ from $(A.1)_2$:-

$$\mathbf{H} = \frac{\mathbf{B}}{\mu} - \frac{\mathbf{v} \times \mathbf{E}}{\mu c_0^2} + \mathbf{v} \times \mathbf{D} \tag{A.2}$$

which then immediately gives $(A.4)_1$

Similarly we can eliminate $\mathbf{D}$ from $(A.1)_2$ using $\mathbf{D}$ from $(A.1)_1$:-

$$\mathbf{D} = -\frac{\mathbf{v} \times \mathbf{H}}{c_0^2} + \varepsilon(\mathbf{E} + \mathbf{v} \times \mathbf{B}) \tag{A.3}$$

which gives $(A.4)_2$

$$\begin{cases} \mathbf{D} - \frac{1}{c_0^2}\left(\mathbf{v} \times \mathbf{D}\right) \times \mathbf{v} = \\ \quad \varepsilon\mathbf{E} - \frac{1}{\mu c_0^4}\left(\mathbf{v} \times \mathbf{E}\right) \times \mathbf{v} + \frac{\mu_r\varepsilon_r - 1}{\mu c_0^2}\left(\mathbf{v} \times \mathbf{B}\right) \\ \mathbf{H} = \frac{\mu_r\varepsilon_r - 1}{\mu}\frac{1}{c_0^2 - v^2}\left(\mathbf{v} \times \mathbf{E}\right) + \\ \quad \frac{1}{\mu}\mathbf{B} - \frac{1}{\mu}\frac{\mu_r\varepsilon_r - 1}{c_0^2 - v^2}\left(\mathbf{v} \times \mathbf{B}\right) \times \mathbf{v}. \end{cases} \tag{A.4}$$

Now we can go on and derive the tensor fields P, Q, L, M in the rectangular

co-ordinate system.

We have the following identity for any vector $\mathbf{A}$, $\mathbf{v}$

$$(\mathbf{v}\times\mathbf{A})\times\mathbf{v} = (\mathbf{v}\cdot\mathbf{v})\mathbf{A} - (\mathbf{v}\cdot\mathbf{A})\mathbf{v} \tag{A.5}$$

Which in rectangular co-ordinate system gives the different components as:-

$$\begin{aligned}((\mathbf{v}\times\mathbf{A})\times\mathbf{v})_x &= v_y^2 A_x - v_x v_y A_y\\ ((\mathbf{v}\times\mathbf{A})\times\mathbf{v})_y &= v_x^2 A_y - v_x v_y A_x\\ ((\mathbf{v}\times\mathbf{A})\times\mathbf{v})_z &= (v_x^2+v_y^2)A_z\end{aligned} \tag{A.6}$$

where the subscript indicates the component along that coordinate direction, and $v_z = 0$ for rotation along z axis. The above identity can be used while splitting the equation (A.4) along the coordinate directions, to get the components of $(\mathbf{v}\times\mathbf{D})\times\mathbf{v}$, $(\mathbf{v}\times\mathbf{E})\times\mathbf{v}$, $(\mathbf{v}\times\mathbf{B})\times\mathbf{v}$.

Hence for equation $(A.4)_1$ we get

$$\begin{aligned}D_x - \tfrac{1}{c_0^2}(v_y^2 D_x - v_x v_y D_y) &= \varepsilon_0\varepsilon_r E_x - \tfrac{1}{\mu c_0^4}(v_y^2 E_x - v_x v_y E_y) + \tfrac{\mu_r\varepsilon_r - 1}{\mu_0\mu_r c_0^2}(v_y B_z)\\ D_y - \tfrac{1}{c_0^2}(v_x^2 D_y - v_x v_y D_x) &= \varepsilon_0\varepsilon_r E_y - \tfrac{1}{\mu c_0^4}(v_x^2 E_y - v_x v_y E_x) - \tfrac{\mu_r\varepsilon_r - 1}{\mu_0\mu_r c_0^2}(v_x B_z)\\ D_z - \tfrac{1}{c_0^2}(v_x^2+v_y^2)D_z &= \varepsilon_0\varepsilon_r E_z - \tfrac{1}{\mu_0\mu_r c_0^4}(v_x^2+v_y^2)E_z + \tfrac{\mu_r\varepsilon_r-1}{\mu_0\mu_r c_0^2}(v_x B_y - v_y B_x)\end{aligned} \tag{A.7}$$

We can write, with ω_s defined in anti-clockwise sense, $v_x = -\omega_s y$, $v_y = \omega_s x$. Now we can extract D_z from equation $(A.7)_3$ and solve for D_x, D_y from eqautions $(A.7)_1$ and $(A.7)_2$ to get the following equation.

$$\begin{aligned}D_x &= (\varepsilon_0\varepsilon_r + \tfrac{\omega_s^2 x^2(\varepsilon_r\mu_r - 1)}{\mu_0\mu_r c_0^2\left(c_0^2 - \omega_s^2(x^2+y^2)\right)})E_x + \tfrac{\omega_s^2 xy(\varepsilon_r\mu_r-1)}{\mu_0\mu_r c_0^2\left(c_0^2-\omega_s^2(x^2+y^2)\right)}E_y + \tfrac{\omega_s x(\varepsilon_r\mu_r-1)}{\mu_0\mu_r\left(c_0^2-\omega_s^2(x^2+y^2)\right)}B_z\\ D_y &= \tfrac{\omega_s^2 xy(\varepsilon_r\mu_r-1)}{\mu_0\mu_r c_0^2\left(c_0^2-\omega_s^2(x^2+y^2)\right)}E_x + (\varepsilon_0\varepsilon_r + \tfrac{\omega_s^2 y^2(\varepsilon_r\mu_r-1)}{\mu_0\mu_r c_0^2\left(c_0^2-\omega_s^2(x^2+y^2)\right)})E_y + \tfrac{\omega_s y(\varepsilon_r\mu_r-1)}{\mu_0\mu_r\left(c_0^2-\omega_s^2(x^2+y^2)\right)}B_z\\ D_z &= (\varepsilon_0\varepsilon_r + \tfrac{\omega_s^2(x^2+y^2)(\varepsilon_r\mu_r-1)}{\mu_0\mu_r c_0^2\left(c_0^2-\omega_s^2(x^2+y^2)\right)})E_z - \tfrac{\omega_s x(\varepsilon_r\mu_r-1)}{\mu_0\mu_r\left(c_0^2-\omega_s^2(x^2+y^2)\right)}B_x - \tfrac{\omega_s y(\varepsilon_r\mu_r-1)}{\mu_0\mu_r\left(c_0^2-\omega_s^2(x^2+y^2)\right)}B_y\end{aligned} \tag{A.8}$$

From equation $(A.4)_2$ we get

$$\begin{aligned}H_x &= \tfrac{\mu_r\varepsilon_r-1}{\mu_0\mu_r(c_0^2-(v_x^2+v_y^2))}v_y E_z + \tfrac{1}{\mu_0\mu_r}B_x - \tfrac{\mu_r\varepsilon_r-1}{\mu_0\mu_r(c_0^2-(v_x^2+v_y^2))}(v_y^2 B_x - v_x v_y B_y)\\ H_y &= -\tfrac{\mu_r\varepsilon_r-1}{\mu_0\mu_r(c_0^2-(v_x^2+v_y^2))}v_x E_z + \tfrac{1}{\mu_0\mu_r}B_y - \tfrac{\mu_r\varepsilon_r-1}{\mu_0\mu_r(c_0^2-(v_x^2+v_y^2))}(v_x^2 B_y - v_x v_y B_x)\\ H_z &= \tfrac{\mu_r\varepsilon_r-1}{\mu_0\mu_r(c_0^2-(v_x^2+v_y^2))}(v_x E_y - v_y E_x) + \tfrac{1}{\mu_0\mu_r}B_z - \tfrac{\mu_r\varepsilon_r-1}{\mu_0\mu_r(c_0^2-(v_x^2+v_y^2))}(v_x^2+v_y^2)B_z\end{aligned} \tag{A.9}$$

which when substituted for v_x, v_y and rearranged gives

$$\begin{aligned}
H_x &= \frac{\omega_s x(\varepsilon_r\mu_r-1)}{\mu_0\mu_r\left(c_0^2-\omega_s^2(x^2+y^2)\right)}E_z + \left(\frac{1}{\mu_0\mu_r} - \frac{\omega_s^2 x^2(\varepsilon_r\mu_r-1)}{\mu_0\mu_r\left(c_0^2-\omega_s^2(x^2+y^2)\right)}\right)B_x - \frac{\omega_s^2 xy(\varepsilon_r\mu_r-1)}{\mu_0\mu_r\left(c_0^2-\omega_s^2(x^2+y^2)\right)}B_y \\
H_y &= \frac{\omega_s y(\varepsilon_r\mu_r-1)}{\mu_0\mu_r\left(c_0^2-\omega_s^2(x^2+y^2)\right)}E_z - \frac{\omega_s^2 xy(\varepsilon_r\mu_r-1)}{\mu_0\mu_r\left(c_0^2-\omega_s^2(x^2+y^2)\right)}B_x + \left(\frac{1}{\mu_0\mu_r} - \frac{\omega_s^2 y^2(\varepsilon_r\mu_r-1)}{\mu_0\mu_r\left(c_0^2-\omega_s^2(x^2+y^2)\right)}\right)B_y \\
H_z &= -\frac{\omega_s x(\varepsilon_r\mu_r-1)}{\mu_0\mu_r\left(c_0^2-\omega_s^2(x^2+y^2)\right)}E_x - \frac{\omega_s y(\varepsilon_r\mu_r-1)}{\mu_0\mu_r\left(c_0^2-\omega_s^2(x^2+y^2)\right)}E_y + \left(\frac{1}{\mu_0\mu_r} - \frac{\omega_s^2(x^2+y^2)(\varepsilon_r\mu_r-1)}{\mu_0\mu_r\left(c_0^2-\omega_s^2(x^2+y^2)\right)}\right)B_z
\end{aligned} \tag{A.10}$$

Equations (A.8) and (A.10) immediately gives the tensor fields P,Q,L,M described in equations (4.17), (4.18), (4.19) and (4.20).

Bibliography

[1] J. G. Van Bladel. *Electromagnetic Fields*. IEEE Press, Piscataway, NJ, USA, 2nd edition, 2007.

[2] A. M. Messiaen and P. E. Vandenplas. High-frequency effect due to the axial drift velocity of a plasma column. *Physical Review*, 149:131–140, September 1966.

[3] C. Yeh. Scattering obliquely incident microwaves by a moving plasma column. *Journal of Applied Physics*, 40(13):5066–5075, December 1969.

[4] T. Shiozawa and S. Seikai. Scattering of electromagnetic waves from an inhomogeneous magnetoplasma column moving in the axial direction. *IEEE Transactions on Antennas and Propagation*, 20(4):455–463, July 1972.

[5] J. V. Parker, J. C. Nickel, and R. W. Gould. Resonance oscillations in a hot nonuniform plasma. *Physics of Fluids*, 7(9):1489–1500, September 1964.

[6] D. Censor. Scattering of electromagnetic waves by a cylinder moving along its axis. *IEEE Transactions on Microwave Theory and Techniques*, 17(3):154–158, March 1969.

[7] Y. Yan. Mass flow measurement of bulk solids in pneumatic pipelines. *Measurement Science and Technology*, 7(12):1687, 1996.

[8] M. Pastorino, M. Raffetto, and A. Randazzo. Electromagnetic inverse scattering of axially moving cylindrical targets. *IEEE Transactions on Geoscience and Remote Sensing*, 53(3):1452–1462, March 2015.

[9] M. Brignone, G. L. Gragnani, M. Pastorino, M. Raffetto, and A. Randazzo. Noise limitations on the recovery of average values of velocity profiles in pipelines by simple imaging systems. *IEEE Geoscience and Remote Sensing Letters*, 13(9):1340–1344, 2016.

[10] J. Van Bladel. Electromagnetic fields in the presence of rotating bodies. *Proceedings of the IEEE*, 64(3):301– 318, March 1976.

[11] D. De Zutter. Scattering by a rotating dielectric sphere. *IEEE Transactions on Antennas and Propagation*, 28(5):643–651, September 1980.

[12] D. De Zutter. Scattering by a rotating circular cylinder with finite conductivity. *IEEE Transactions on Antennas and Propagation*, 31(1):166–169, January 1983.

[13] A. Einstein. Zur Elektrodynamik bewegter Körper. *Annalen der Physik*, 17(891), 1905.

[14] D. K. Cheng and J.-A. Kong. Covariant descriptions of bianisotropic media. *Proceedings of the IEEE*, 56(3):248–251, March 1968.

[15] C. Yeh and K. F. Casey. Reflection and transmission of electromagnetic waves by a moving dielectric slab. *Physical Review*, 144(2):665–669, 1966.

[16] C. Yeh. Reflection and transmission of electromagnetic waves by a moving dielectric slab. ii. parallel polarization. *Physical Review*, 167(3):875–877, 1968.

[17] A. Z. Ilic and M. M. Ilic. Higher-order frequency-domain FEM analysis of EM scattering off a moving dielectric slab. *IEEE Antennas and Wireless Propagation Letters*, 12:890–893, 2013.

[18] S. Caorsi, M. Pastorino, and M. Raffetto. Electromagnetic scattering by a multilayer elliptic cylinder under transverse-magnetic illumination: series solution in terms of Mathieu functions. *IEEE Transactions on Antennas and Propagation*, 45(6):926–935, June 1997.

[19] S. Caorsi, M. Pastorino, and M. Raffetto. Scattering by a conducting elliptic cylinder with a multilayer dielectric coating. *Radio Science*, 32(6):2155–2166, November-December 1997.

[20] M. Brignone and M. Raffetto. Well posedness and finite element approximability of two-dimensional time-harmonic electromagnetic problems involving nonconducting moving objects with stationary boundaries. *ESAIM: Mathematical Modelling and Numerical Analysis*, 49(4):1157–1192, July-August 2015.

[21] J. Van Bladel. Rotating dielectric sphere in a low-frequency field. *Proceedings of the IEEE*, 67(12):1654–1655, December 1979.

[22] D. De Zutter and D. Goethals. Scattering by a rotating conducting sphere. *IEEE Transactions on Antennas and Propagation*, 32(1):95–98, January 1984.

[23] R. D. Graglia, A. Freni, and G. Pelosi. A finite element approach to the electromagnetic interaction with rotating penetrable cylinders of arbitrary cross section. *IEEE Transactions on Antennas and Propagation*, 41(5):635–650, May 1993.

[24] P. Fernandes and M. Raffetto. Well posedness and finite element approximability of time-harmonic electromagnetic boundary value problems involving bianisotropic materials and metamaterials. *Mathematical Models and Methods in Applied Sciences*, 19(12):2299–2335, December 2009. DOI No: 10.1142/S0218202509004121.

[25] P. Kalarickel Ramakrishnan and M. Raffetto. Fisrt error analyses for finite element solutions of boundary value problems involving cylinders moving in axial direction. In *2015 International Conference on Electromagnetics in Advanced Applications (ICEAA)*, pages 305–308, Sept 2015.

[26] M. Brignone, P. K. Ramakrishnan, and M. Raffetto. A first numerical assessment of the reliability of finite element simulators for time-harmonic electromagnetic problems involving rotating axisymmetric objects. In *URSI International Symposium on Electromagnetic Theory(EMTS)*, pages 787–790, Aug 2016.

[27] K.Tanaka and K:Hazama. Reflection and transmission of electromagnetic waves by a moving inhomogeneous medium. *Radio Sci.*, 7(10):973–978, Oct. 1989.

[28] T. Shiozawa and I. Kawano. Electromagnetic scattering by an infinitely long cylinder moving along its axis. *Electronics and Communications in Japan*, 53-B(7):45–51, 1970.

[29] V. Girault and P. A. Raviart. *Finite element methods for Navier–Stokes equations*. Springer–Verlag, Berlin, 1986.

[30] P. Monk. *Finite element methods for Maxwell's equations*. Oxford Science Publications, Oxford, 2003.

[31] J. A. Kong. *Theory of Electromagnetic Waves*. Wiley, New York, 1975.

[32] P. Fernandes, M. Ottonello, and M. Raffetto. Regularity of time-harmonic electromagnetic fields in the interior of bianisotropic materials and metamaterials. *The IMA Journal of Applied Mathematics*, 79(1):54–93, February 2014.

[33] J. Jin. *The finite element method in electromagnetics*. John Wiley & Sons, New York, 1993.

[34] G. Franceschetti. *Campi elettromagnetici*. Bollati Boringhieri, Turin, Italy, 1988. In Italian.

[35] P. G. Ciarlet. *Basic error estimates for elliptic problems*. Elsevier Science Publishers B. V. (North-Holland), Amsterdam, 1991.

[36] R. Barrett, M. Berry, T. F. Chan, J. Demmel, J. Donato, J. Dongarra, V. Eijkhout, R. Pozo, C. Romine, and H. Van der Vorst. *Templates for the Solution of Linear Systems: Building Blocks for Iterative Methods, 2nd Edition*. SIAM, Philadelphia, PA, 1994.

[37] A. Freni, C. Mias, and R. L. Ferrari. Finite element analysis of electromagnetic wave scattering by a cylinder moving along its axis surrounded by a longitudinal corrugated structure. *IEEE Transactions on Magnetics*, 32(3):874–877, May 1996.

[38] A. Sommerfeld. *Electrodynamics*. Lectures on theoretical physics. Academic Press, 1959.

[39] P. G. Ciarlet and J. L. Lions (Eds.). *Handbook of Numerical Analysis, vol. II, Finite Element Methods, Part 1*. North-Holland, Amsterdam, 1991.

[40] M. Pastorino and M. Raffetto. Scattering of electromagnetic waves from a multilayer elliptic cylinder moving in the axial direction. *IEEE Transactions on Antennas and Propagation*, 61(9):4741–4753, September 2013.

[41] J. D. Jackson. *Classical electrodynamics*. Wiley, New York, 3rd edition, 1999.

[42] G. Cevini, G. Oliveri, and M. Raffetto. Further comments on the performances of finite element simulators for the solution of electromagnetic problems involving metamaterials. *Microwave and Optical Technology Letters*, 48(12):2524–2529, 2006.

[43] M. Pastorino. *Microwave Imaging*. Wiley, New York, 2010.

[44] J. L. Volakis, A. Chatterjee, and L. C. Kempel. *Finite element method for electromagnetics: antennas, microwave circuits, and scattering applications*. IEEE Press, Piscataway, NJ, USA, 1998.

[45] M. Brignone and M. Raffetto. First results on the reliability of finite element simulators for the solution of time-harmonic electromagnetic problems involving moving objects with stationary boundaries. In *2013 International Conference on Electromagnetics in Advanced Applications (ICEAA)*, pages 159–162, September 2013.

[46] R. F. Harrington. *Field computation by moment methods*. IEEE Press, Piscataway, NJ, USA, 1993.

[47] P. Fernandes and M. Raffetto. Existence, uniqueness and finite element approximation of the solution of time-harmonic electromagnetic boundary value problems involving metamaterials. *COMPEL*, 24(4):1450–1469, 2005.

[48] S. Caorsi, P. Fernandes, and M. Raffetto. On the convergence of Galerkin finite element approximations of electromagnetic eigenproblems. *SIAM Journal on Numerical Analysis*, 38(2):580–607, 2000.

[49] S. Caorsi, P. Fernandes, and M. Raffetto. Spurious-free approximations of electromagnetic eigenproblems by means of Nedelec-type elements. *Mathematical Modelling and Numerical Analysis*, 35(2):331–354, 2001.

[50] T. S. Mo. Theory of electrodynamics in media in noninertial frames and applications. *Journal of Mathematical Physics*, 11(8):2589–2610, 1970.

[51] T. Shiozawa. Phenomenological and electron-theoretical study of the electrodynamics of rotating systems. *Proceedings of the IEEE*, 61(12):1694–1702, December 1973.

[52] P. G. Ciarlet. *The finite element method for elliptic problems*. North-Holland, Amsterdam, 1978.

[53] Jonathan Richard Shewchuk. Triangle: Engineering a 2D Quality Mesh Generator and Delaunay Triangulator. In Ming C. Lin and Dinesh Manocha, editors, *Applied Computational Geometry: Towards Geometric Engineering*, volume 1148 of *Lecture Notes in Computer Science*, pages 203–222. Springer-Verlag, May 1996. From the First ACM Workshop on Applied Computational Geometry.

[54] Hang Si. TetView. `http://tetgen.berlios.de/tetview.html`, 2004.

[55] T. X. Wu and D. L. Jaggard. A comprehensive study of discontinuities in chirowaveguides. *IEEE Transactions on Microwave Theory and Techniques*, 50(10):2320–2330, October 2002.

[56] P. Alotto and L. Codecasa. A fit formulation of bianisotropic materials over polyhedral grids. *IEEE Transactions on Magnetics*, 50(2):349–352, Feb 2014.